

MEMS & BIOMEMS

A Versatile MEMS Quadrupole Platform for Portable Mass Spectrometry Using the First and Second Stability Regions	4-1
First Principles Optimization of Mass-producible Microscaled Linear Quadrupoles for Operation in Higher Stability Regions	4-2
A Single-gated Open Architecture Carbon Nanotube Array for Efficient Field Ionization.....	4-3
A Fully Micro-fabricated Planar Array of Electrospray Emitters for Space-propulsion Applications	4-4
Carbon Nanotube Electron Sources for Space Propulsion Applications	4-5
Carbon Nanotubes for Electrospray Nanofluidic Applications.....	4-6
A High-density Electron Source that Uses Un-gated Transistors for Ballasting	4-7
Nanoelectromechanical Switches and Memories	4-8
Exciton Coupled Surface Plasmon Resonance Biosensor	4-9
Micromechanical Substrates for Reconfigurable Cell Culture	4-10
Aligned Multimask Patterning of Biomolecules and Cells	4-11
Collective Hydrodynamics and Kinetics of Sickle Cell Vaso-occlusion and Rescue in a Microfluidic Device	4-12
Plasma-activated Inter-layer Bonding of Thermoplastics for Micro- and Nano-fluidic Manufacturing	4-13
Environmentally Benign Manufacturing of Three-dimensional Integrated Circuits	4-14
An Implantable MEMS Drug-delivery Device.....	4-15
High Speed Three-dimensional Scanner for <i>in vivo</i> Non-invasive Optical Biopsy using Two-photon Microscopy	4-16
Electromagnetically-driven Meso-scale Nanopositioners for Nano-scale Manufacturing and Measurement.....	4-17
Barcoded Microparticles for Multiplexed Detection	4-18
Single-molecule DNA Mapping in a Fluidic Device	4-19
DNA Dynamics in Nanofluidic Devices	4-20
Microfluidic Bubble Logic	4-21
Perfused Multiwell Tissue Culture Plates for Development of Drug and Disease Models	4-22
A Patterned Anisotropic Nanofilter Array for Continuous-flow Separation of DNA and Proteins	4-23
Cell Stimulation, Lysis, and Separation in Microdevices	4-24
Microreactors for Synthesis of Quantum Dots	4-25
Microfluidic Synthesis and Surface Engineering of Colloidal Nanoparticles	4-26
Organic Synthesis in Microreactor Systems	4-27
Autothermal Catalytic Micromembrane Devices for Portable High-purity Hydrogen Generation	4-28
Thermal Management in Devices for Portable Hydrogen Generation	4-29
Microfluidic Systems for the Study of Vascular Networks.....	4-30
Patterning and Processing of Thermosensitive Hydrogels for Microfluidics Applications	4-31
A Large-strain, Arrayable Piezoelectric Microcellular Actuator by Folding Assembly	4-32
Thermal Ink Jet Printing of Lead Zirconate Titanate Thin Films	4-33
Piezoelectric Micro-power-generator: MEMS Energy-harvesting Device for Self-powered Wireless Corrosion-monitoring System.....	4-34
Lateral-line-inspired MEMS-array Pressure Sensing for Passive Underwater Navigation	4-35
Fabrication of a Fully-integrated Multiwatt μ TurboGenerator.....	4-36
A Portable Power Source Based on MEMS and Carbon Nanotubes	4-37
A MEMS Steam Generator.....	4-38
Microscale Singlet Oxygen Generator for MEMS-based COIL Lasers	4-39
An Integrated Microelectronic Device for Label-free Nucleic Acid Amplification and Detection.....	4-40
Monitoring of Heparin and its Low Molecular Weight Analogs by Silicon Field Effect	4-41
Weighing of Biomolecules, Single Cells and Single Nanoparticles in Fluid	4-42
Integrated System for Cancer Biomarker Detection.....	4-43
Passive Microwave Transponders for Passive, Real-time, and High-sample-rate Localization	4-44
Macroscopic Interfaces to Parallel Integrated Bioreactor Arrays.....	4-45
MIT-OSU-HP Focus Center on Non-lithographic Technologies for MEMS and NEMS	4-46
A Micromachined Printhead for the Evaporative Printing of Organic Materials at Ambient Pressure	4-47
Surface Micromachining Processes using Non-lithographic Technologies	4-48
Micromechanical Actuators for Insect Flight Mechanics	4-49
MEMS Micro-vacuum Pump for Portable Gas Analyzers	4-50
Microfabricated Electrodes for Solid Oxide Fuel Cells	4-51
A MEMS-relay for Power Applications	4-52
A Silicon-etched, Electrical-contact Tester.....	4-53
Microfluidic Studies of Biological Cell Deformability and Rheology	4-54
Phase Change Materials for Actuation in MEMS	4-55
Microfabricated Thin-film Electrolytes and Electrodes for Solid Oxide Fuel Cells	4-56
Nanowire- and Microsphere-templated Gas Sensors	4-57
BioMEMS for Control of the Stem Cell Microenvironment	4-58
Microfabricated Devices for Sorting Cells Using Complex Phenotypes	4-59
Combined Microfluidic/Dielectrophoretic Microorganism Concentrators	4-60
DEP Cell-patterning for Controlling Cellular Organization	4-61
Iso-dielectric Cell Separation	4-62
MEMS Vibration Harvesting for Wireless Sensors	4-63
Design, Fabrication, and Testing of Multilayered Microfabricated Solid Oxide Fuel Cells (SOFCs)	4-64

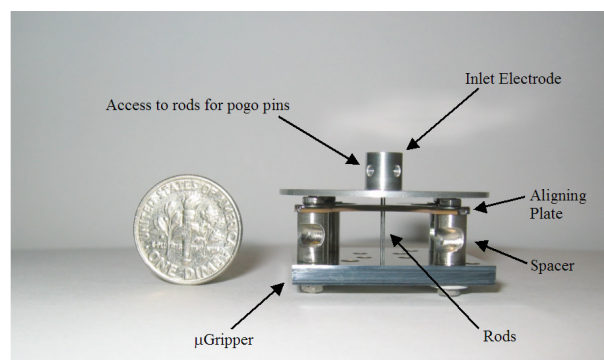
A Versatile MEMS Quadrupole Platform for Portable Mass Spectrometry Using the First and Second Stability Regions

L.F. Velásquez-García, K. Cheung, A.I. Akinwande
Sponsorship: DARPA

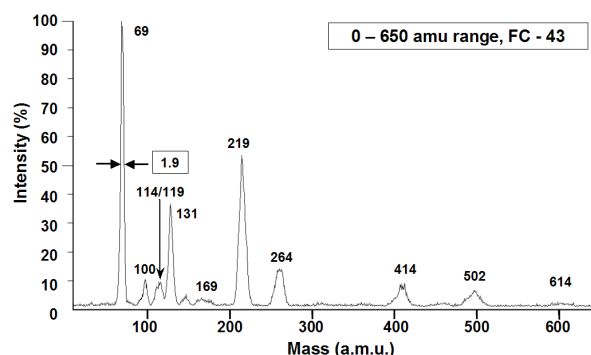
The Micro Gas Analyzer Program aims to develop portable, low-power, fast and low-false-alarm-rate gas analyzer technology for a wide range of applications. One of the subsystems of the gas analyzer is a mass filter. An array of micro-fabricated quadrupole mass filters is being developed for this purpose. The quadrupoles will sort out the ions based on their specific charges. Both high sensitivity and high resolution are needed over a wide range of ion masses, from 15 to 650 amu. In order to achieve this performance, multiple micro-fabricated quadrupoles, each operating at a specific stability region and mass range, are operated in parallel.

The proof-of-concept device is a single, linear quadrupole that has a micro-fabricated mounting head with meso-scaled DRIE-patterned springs. The mounting head allows micron-precision hand assembly of the quadrupole rods [1] –critical for good resolution and ion transmission. The micro-fabricated mounting head can implement quadrupoles with a wide range of aspect ratios for a given electrode diameter. The springs can be individually actuated using spring tip handlers. The current version of the spring-

head is able to interact with rods with diameters from 1588 μm down to 250 μm . The quadrupoles that have been implemented thus far span the aspect ratio range from 30 to 60. The choice of electrode diameter takes into account the dimensional uncertainties and alignment capabilities with respect to the expected resolution and transmission goals. Figure 1 shows an assembled MEMS quadrupole with 250-micrometer diameter rods. Figure 2 shows the experimental data of one of these quadrupoles using FC-43 as a calibration compound, where a mass resolution of 2 amu and a full mass range of 650 amu are demonstrated, while using a 1.44 MHz RF power supply to drive the quadrupole with a constant-width circuit made by the Extrel company (Pittsburgh, PA). To obtain better resolution, the MEMS quadrupoles have been driven with up to 4 MHz RF sources, resulting in 0.7 amu peak width. Also, the devices have been driven in the second stability regions to obtain 0.4 amu of peak width and smoother peaks. Current research efforts concentrate on developing RF power supplies of higher frequency and further exploration of the second stability region to obtain better performance.



▲ Figure 1: A micro-fabricated quadrupole with electrode diameter equal to 250 micrometers, near a dime for size comparison. The micro-fabricated part of the device is the square base, which contains a system of meso-scaled DRIE-patterned springs.



▲ Figure 2: Experimental characterization of a MEMS quadrupole, using the compound FC-43 to get peaks in the 1 – 650 amu mass range. The peak width is estimated at 2 amu, using a 1.44-MHz-RF-power supply. Peak widths as small as 0.4 amu have been obtained.

REFERENCES

- [1] L.F. Velásquez-García and A.I. Akinwande, "Precision hand assembly of MEMS subsystems using DRIE-patterned deflection spring structures: An example of an out-of-plane substrate assembly," *Journal of MicroElectroMechanical Systems*, to be published.

First Principles Optimization of Mass-producible Microscaled Linear Quadrupoles for Operation in Higher Stability Regions

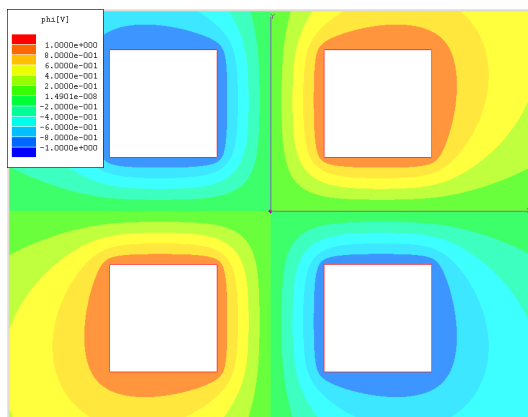
K. Cheung, L.F. Velásquez-García, A.I. Akinwande
Sponsorship: DARPA

In recent years, there has been a desire to scale down linear quadrupoles. The key advantages of this miniaturization are the portability it enables and the reduction of pump-power needed due to the relaxation on operational pressure. Various attempts at making microscaled linear quadrupoles met with varying degrees of success [1-2]. Producing these devices involved some combination of precision machining or microfabrication and downstream assembly. For miniature quadrupole mass filters to be mass-produced cheaply and efficiently, manual assembly should be removed from the process.

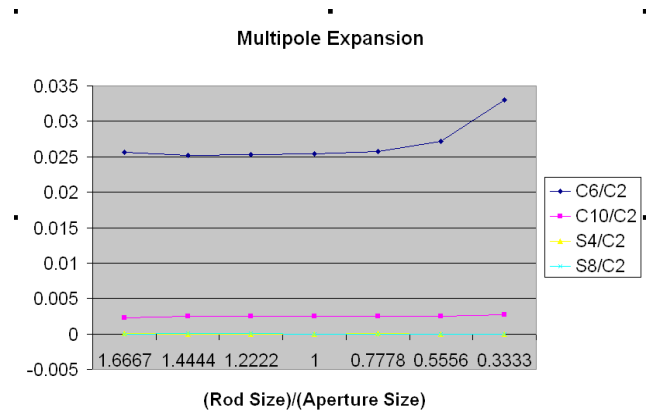
A purely microfabricated quadrupole mass filter comprising a planar design and a rectangular electrode geometry is proposed. Quadrupole resolution is inversely-proportional to the square of the electrode length, thus favoring a planar design since electrodes can be made quite long. Rectangular rods are considered since that is the most amenable geometric shape for planar microfabrication. This deviation from the conventional round rod geometry calls for optimization and analysis. Electrode designs were parameterized, and the potential fields were solved using Maxwell

3D (Figure 1). The fields were decomposed using a multipole expansion to examine the higher-order coefficients (Figure 2). This process was used to minimize the significant high-order terms, thus optimizing the design and determining the ultimate limitations of the device.

Higher-order field contributions arising from geometric non-idealities lead to non-linear resonances. These resonances manifest as peak splitting that is typically observed in quadrupole mass spectra. Reported work involving linear quadrupoles operated in the second stability region show improved peak shape without these splits [3]. It is believed that operating the device in the second stability region will provide a means to overcome the non-linear resonances introduced by the square electrode geometry. This study was conducted to justify a fully microfabricated, mass-producible, MEMS linear quadrupole mass filter. Successful implementation of such devices will lead into arrayed configurations for parallel analysis and aligned quadrupoles operated in tandem for enhanced resolution.



▲ Figure 1: Potential field solution generated by Maxwell 3D using a rectangular electrode geometry. Geometries were parameterized and solved.



▲ Figure 2: Dependence of the coefficients derived from a multipole expansion on the ratio of rod size to aperture size. The C2 refers to an ideal quadrupole field.

REFERENCES

- [1] M. Gear, R.R.A. Syms, S. Wright, and A.S. Holmes, "Monolithic MEMS Quadrupole mass spectrometers by deep silicon etching," *Journal of Microelectromechanical Systems*, vol. 14, no. 5, pp. 1156-1166, Oct. 2005.
- [2] J.J Tunstall, S. Taylor, R.R.A. Syms, T.Tate, and M.M. Ahmad, "Silicon micromachined mass filter for a low-power, low-cost quadrupole mass spectrometer," in *Proc. IEEE Eleventh Annual International Workshop on Micro Electro Mechanical Systems*, 1998, pp. 438-442.
- [3] L.F. Velazquez-Garcia, K. Cheung, and A.I. Akinwande, "A versatile MEMS quadrupole platform for portable mass spectrometry using the first and second stability regions," *Journal of Microelectromechanical Systems*, to be published.

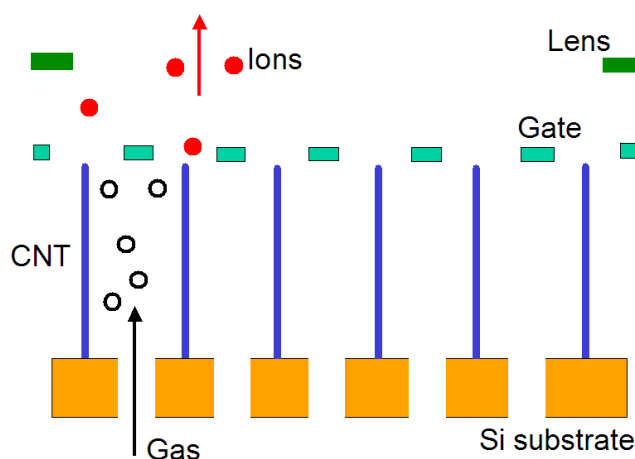
A Single-gated Open Architecture Carbon Nanotube Array for Efficient Field Ionization

L.F. Velásquez-García, A.I. Akinwande
Sponsorship: DARPA

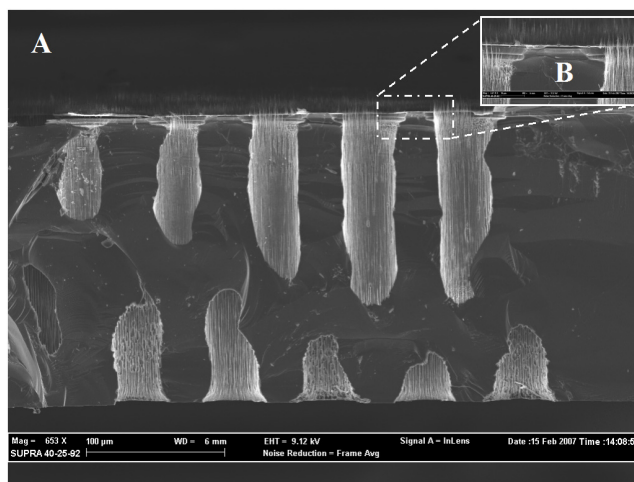
Mass spectrometers require a suitable ionizer to be able to discern the chemical composition of the sample that they are analyzing. Traditional ionizers for gases use either chemical ionization (CI) or electron impact ionization (EI). In the latter case, electrons from thermionic sources produce ions by colliding with neutral molecules. More efficient carbon nanotube-based field emitted electron impact ionizers have been developed [1]. However, one of the drawbacks of electron impact ionization is that the sample is transformed into fragmentation products. Several samples could have similar fragmentation spectra but be quite different compounds, with radically different properties (for example, one substance can be a poisonous agent while another is a harmless material). Therefore, an approach to reduce the fragmentation products would improve the informational power of the mass spectrometer.

Field ionization soft-ionizes molecules, thus reducing the fragmentation products. In the field ionization scheme, ions are created by directly tunneling electrons from the outer shell of neutral

molecules by virtue of a very high electric field [2]. The electric field is produced by high aspect ratio field enhancers and the application of a large (up to 1 kV) bias voltage. Carbon nanotubes are ideal field enhancers because of their high aspect ratio and their reduced tip radius. A good field ionizer should work in the field-limited regime instead of the molecular flux-limited regime, where all the molecules that approach the high field region are thus ionized. In the case of the electron impact ionizers, a closed architecture is implemented because it is intended to protect the field enhancers from back streaming ions [3]. Therefore, an open architecture, where the field enhancers surround a through-hole, is a more suitable approach to produce field ionization. We plan to implement a single-gated field ionizer array with an open architecture. Figure 1 shows a schematic of the open architecture concept. Figure 2 shows a cross section of the device. Current research effort focuses on device characterization.



▲ Figure 1: Schematic of a Field ionizer array. The gas inlet provides neutral species to the field enhancers. If the molecules of the gas come close enough to the CNT tips, an electron from the outer shell of the molecule will tunnel to the CNT, thus ionizing the molecule.



▲ Figure 2: A single-gated CNT field ionizer array grown at MIT. Field view of an array cross-section (A), and detail of two adjacent field ionizers (B). The ionizer well has a film of silicon dioxide 5 μm thick below the gate that acts as electrical insulator between the gate and the CNTs. The CNT catalyst was Ni 7.5 nm thick.

REFERENCES

- [1] L.-Y. Chen, "Double-gated field emission arrays," Ph.D. thesis, Massachusetts Institute of Technology, Cambridge, MA, 2007.
- [2] R. Gomer, *Field Emission and Field Ionization*, New York, NY: American Institute of Physics, 1961, rpt. 1993
- [3] L. Dvorson, I. Kymissis, and A.I. Akinwande, "Double-gated silicon field emitters," *J. of Vac. Sci. and Technol. B*, vol. 21, no. 1, pp. 486-494, Jan. 2003.

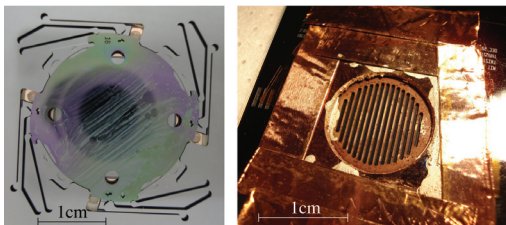
A Fully Micro-fabricated Planar Array of Electro spray Emitters for Space-propulsion Applications

B. Gassend, L.F. Velasquez-Garcia, A.I. Akinwande, M. Martinez-Sanchez
 Sponsorship: AFOSR, DARPA

Electrospray thrusters work by extracting ions or charged droplets directly from a liquid surface using an electrostatic field and accelerating them in that field to produce thrust [1]. This method could lead to more efficient and precise thrusters for space propulsion applications. Emission occurs from sharp emitter tips, which enhance the electric field and constrain the emission location. The electro spray process limits the thrust from a single tip. To get into the millinewton range will require an array with tens of thousands of emitters. Batch micro-fabrication is well suited to making this array.

We have designed, built, and tested a thruster made in silicon using deep reactive ion etching (DRIE) and wafer-bonding technology (see Figure 1). This thruster comprises two components. The emitter die has up to 517 emitters in a 0.75 cm² area, formed using DRIE and SF₆ etching, and is plasma treated so that liquid can be transported to the tips in a porous black silicon surface layer. The extractor die incorporates the extractor electrode, a Pyrex layer for insulation, and the springs, which are used to reversibly clamp the emitter die [2]. This versatile assembly method allows the extractor die to be reused with multiple emitter dies and potentially with emitter concepts radically different from the one we have experimented with.

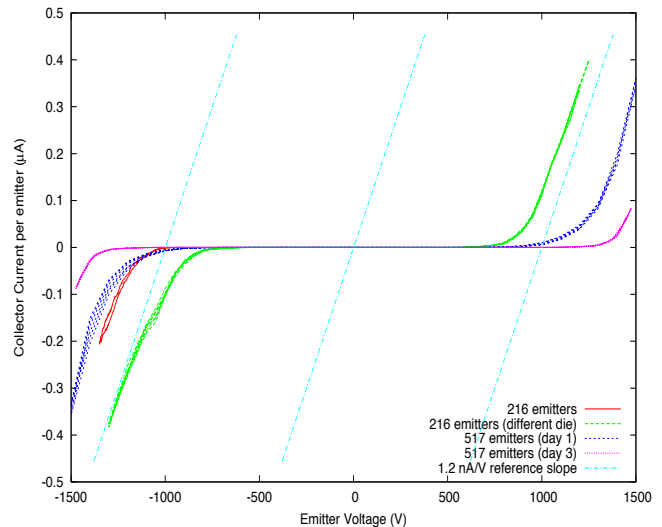
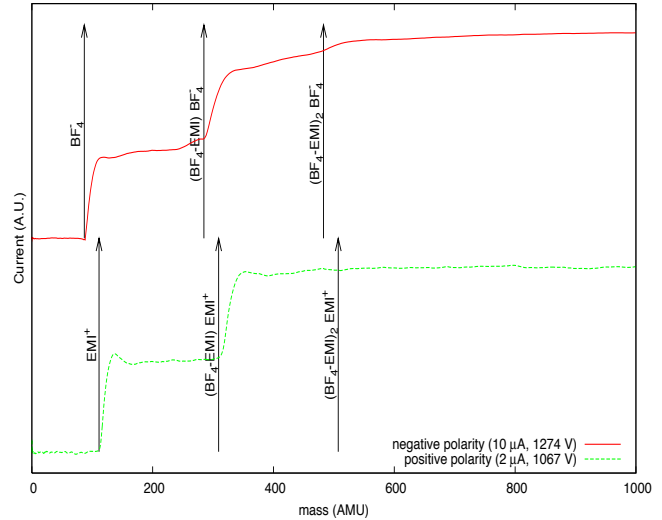
Figure 2 shows data collected when firing the thruster with the ionic liquid EMI-BF₄. Measurable emissions occurred for extraction voltages down to 700 V. The current collected on the extractor electrode was less than 3% of the emitted current over a wide operating range and often less than 0.1 %. Beam-divergence half-angles were between 15 and 30 degrees, depending on the operating conditions. Emitted currents of 500 nA/emitter were observed in stable operation, for expected thrusts of 25 nN/emitter. Time-of-flight measurements prove operation in the ion emission regime, which is most efficient for propulsion.



▲ Figure 1: The assembly mechanism (top-left), the extractor electrodes (top-right), diagram of the thruster (bottom).

REFERENCES

- [1] M. Gamero-Castaño and V. Hruby, "Electrospray as a source of nanoparticles for efficient colloid thrusters," *Journal of Power and Propulsion*, vol. 17, no. 5, pp. 977-987, Sep.-Oct. 2001.
- [2] B. Gassend, L.F. Velasquez-Garcia, A.I. Akinwande, and M. Martinez-Sanchez, "Mechanical assembly of electro spray thruster grid," in *Proc. 29th International Electric Propulsion Conference*, Princeton, NJ, Nov. 2005.



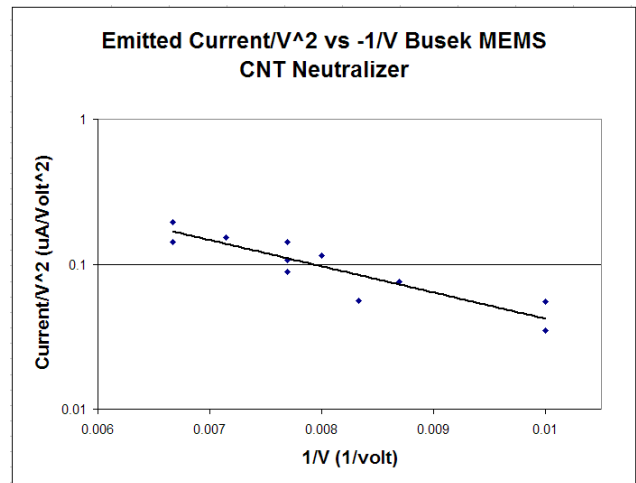
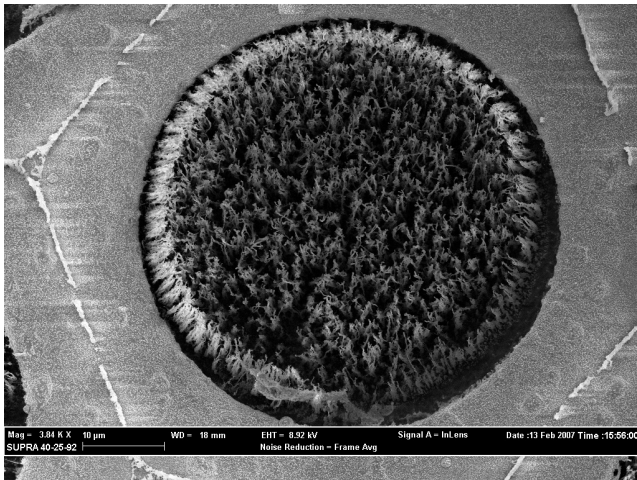
▲ Figure 2: Time of flight data (top) and current-voltage characteristic (bottom) of the thruster.

Carbon Nanotube Electron Sources for Space Propulsion Applications

L.F. Velásquez-García, A.I. Akinwande
Sponsorship: DARPA

Low-power, low-voltage, efficient field emission neutralizers for FEEPs [1], colloid thrusters [2], and other micro-propulsion engines are attractive for nanosatellites because they do not use mass flowrate to operate, unlike more conventional neutralizing solutions such as hollow cathodes [3]. Electrons are field-emitted from the surface of metals and semiconductors by the application of a high electrostatic field. Field emitters use high aspect ratio structures to generate very high fields even when low voltages are applied. The ideal field enhancing structure is a rounded whisker [4]. Micro-engineered field emission neutralizers would have smaller starting voltages, better area usage, and more uniform I-V characteristics, compared to macro/meso fabricated field emitter versions. Plasma-Enhanced Chemical Vapor Deposited (PECVD) Car-

bon Nanotubes (CNTs) are rounded whiskers with 100 nm or less of tip radius and 13 μm or more tall. The adoption of CNTs as electron-emitting substrate has recently been shown to have advantages compared to Spindt emitters because of the higher aspect ratio of CNTs and their superior resistance to harsh environments. This research focuses on the development of a batch-fabricated MEMS neutralizer that uses PECVD CNTs as field enhancers (Figure 1). As a reference, a previously made Busek-MIT MEMS CNT device that uses a randomly oriented CNT matrix produced by Busek Co. (Natick MA) with a proprietary arc-based process yielded devices with Fowler-Nordheim emission, startup voltage as low as 100 V, and electron currents as large as 3.2 mA/cm² with about 20% of gate current interception.



▲ Figure 1: Top view of a 14- μm -tall CNF forest inside a microfabricated well. The well has integrated a gate to bias voltage to the CNT forest to produce field emission.

▲ Figure 2: The I-V characterization of a similar CNT-based field emitter array. The device was jointly developed with the Busek company (Natick, MA)

REFERENCES

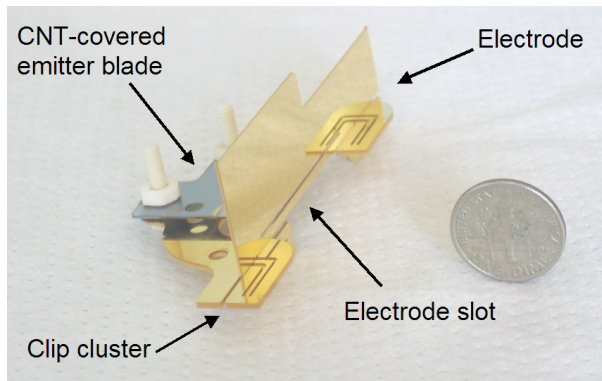
- [1] M. Tajmar, A. Genovese, and W. Steiger, "Indium field emission propulsion microthruster experimental characterization," *J. of Propulsion and Power*, vol. 20, no. 2, pp. 211-218, Mar.-Apr. 2004.
- [2] M. Gamero and V. Hruby, "Electrospray as a source of nanoparticles for efficient colloid thrusters," *J. of Propulsion and Power*, vol. 17, no. 5, pp. 977-987, Sep.-Oct. 2001.
- [3] I. Kameyama and P. Wilbur, "Measurements of ions from high-current hollow cathodes using electrostatic energy analyzer," *J. of Propulsion and Power*, vol. 16, no. 3, pp. 529-535, May-June 2000.
- [4] T. Utsumi, "Vacuum microelectronics: What's new and exciting," *IEEE Transactions on Electron Devices*, vol. 38, no. 10, pp. 2276-2283, Oct. 1991.

Carbon Nanotubes for Electro spray Nanofluidic Applications

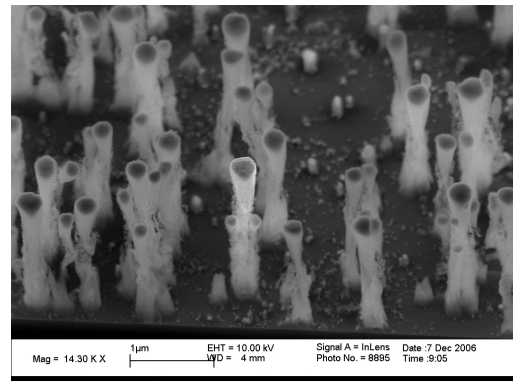
L.F. Velásquez-García, A.I. Akinwande
Sponsorship: DARPA

Electrospray is the technique to soft-ionize liquids by applying a high electric potential to a liquid meniscus. The liquid meniscus is deformed into a cone [1], and charged species are emitted from its apex. The emission can be solvated ions, charged droplets, or a mix of the two. This low-divergence charged species source can be used in diverse applications such as mass spectrometry, propulsion, printing, and etching. Our research group has successfully developed several multiplexed MEMS electro spray sources, mainly intended for space propulsion applications. These devices include internal pressure-fed spouts that emit charged droplets [2] and externally surface tension fed spouts that emit solvated ions [3]. In all cases, the emitter field enhancers and the hydraulic impedance are provided using silicon-based structures. Furthermore, the devices use a 3D packaging technology that allows decoupling the process flows of the subsystems without loss in emitter density [4]. Consequently, it is possible to use radically different fabrication techniques and materials to implement MEMS electro spray arrays.

This project intends to investigate the application of Plasma Enhanced Chemical Vapor Deposition Carbon Nanotubes (PECVD CNTs) in multiplexed electro spray sources. Two research directions are currently pursued: the use of CNTs as hydraulic impedance to ballast the emitter array (both in internal and external architectures) and the use of CNTs as emitter field enhancers. On the one hand, PECVD CNT forests can be custom tailored to match a desired morphology. On the other hand, PECVD CNTs have remarkable field enhancing properties. Figure 1 shows a silicon-based externally fed electro spray linear emitter array that uses PECVD CNTs as hydraulic impedance, while Figure 2 shows the PECVD CNT forest grown on top of the silicon structures, using our group's reactor. Current research is focused on exploring the wettability of CNT forests using different liquids, catalysts, and growth conditions. These results will be used to choose the proper nanostructure to be used in an externally fed MEMS electro spray head that will eventually include CNT-based field enhancers.



▲ Figure 1: A 145 externally fed electro spray linear array. The emitter array is about 1-inch long.



▲ Figure 2: An SEM of a zoomed PECVD CNT forest used as hydraulic impedance for the electro spray array. The CNT height is about 1 µm.

REFERENCES

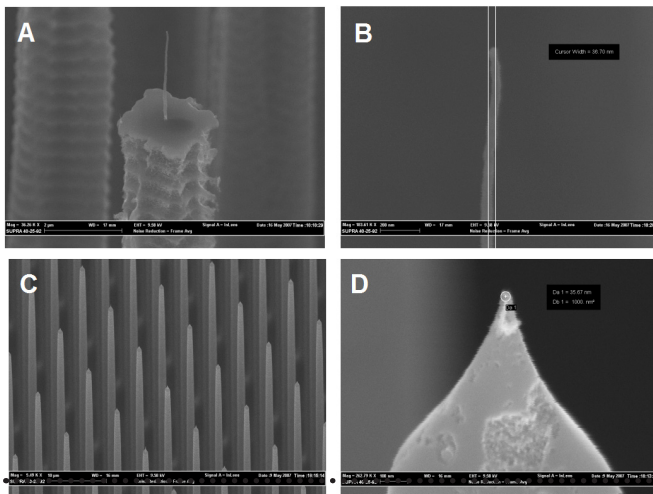
- [1] G.I. Taylor, "Disintegration of water drops in an electric field," *Proc. R. Soc. London A*, vol. 280, no. 1382, pp. 383-397, July 1964.
- [2] L.F. Velásquez-García, A.I. Akinwande, and M. Martínez-Sánchez, "A micro-fabricated linear array of electro spray emitters for thruster applications," *Journal of MicroElectroMechanical Systems*, vol. 15, no. 5, pp. 1260-1271, Oct. 2006.
- [3] L.F. Velásquez-García, A.I. Akinwande, and M. Martínez-Sánchez, "A planar array of micro-fabricated electro spray emitters for thruster applications," *Journal of MicroElectroMechanical Systems*, vol. 15, no. 5, pp. 1272-1280, Oct. 2006.
- [4] L.F. Velásquez-García and A.I. Akinwande, "Precision hand assembly of MEMS subsystems using DRIE-patterned deflection spring structures: An example of an out-of-plane substrate assembly," *Journal of MicroElectroMechanical Systems*, to be published.

A High-density Electron Source that Uses Un-gated Transistors for Ballasting

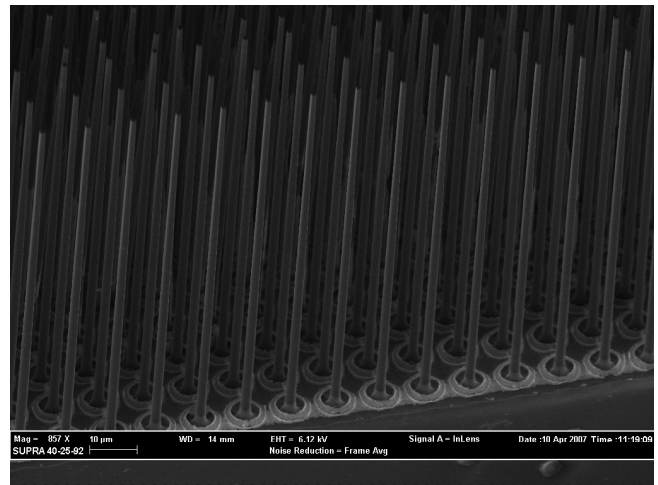
L.F. Velásquez-García, A.I. Akinwande
Sponsorship: AFRL

Electrons are field emitted from the surface of metals and semiconductors when the potential barrier (work function) that holds electrons within the metal or semiconductor is deformed by the application of a high electrostatic field. Field emitters use high aspect ratio structures with tips that have nanometer dimensions to produce a high electrostatic field with a low applied voltage. We are implementing two types of field enhancers: carbon nanofibers (CNFs) and silicon conical tips (Figure 1). Spatial variation of tip radius results in the spatial variation of the emission currents and non-uniform turn-on voltages. Small changes in the tip radius result in huge changes in the current density because of the exponential dependence of the emitted current on the bias voltage, as described by the Fowler-Nordheim theory. If the emitters are ballasted, the spatial non-uniformity can then be substantially decreased. Furthermore, ballasting individual emitters prevents destructive emission from the sharper tips allowing higher overall current emission because of the inclusion of duller tips. Ballasting also results

in more reliable operation. The use of large resistors in series with the field emitters is an unattractive ballasting approach because of the resulting low emission currents and power dissipation in the resistors. A better approach for ballasting field emitters is the use of un-gated field effect transistors that effectively provide high dynamic resistance with large saturation currents. In the past our research group demonstrated the use of a MOSFET to ballast the emission of electrons from silicon tips [1]. We plan to implement vertical un-gated transistors in series to the field emitters to obtain spatial uniformity in the current emission and I-V characteristics of the array [2]. The ballast structure is an n-doped, single-crystal silicon column, patterned using Deep Reactive Etching, and thinned using wet oxidation. Figure 2 shows a cross section of the un-gated transistors consisting of a 1-million elements in 1 cm². The field emitters are formed on top of the columns. Current efforts focus on device testing.



▲ Figure 1: A) An isolated 4 μm -tall CNF on top of a 100 μm -tall silicon column; B) Zoom of the CNF tip –tip diameter equal to 36 nm; C) Field of silicon tips on top of 100 μm -tall silicon columns; D) Zoom of a silicon tip -tip diameter equal to 35 nm.



▲ Figure 2: A 1000 \times 1000 array of 100- μm -tall, 1- μm -wide silicon columns, spaced 10 μm . The columns are un-gated transistors that control the current that the tips field-emit.

REFERENCES

- [1] C.-Y. Hong and A.I. Akinwande, "Temporal and spatial current stability of field emission arrays," *IEEE transactions on Electron Devices*, vol. 52, no. 10, pp. 2323, Oct. 2005.
- [2] H. Takemura, et. al., "A novel vertical current limiter fabricated with a Deep-trench-forming technology for highly reliable field emitter arrays," *Technical Digest of the IEEE International Electron Device Meeting*, Dec. 1997, pp. 709-712.

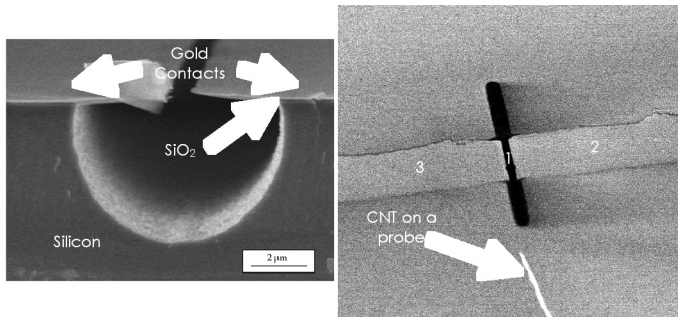
Nanoelectromechanical Switches and Memories

K.M. Milaninia, M.A. Baldo
Sponsorship: SRC/FCRP MSD, ISN

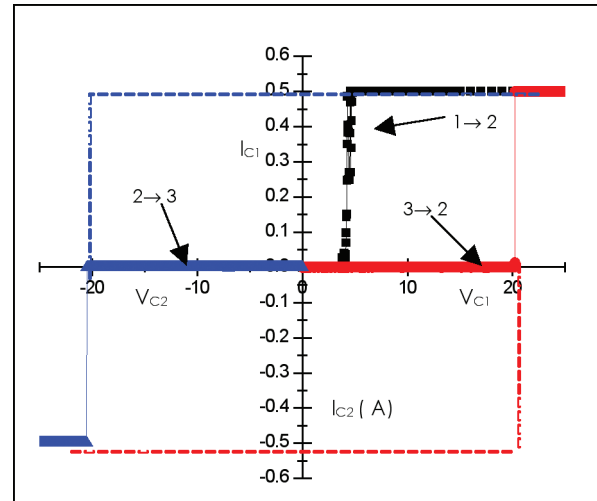
The ability to change shape is a compelling attraction of molecular semiconductors. Compared to rigid inorganic materials, molecules are soft and malleable, and their conformational changes are essential to the functionality of biological systems. Applications of nano-electro-mechanical (NEM) molecular devices include memories and transistors: Information can be stored in the conformation of molecules, potentially leading to very high density memories, and molecular transistors that change shape under bias could exhibit sub-threshold slopes of $\ll 60$ mV/decade [1]. Indeed, as an example of the potential of NEMs, voltage-gated ion channels possess sub-threshold slopes of approximately 15 mV/decade [2].

Although many materials are available for NEM applications, carbon nanotubes exhibit low resistance and good mechanical properties. In this project, we are constructing an NEM testbed. The proposed design for our relay is shown in Figure 1. Nano-

tubes are directly grown at the bottom of an electron-beam defined trench etched in Si. Leaving tube growth to the final step gives us better control of the nanotube and removes the need for additional steps that are required for the removal of surfactants and organics from the surface of the nanotubes. Because the nanotubes are vertically oriented, we are able to take advantage of the smallest size feature of the carbon nanotube, its diameter, which enables us to create dense arrays of relays for applications such as memory or logic devices. The vertical orientation allows NEM structures with very large aspect ratios. Theoretical results [3] have shown that increasing the aspect ratio of a carbon nanotube reduces the voltage needed to pull in the nanotube, thereby reducing the power consumption. Furthermore, because of the ability to easily functionalize the surface of nanotubes, we can functionalize the tube with multiple charges to lower the pull-in voltage even further.



▲ Figure 1: Testing is performed by introducing a probe-mounted CNT in between two gold contacts on silicon and then sweeping it from the center position (1), to the right contact (2), and subsequently to the third contact (3), and then back.



▲ Figure 2: An I-V of the device being switched from state 1→2 by applying a bias between Contact 1 and CNT, then switched from state 2→3 by applying a bias between Contact 2 and CNT, and finally switched from state 3→2 by applying a bias between Contact 1 and CNT.

REFERENCES

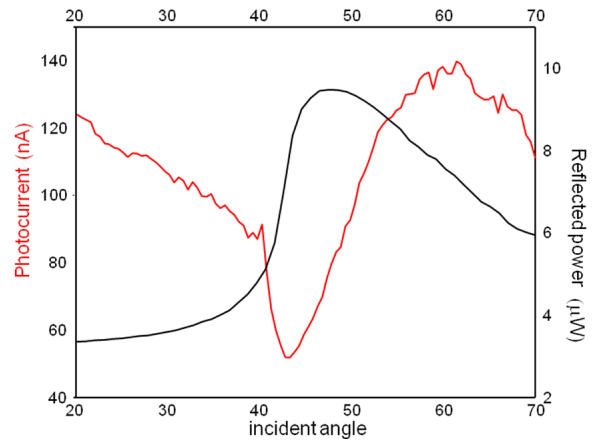
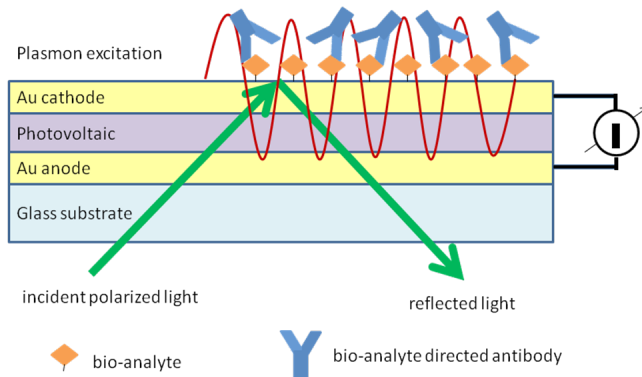
- [1] A.W. Ghosh, T. Rakshit, and S. Datta, "Gating of a molecular transistor: Electrostatic and conformational," *Nano Letters*, vol. 4, no. 4, pp. 565-568, Apr. 2004.
- [2] A.L. Hodgkin and A.F. Huxley, "Currents carried by sodium, potassium ions through the membrane of the giant squid axon of *Logilo*," *Journal of Physiology*, vol. 4, no. 116, pp. 449-472, 1952.
- [3] M. Dequesnes, S.V. Rotkin, and N.R. Aluru, "Calculation of pull-in voltages for carbon-nanotube-based nanoelectromechanical switches," *Nanotechnology*, vol. 13, no. 1, pp. 120-131, Feb. 2002.

Exciton Coupled Surface Plasmon Resonance Biosensor

M. Bora, M.A. Baldo
Sponsorship: ISN

The development of portable and cost-effective biological sensors promises benefits to medical care, pharmaceutical testing, and the detection of biological warfare agents. Electronic devices are compact and readily integrated into microfluidic substrates, making them a promising alternative to today's bio-detection requirements. Our sensor design aims to exploit the sensitivity of surface plasmon resonance (SPR). Unlike conventional SPR sensors, the plasmon is detected in the near field using a thin film organic photovoltaic (PV). High absorption coefficients make organic semiconductors ideal candidates for the detection of surface plasmons. Organic materials are also easily deposited on microfluidics, enabling use of these devices outside the laboratory environment in a convenient portable package.

In the initial demonstration, plasmon modes are excited in the top surface of the gold cathode by a p-polarized laser beam, when the horizontal component of the light wavevector matches the plasmon wavevector [1]. The plasmon is absorbed by the organic semiconductor and split into holes and electrons at the interface between the donor and acceptor layers composing the PV cell (Figure 1). The plasmon resonance measured indirectly as reflected power and photocurrent (Figure 2) has a strong angular location dependence on the adjacent layer's dielectric constant that is altered upon binding of bio-molecular species. The steep slope of the resonance enables sensitive detection as well as measurement of kinetic parameters of the binding event.



▲ Figure 1: Device structure for biosensor. An organic photovoltaic cell converts the plasmon excitation resonance into photocurrent, resulting in direct probing of the environment above the top surface of the gold cathode.

▲ Figure 2: Plasmon resonance conversion to photocurrent. A dip in reflectivity above the total internal reflection angle of 43° corresponds to a proportional increase in photocurrent.

REFERENCES

[1] J.K. Mapel, K. Celebi, M. Singh, and M.A. Baldo, "Plasmonic excitation of organic double heterostructure solar cells," *Applied Physics Letters*, vol. 90, no. 12, pp. 121102:1-3, Mar. 2007.

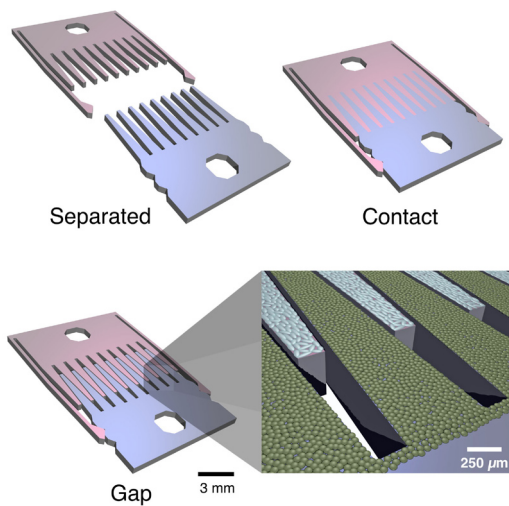
Micromechanical Substrates for Reconfigurable Cell Culture

E. Hui, S.N. Bhatia
Sponsorship: NIH NIDDK

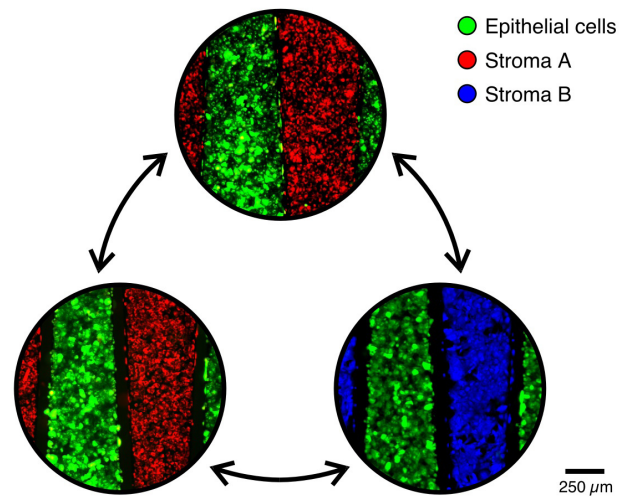
We have previously demonstrated the use of microfabricated cell culture substrates (Figure 1) to implement reconfigurable cell culture (Figure 2) [1]. Specifically, we studied interactions between liver hepatocytes and supportive stromal cells. We found that preservation of liver-specific function depended on signaling from the stroma. Specifically, signaling both through direct contact and through diffusible secreted factors was important. However, while the secreted factors needed to be maintained for the entire duration of culture (2 weeks), direct contact was required only for an 18-hour period early in culture. In addition, the secreted factors were found to have a limited effective range of less than 400 μm .

Through FEM diffusion modeling, we showed that a half-life on the order of hours would result in such short-range signaling.

Currently, we are exploring the use of this platform in a variety of applications including identification of the signaling factors in hepatocyte co-culture, stabilizing liver endothelial cells in culture, toxicity models for drug testing, preconditioning of hepatocytes prior to encapsulation in a 3D gel, and patterning cells directly on the combs to study contact signaling mechanisms.



▲ Figure 1: Micromechanical substrate is composed of two parts that may be locked together with the fingers in contact or separated by a narrow gap of 80 μm . Switching between these states modulates interactions between cells adhered to the top surface of the fingers.



▲ Figure 2: Fluorescent microscopy of dyed cells on the comb substrates, illustrating the various manipulations possible. Cell populations can be brought into and out of contact with each other. A single population can also be swapped out and replaced.

REFERENCES

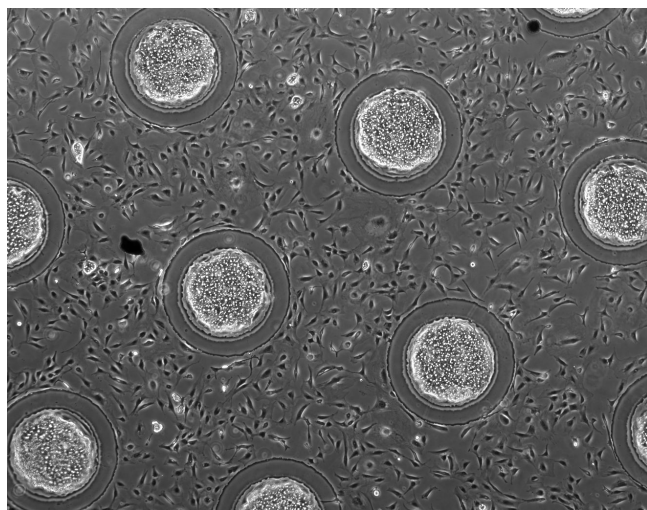
- [1] E.E. Hui and S.N. Bhatia, "Micromechanical control of cell-cell interactions," in *Proceedings of the National Academy of Sciences of the United States of America*, vol. 104, no. 14, Apr. 2007, pp. 5722-5726.

Aligned Multimask Patterning of Biomolecules and Cells

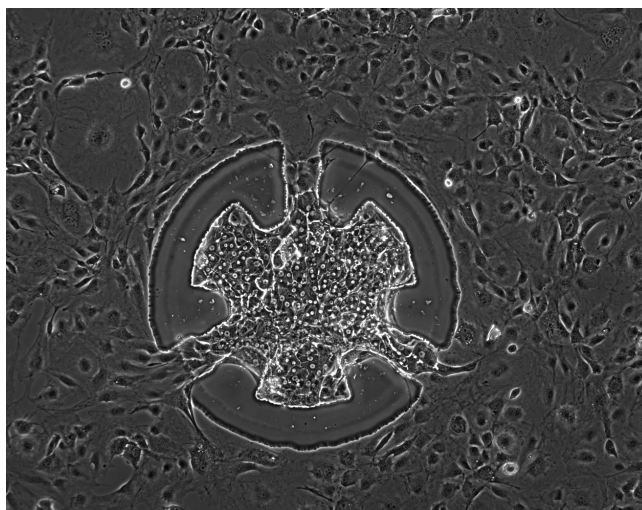
E. Hui, S.N. Bhatia
Sponsorship: NIH NIDDK

Surface engineering of cell culture substrates has developed into a powerful tool for controlling multicellular organization at the micrometer scale. This new capability has brought valuable insight into the biological mechanisms by which the cellular micro-environment determines cell fate and function. However, studies requiring more complex tissue structures have been hindered by limitations in surface patterning. Typically, molecules that mediate cell attachment are patterned against a non-adhesive background, allowing arrays of a single cell type to be formed with control of cell positioning and relative spacing. Alternatively, patterns composed of two different adhesive regions can be employed to form patterned co-cultures of two different cell types, as long as one cell type selectively attaches to a specific region. However, there have been a few examples where multiple attachment chemistries have been successfully combined with non-adhesive surfaces in a multicomponent pattern. This has prevented the realization of configurations in which cell-cell contact and spacing between *different* cell types are controlled.

The use of photolithography with multiple aligned masks is well established for generalized multicomponent patterning, but it is often too harsh for biomolecules. We report a two-mask photolithographic process that is tuned to preserve bioactivity in patterns composed of covalently coupled polyethylene glycol (PEG), adsorbed extracellular matrix protein (e.g., collagen I), and adsorbed serum proteins (e.g., vitronectin). Thereby, we pattern two cell types—primary hepatocytes and 3T3 fibroblasts—demonstrating control over contact and spacing (20-200 μm) between the two cell types for over one week. This method is applicable to the study of intercellular communication in cell biology and tissue engineering.



▲ Figure 1: Hepatocyte islands isolated from surrounding fibroblast support cells by “moats” of PEG-disilane. The moats prevent contact interactions between the two cell types, while preserving communication via diffusible secreted factors.



▲ Figure 2: A closer view of an alternative configuration. Here, the moat is discontinuous in 3 locations. These “bridges” allow local contact at specific points of the hepatocyte island, while contact remains prevented over the rest of the island.

REFERENCES

- [1] E.E. Hui and S.N. Bhatia, “Microscale control of cell contact and spacing via three-component surface patterning,” *Langmuir*, vol. 23, no. 8, pp. 4103-4107, Apr. 2007.

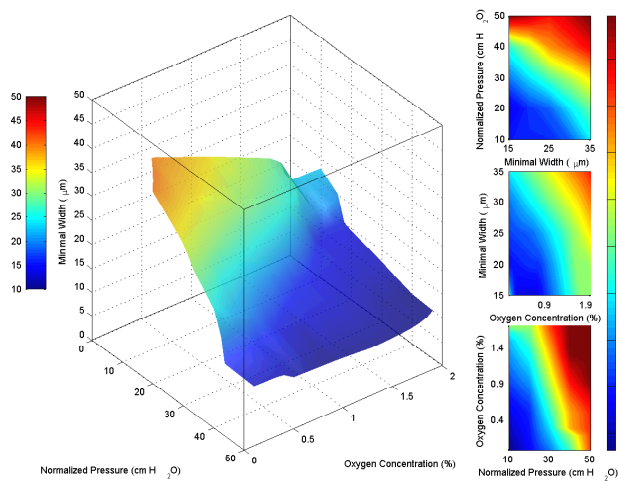
Collective Hydrodynamics and Kinetics of Sickle Cell Vaso-occlusion and Rescue in a Microfluidic Device

D.T. Eddington, J.M. Higgins, L. Mahadevan, S.N. Bhatia
Sponsorship: NIH

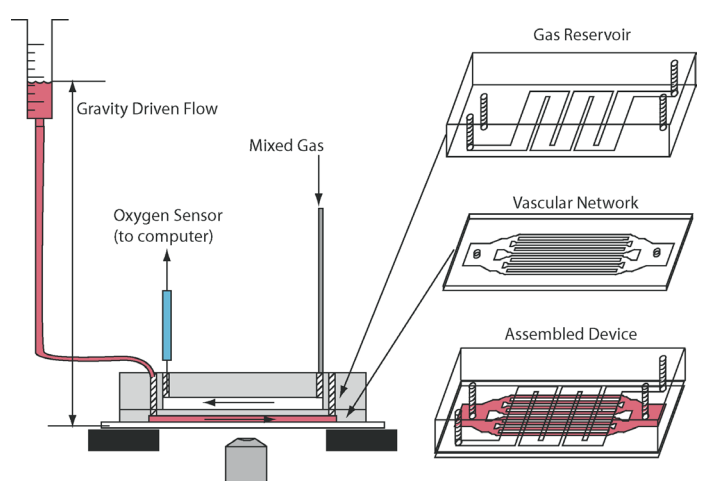
The pathophysiology of sickle cell disease, the first to be implicated with a genetic origin, is complicated by the multi-scale nature of the processes that link the molecular genotype to the organismal phenotype. Here, we show that it is possible to evoke, control and inhibit the vaso-occlusive crisis event in sickle cell disease using an artificial microfluidic environment. We use a combination of geometric, physical, chemical and biological means to quantify the phase space for the onset of a jamming crisis, as well as its dissolution, as shown in Figure 1.

The microfluidic chip designed to independently vary the various parameters that control the onset of vaso-occlusion in a sickle cell crisis is shown in Figure 2. This device allows us to dissect and probe the hierarchical dynamics of this multi-scale process by manipulating the geometrical, physical, chemical and biological determinants of the process. The chip consists of a series of bifurcating channels of varying diameters that grossly mimics the geometry of vasculature. By controlling the physical pressure

gradient across the chip, we can vary the kinetic time scale for transit of red blood cells. The channels are separated from a gas reservoir by a thin gas-permeable polydimethylsiloxane (PDMS) membrane. As the geometries are microscopic, gas diffusion is rapid and the oxygen concentration in the microchannels is governed by the concentration in the gas reservoir. By changing the mixture of this reservoir, we control oxygen concentrations in the channels and hence the onset of microscopic hemoglobin polymerization. By using blood with varying concentrations of HbS and different hematocrits, we can mimic the variability among individuals. This device was used to study the phase space of jamming governed by pressure, channel dimensions and oxygen concentration as shown in Figure 1. Our experimental study integrates the dynamics of collective processes at the molecular, polymer, cellular and multi-cellular level; lays the foundation for a quantitative understanding of the rate limiting processes; provides a potential tool for optimizing and individualizing treatment; and serves as a bench test for dynamical drugs.



▲ Figure 1: Phase space of vaso-occlusion. The colored surface represents a fitted hypersurface in 4-dimensional space: width, pressure, oxygen concentration, and occlusion time. The isosurface was computed from 43 data points using Delaunay triangulation. All points on the hypersurface correspond to triples of height, pressure, and oxygen concentration where the fitted time to occlusion was 500 seconds. The color of each point on the surface characterizes the minimal width in the device and is redundant with the point's vertical (width) coordinate. The filled contour plots represent slices through the fitted volume at specific planes (top: oxygen concentration = 0.5%, middle: normalized pressure = 20 cm H₂O, bottom: minimal width = 25 μm). This phase space describes the behavior of patients whose samples contained hemoglobin S concentrations of at least 65% (mean 86%, standard deviation 6.7%).



▲ Figure 2: Fabrication and schematic of the device. The oxygen channels and vascular network were fabricated in separate steps. After removal of the device from the SU8 mold master, holes were cored and networks were bonded via oxygen plasma activation and then attached to a glass slide. The widest cross section in the vascular network on the left and right of the device is 4 mm x 12 μm. The vascular network then bifurcates, maintaining a roughly equal cross-sectional area. An open 5 mL syringe was connected to the device and raised and lowered to increase or decrease the flow rates through the device. The gas channels were connected to two rotometers regulating the ratio of 0% and 10% oxygen in the gas mixture that was fed into the device. The outlet of the gas network had an oxygen sensor to validate the oxygen concentration in the microchannels.

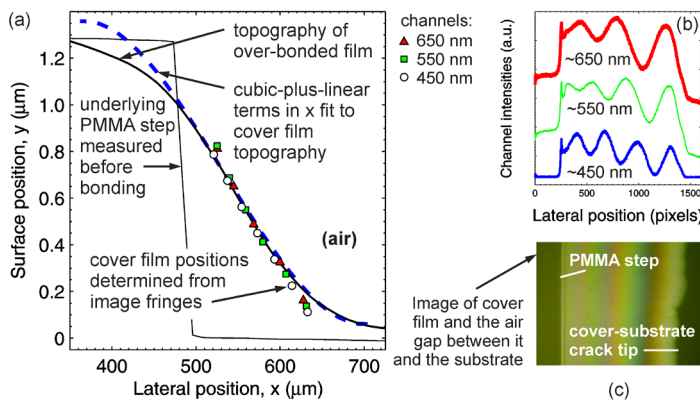
Plasma-activated Inter-layer Bonding of Thermoplastics for Micro- and Nano-fluidic Manufacturing

H.K. Taylor, M. Dirckx, D.S. Boning
Sponsorship: Singapore-MIT Alliance

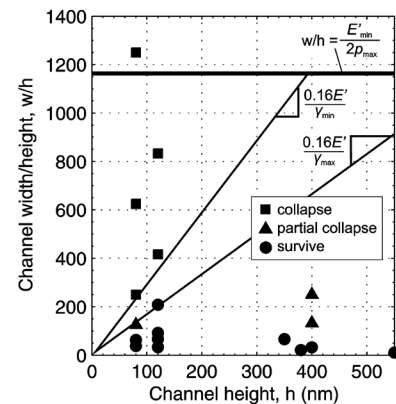
Plasma-activated polymer–polymer bonding is a promising way of encapsulating micro- and nano-fluidic channels across large substrate areas, without the substantial distortion of channel geometries that can plague thermally- and solvent-assisted bonding. The process involves treating the surfaces to be bonded with an oxygen or air plasma, and then pressing the surfaces together to allow an irreversible chemical bond to form [1]. A convenient method is desired for measuring the toughness of such a bonded interface. Simple crack-opening tests (whereby a blade prizes apart the two bonded layers and the length of the inter-layer crack determines the bond toughness [2]) are clumsy and hard to automate. We propose that built-in microscopic crack-opening test sites be distributed across manufactured substrates [3]. At each test site, a polymeric film bonded over a step in the substrate would peel back from the step after bonding, by a distance depending on the toughness of the bond. The presence of a wedge-shaped air gap between the covering film and the substrate leads to visible interference fringes, the spacing of which can be used to extract the bond strength (Figure 1). Arrays of these *in situ*

cracks might be imaged without removing the substrate from a production line and would allow us to monitor both substrate-to-substrate and cross-substrate bond toughness variation.

Bond toughness and polymer layers' surface energies are of particular relevance in planning the fabrication of very shallow fluidic channels whose widths, w , are much larger than their depths, h . The risk of channels' collapsing during fabrication must be controlled. For channels with $h \sim 1 \mu\text{m}$ or less that are fabricated with thermoplastics, we expect collapsing to occur through local deformation of the surrounding material rather than through plate-like bending of the cover plate [4]. Our analysis suggests that the pressure applied during bonding, together with the polymer–polymer interface energies that exist before and after plasma-activated bonding, will delineate, on a w/h against h plot, regions in which collapsing will and will not occur. We have demonstrated nanochannels fabricated from polymethylmethacrylate (PMMA) that are 80 nm deep and 10 μm wide and other channels that are 110 nm deep and 20 μm wide (Figure 2).



▲ Figure 1: Results from a prototype bond toughness measurement feature. The topography of the film covering one side of a PMMA ridge (a) is determined with white-light interferometry (black line); a cubic-plus-linear function of the lateral position has been fit to the film topography, showing good agreement with an analytical small-deflections model of the cover plate. Symbols indicate the varying height of the air gap between substrate and cover film, obtained by interpreting a color interference image of the sample (c). The average red, green, and blue intensities present in the image are plotted (b) above the image.



▲ Figure 2: The PMMA nanochannel fabrication results. Our analysis suggests that provided $w/h < E'/2p$ (where E' is the plate modulus and p is the pressure applied during bonding), channel collapsing is determined by the channel dimensions, the material's stiffness, and the surface energy change γ that occurs when a polymer–polymer interface is reversibly formed or broken. Possible lines separating regions of collapsed and intact channels are suggested; many more channel sizes need to be tested to map the w/h – h space confidently.

REFERENCES

- [1] L. Brown, T. Koerner, J.H. Horton, and R.D. Oleschuk, "Fabrication and characterization of poly(methylmethacrylate) microfluidic devices bonded using surface modifications and solvents," *Lab on a Chip*, vol. 6, pp. 66–73, Jan. 2006.
- [2] W.P. Maszara, G. Goetz, A. Caviglia, and J.B. McKittrick, "Bonding of silicon wafers for silicon-on-insulator," *Journal of Applied Physics*, vol. 64, pp. 4943–4950, Nov. 1988.
- [3] R.D. Horning, D.W. Burns, and A.I. Akinwande, "A test structure for bond strength measurement and process diagnostics," in *Proc. 1st International Symposium on Semiconductor Wafer Bonding: Science, Technology and Applications*, 1992, pp. 386–393.
- [4] Q.-Y. Tong and U. Gösele, *Semiconductor Wafer Bonding: Science and Technology*. New York: Wiley, 1999.

Environmentally Benign Manufacturing of Three-dimensional Integrated Circuits

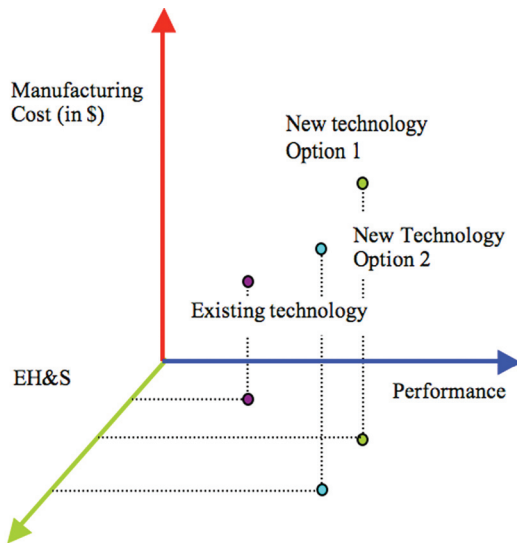
A. Somani, D.S. Boning

Sponsorship: SRC/SEMATECH Engineering Research Center for Environmentally Benign Semiconductor Manufacturing

Along with scaling down in size, novel materials have been introduced into the semiconductor industry to enable continued improvements in performance and cost as predicted by Moore’s law. It has become important now more than ever to include an environmental impact evaluation of future technologies, before they are introduced into manufacturing, in order to identify potentially environmentally harmful materials or processes and understand their implications, costs, and mitigation requirements. In this project we introduce a methodology to compare alternative options on the environmental axis, along with the cost and performance axes, in order to create environmentally aware and benign technologies. This methodology also helps to identify potential performance and cost issues in novel technologies by taking a transparent and bottoms-up assessment approach.

This methodology is applied to the evaluation of the MIT 3D IC technology in comparison to a standard CMOS 2D IC approach. Both options are compared on all three axes—performance, cost, and environmental impact. The “handle wafer” unit process in

the existing 3D IC technology, which is a crucial process for back-to-face integration, is found to have a large environmental impact because of its use of thick metal sacrificial layers and high-energy consumption. We explore three different handle wafer options: between-die channel, oxide release layer, and alternative low-temperature permanent bonding. The first two approaches use a chemical handle wafer-release mechanism while the third explores solid liquid inter-diffusion (SLID) bonding using copper-indium at 200°C. Preliminary results for copper-indium bonding indicate that a sub-micron thick multi-layer copper-indium stack, when bonded to a 300-nm-thick copper film, results in large voids in the bonding interface primarily due to rough as-deposited films. Finally, we conduct an overall assessment of these and other proposed handle wafer technologies. The overall assessment shows that none but the oxide release layer approach appears promising; however, each process option has its strengths and weaknesses, which need to be understood and pursued accordingly.



▲ Figure 1: Three axes to manufacturing: Cost, performance and EH&S impact. Emerging silicon technologies can be mapped into three-dimensions for environmentally conscious technologies.

	Al Release Layer	Between-die Channel	Smart Cut	Oxide Release Layer
Performance	✘	✓	✓	●
Cost	✘	●	✘	✓
Environmental Impact	✘	✘	✓	●

▲ Table 1: Demonstration of integrated assessment of handle wafer options. A ✓ indicates acceptable, and a ● indicates further work is required, while ✘ indicates that an area of high concern. The oxide release layer approach has no ✘, which makes it most appropriate.

REFERENCES

- [1] A. Somani, “Environmentally benign manufacturing of three-dimensional integrated circuits,” PhD thesis, Massachusetts Institute of Technology, Cambridge, MA, 2007.

An Implantable MEMS Drug-delivery Device

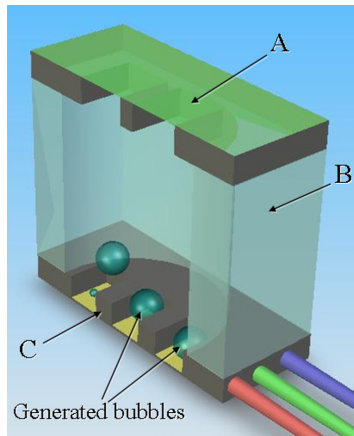
H.L. Ho Duc, N. Elman, M.J. Cima
Sponsorship: ARO, ISN

A novel drug-delivery system based on MEMS technology is being developed. This implantable microchip is capable of delivering vasopressin, a known vasoconstrictor that can prevent or delay death by hemorrhagic shock [1]. The device is specially tailored to treat hemorrhagic shock in ambulatory settings and is intended for *in vivo* use as a micro-implant in the peritoneum for people in high-risk situations.

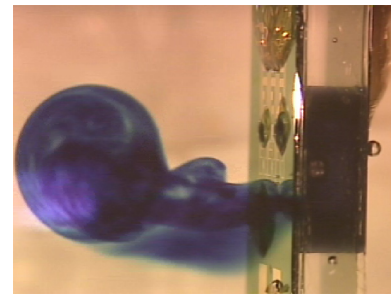
The device has a modular design and is composed of three layers (shown schematically in Figure 1): a large reservoir layer, where the drug solution is stored; a membrane layer from where the drug is ejected; and a bubble-generating layer, where bubbles are formed. The reservoir layer is defined by drilling through a Pyrex 7740 wafer with a diamond bit. Wafer thickness and hole diameter can be modified to change reservoir capacity. The membrane layer is composed of silicon nitride membranes cover-

ing through-holes etched by DRIE into a silicon substrate. Thin gold fuses can be patterned on the membranes to detect ruptures, which then shows as an open circuit. The bubble-generating layer is defined by micro-resistors, which can quickly and locally heat the contained fluid to generate bubbles. The pressure exerted by these bubbles causes rupture of the silicon nitride membranes and forces the contained solution out of the device.

In vitro operation of the device has been demonstrated, as shown in Figure 2. Further developments of this device include reduction of power consumption during activation, wireless activation, and adaptation of the device for a pen-size, transdermal delivery system. We believe that the ramifications of this MEMS-based drug delivery system can be useful for a vast number of medical applications.



▲ Figure 1: Schematic representation of drug delivery system with (A) membrane layer, (B) reservoir layer containing the drug solution and (C) bubble-generating layer.



▲ Figure 2: *In vitro* release of methylene blue solution from the drug delivery system.

REFERENCES

- [1] W. Voelckel, C. Raedler, V. Wenzel, K. Lindner, A. Krismer, C. Schmittinger, H. Herff, K. Rheinberger, and A. Konigsrainer, "Arginine vasopressin, but not epinephrine, improves survival in uncontrolled hemorrhagic shock after liver trauma in pigs," *Critical Care Medicine*, vol. 31, no. 4, pp. 1160-1165, Apr. 2003.

High Speed Three-dimensional Scanner for *in vivo* Non-invasive Optical Biopsy using Two-photon Microscopy

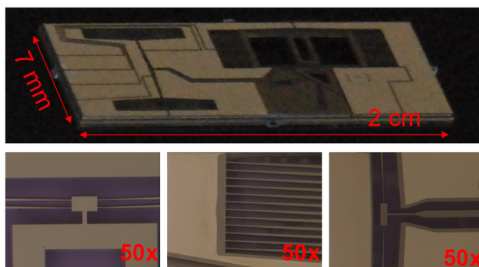
S.-C. Chen, H. Choi, P.T. So, M.L. Culpepper
Sponsorship: NIH

We have recently demonstrated the modeling, design, and micro-fabrication process of a millimeter-scale, high-speed endoscopic scanner that is to be integrated at the distal end of an endomicroscope [1]. The scanner system consists of (1) an active Silicon optical bench (SOB), as shown in Figure 1, which constrains, aligns, and thermally actuates (1) mm-size optics (GRIN lens and prism) at 5 Hz and (2) a slim fiber resonator that excites the double-clad photonic bandgap fiber at ~ 1 kHz. The scanner system has a 7-millimeter device envelope with a range of 100 micrometers in X, Y and Z. The design of a two-photon endoscope requires scanning of focused light to create tissue images, and scanning actuator technology still proves to be a bottleneck for practical endoscope design. The performance (force-speed-stroke) criteria for the prototype endomicroscope design are generated based on clinical needs. The strict force, speed, and stroke requirements (~ 10 mN, 1 kHz, and 100 μm) call for a new method for actuation. The low voltage requirement for future *in vivo* examination/operation makes a new class of thermomechanical actuators (TMAs) a suitable candidate among other micro-actuation technologies.

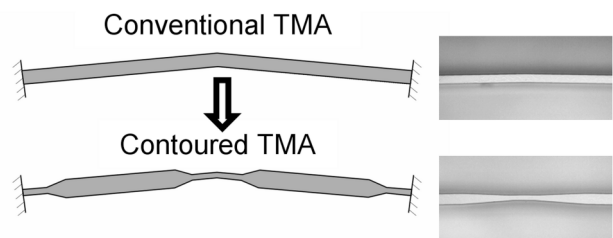
The two-photon imaging technique requires scanning of focused light to create tissue images. The endoscopic scanner may enable the design and construction of a miniaturized two-photon microscopic system to image the surface and sub-surface cells (up to 200 microns depth) of internal tissues with sub-cellular resolution. The two-photon endomicroscope is designed to perform non-invasive, *in vivo*, optical biopsy, which has numerous benefits

over excisional biopsy. For example, non-invasive optical screening may decrease the number of excision biopsies required, and optical biopsy can provide more informed selection of excisional biopsy sites, minimizing incorrect diagnosis due to random sampling. This is useful for detecting cancer at an early stage among other diseases.

The chevron TMAs on the SOB are optimized through the geometric contouring method [2] to provide enhanced force, displacement and reduced power consumption compared to common chevron actuators. This also allows the TMAs to be operated at lower temperature and thus makes the TMAs more suitable for precision actuation. Figure 2 presents an example of a contoured chevron TMA. Early models and experiments of the contour shaping method have confirmed that the maximum achievable thermal strain of a driving beam may be increased by 29%, the actuator stroke may be increased by a factor of 3 or more, and identical force or displacement characteristics may be achieved with 90% reduction in power. A new high-speed pulsing technique has also been investigated recently; it enhances the dynamic performance of the contoured TMAs [3]. Preliminary simulation results indicate a 12% bandwidth increase, 30% stroke enhancement, and 70% power reduction. This technique, together with the geometric contouring method for TMAs, may potentially increase the bandwidth of the endoscopic scanner by a factor of 10 and therefore meet the functional requirements for a two-photon scanning endomicroscope.



▲ Figure 1: Silicon optical bench with integrated contoured TMAs and flexural bearings that generates linear and rotary motions.



▲ Figure 2: Example of a conventional and contoured chevron TMAs.

REFERENCES

- [1] S. Chen, H. Choi, D. Kim, L. Munro, M.L. Culpepper, and P.T. So, "Design of a high-speed, micro-scale fast scanning stage for two-photon endomicroscopy," *Proceedings of the Annual Meeting of the ASPE*, Monterey, CA, Oct. 2006, pp. 279 – 282.
- [2] S. Chen and M.L. Culpepper, "Design of contoured microscale thermomechanical actuators," *Journal of Microelectromechanical Systems*, vol. 15, no. 5, pp. 1226 – 34, Oct. 2006.
- [3] S. Chen and M.L. Culpepper, Massachusetts Institute of Technology, "High-speed pulsing technique for non-uniform heat generation thermal system," MIT Technology Disclosure, filed Apr. 2007.

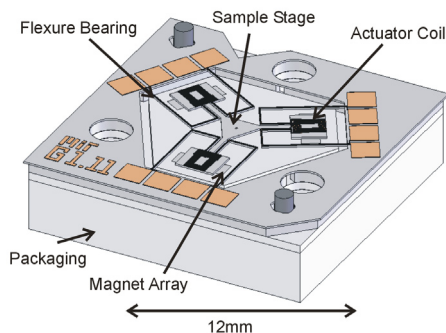
Electromagnetically-driven Meso-scale Nanopositioners for Nano-scale Manufacturing and Measurement

D. Golda, M.L. Culpepper
Sponsorship: NSF, NIH

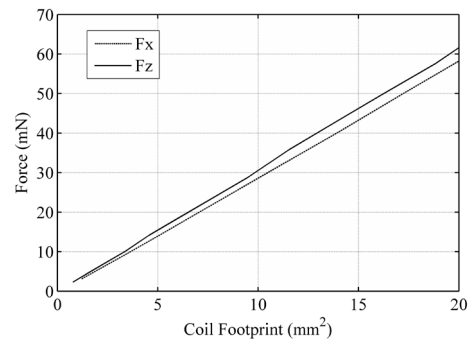
Nanopositioners – be they nano-, micro-, or macro-scale in physical size – enable us to move large or small parts with nanometer-level or better precision. They therefore set the limits on our ability to measure, understand, manipulate, and affect physical systems. Six-axis small-scale nanopositioners enable a combination of faster speed and better resolution. They are therefore important in scientific and commercial applications where speed and small-dimensions are important: biological sciences, data storage and nanomanufacturing equipment and instruments [1-4]. Emerging applications in these fields will benefit from portable, multi-axis nanopositioners that are capable of nanometer-level positioning over tens-of-microns at speeds of hundreds to thousands of Hertz. Toward this end, our work aims to create a meso-scale, high-speed, six-axis nanopositioner.

The nanopositioner is designed to operate with a range-of-motion of larger than 10 micrometers in the X-, Y- and Z- directions, possess a natural frequency of 1 kHz, and exhibit better-

than-10-nm resolution. The nanopositioning system, shown in Figure 1, is composed of three sets of micro-actuators. Within each set, micro-coils are suspended above a linear array of 1 mm³ permanent magnets via a silicon flexure system [5]. Each actuator is composed of two independent coils that apply in-plane and out-of-plane forces to the flexure. The actuator inputs are combined to control the stage position in six axes. Figure 2, which shows the actuator's force output capability vs. coil footprint, was generated using a numerical model. The micro-coils consist of two stacked copper micro-coils that are electrically isolated by a layer of silicon dioxide. They are created by electroplating copper within silicon and photoresist molds. The flexures are etched using deep reactive-ion etching. The system will be applied to the high-speed and precise positioning of small parts such as probes and thin-films. The system is scheduled to be integrated into a bench-top scanning-probe microscope and within a nano-electro-discharge machining station [4].



▲ Figure 1: Solid model representation of the proposed meso-scale nanopositioner that shows the permanent magnets, microfabricated silicon flexures, and copper coils.



▲ Figure 2: Maximum in-plane (Fx) and out-of-plane (Fz) actuator forces vs. micro-coil footprint. The micro-coils used in the nanopositioner are designed with a footprint of 4 mm², resulting in a maximum output force of 10 mN.

REFERENCES

- [1] H. Rothuizen, U. Drechsler, G. Genolet, W. Haberle, M. Lutwyche, R. Stutz, R. Widmer, and P. Vettiger, "Fabrication of a micromachined magnetic X/Y/Z scanner for parallel scanning probe applications," *Microelectronic Engineering*, vol. 53, pp. 509-512, June 2000.
- [2] H. Rothuizen, M. Despont, U. Drechsler, G. Genolet, W. Haberle, M. Lutwyche, R. Stutz, and P. Vettiger, "Compact copper/epoxy-based electromagnetic scanner for scanning probe applications," in *Proc. 15th IEEE International Conference on Micro Electro Mechanical Systems MEMS*, Las Vegas, NV, Jan. 20-24 2002, pp. 582-585.
- [3] A. Pantazi, M.A. Lantz, G. Cherubini, H. Pozidis, and E. Eleftheriou, "A servomechanism for a micro-electromechanical-system-based scanning-probe data storage device," *Nanotechnology*, vol. 15, no. 10, pp. 612-621, Oct. 2004.
- [4] A.P. Malshe, K. Virwani, K.P. Rajurkar, and D. Deshpande, "Investigation of nanoscale electro machining (nano-EM) in dielectric oil," presented at *55th CIRP General Assembly*, Antalya, Turkey, 2005.
- [5] D. Golda and M. L. Culpepper, "Two-axis electromagnetic moving-coil micro-actuator," in *Proc. ASME International Mechanical Engineering Congress and Exposition*, Chicago, IL, Nov. 5-10 2006.

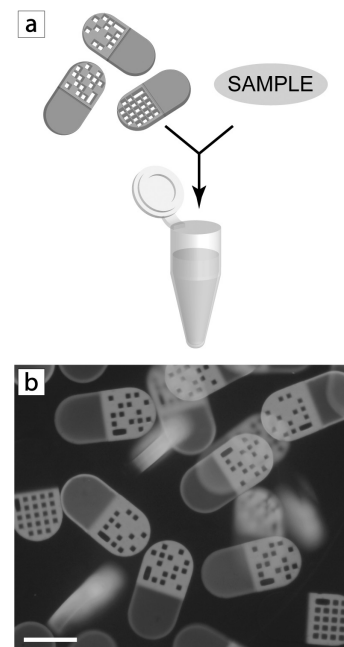
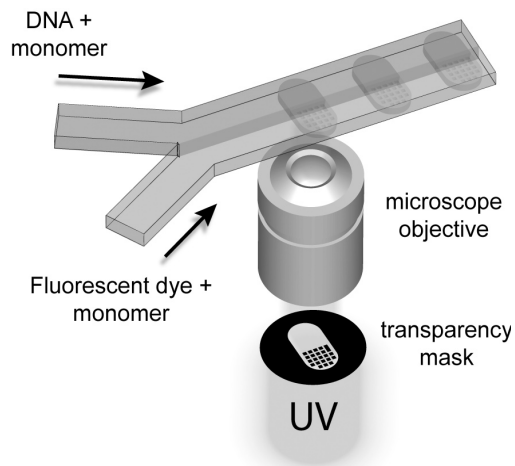
Barcoded Microparticles for Multiplexed Detection

D. Pregibon, M. Toner, P.S. Doyle
Sponsorship: NSF

The detection of multiple targets in a single sample is important for many applications, including medical diagnostics, genotyping, and drug discovery. The current approaches to multiplexing, such as planar arrays (such as DNA microarrays) and suspension (particle-based) arrays, require expensive or cumbersome means of encoding, decoding, or functionalizing substrates. Currently, commercially available approaches for multiplexed analysis are cost-prohibitive for high sample throughput, low-cost applications such as bedside diagnostics.

We have developed a method [1], based on multifunctional barcoded particles, for the sensitive and accurate multiplexed detection of biomolecules. Our method is unique in that (1) we can fabricate, encode, and functionalize particles in a single step, (2) the particles are composed of poly(ethylene glycol) hydrogel to

increase both sensitivity and specificity, and (3) only a single fluorescent wavelength is required to decode the particles and quantify the corresponding targets. Using an efficient one-step method based on continuous-flow lithography, we synthesize microparticles with multiple functional regions (Figure 1). Each particle bears a fluorescent dot-pattern barcode (capable of providing over a million unique codes) to identify the target(s) it is looking for and one or more spatially separated regions containing a probe where those targets can bind and be detected via fluorescence. In this way, particles from a library can be mixed and incubated in a single sample to simultaneously detect many targets, such as DNA oligomers (Figure 2). The detection of targets is not only sensitive but also extremely specific due to the porous and bio-inert nature of the hydrogel structure that allows target molecules to diffuse and bind deep into the transparent particle surfaces.



▲ Figure 1: Schematic of one-step particle synthesis in a microfluidic device. Two monomer streams (one with a DNA probe and the other with a fluorescent dye) are flowed adjacently along a channel where they are repeatedly hit with burst of UV light shone through a microscope objective.

▲ Figure 2: (a) Schematic of multiplexed sample analysis. Particles (with unique barcodes corresponding to their target) are mixed and incubated in a single sample. (b) Fluorescence image of particles after incubation with DNA oligomers targets. Positive detection is indicated by fluorescence in the probe-region of the particles. Scalebar = 100 μm .

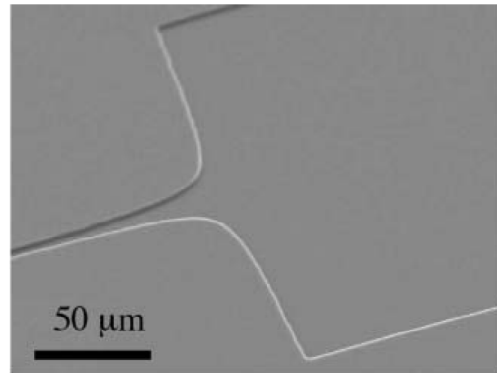
REFERENCES

[1] D.C. Pregibon, M. Toner, and P.S. Doyle, "Multifunctional encoded particles for high-throughput biomolecule analysis," *Science*, vol. 315, no. 5817, pp. 1393-1396, Mar. 2007.

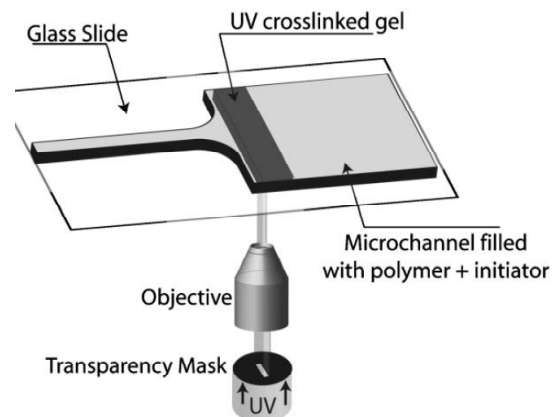
Single-molecule DNA Mapping in a Fluidic Device

J. Tang, G. Randall, P.S. Doyle
Sponsorship: NSF

The ability to controllably and continuously stretch large DNA molecules in a microfluidic format is important for gene-mapping technologies such as Direct Linear Analysis (DLA). We have recently shown that electric field gradients can be readily generated in a microfluidic device and the resulting field is purely elongational. We have performed a single-molecule fluorescence microscopy analysis of T4 DNA (169 kbp), stretching in the electric field gradients in a hyperbolic contraction microchannel. In addition, we are able to selectively pattern a crosslinked gel anywhere inside the microchannel. With an applied electric field, DNA molecules are forced to reptate through the gel and they stretch moderately as they exit the gel. By placing a gel immediately in front of the hyperbolic contraction, we bypass “molecular individualism” and achieve highly uniform and complete stretching of T4 DNA. This device offers a new method to efficiently stretch DNA for single-molecule mapping studies.



▲ Figure 1: An SEM image of a PDMS hyperbolic channel.



▲ Figure 2: Schematic diagram of the method used to create a gel filter just before the hyperbolic contraction.

REFERENCES

[1] G.C. Randall, K.M. Schultz, and P.S. Doyle, “Methods to electrophoretically stretch DNA: Microcontractions, gels, and hybrid gel-microcontraction devices,” *Lab on a Chip*, vol. 6, no. 4, pp. 516-525, Mar. 2006.

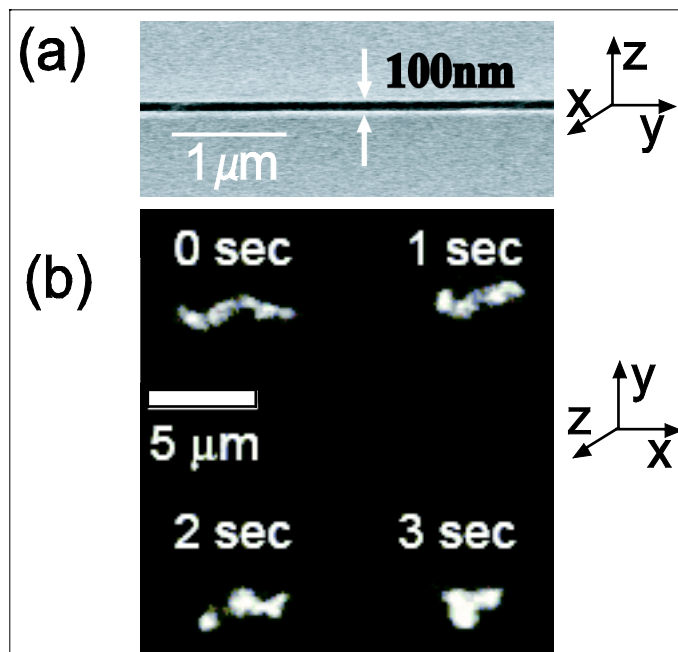
DNA Dynamics in Nanofluidic Devices

A. Balducci, C.-C. Hsieh, P.S. Doyle

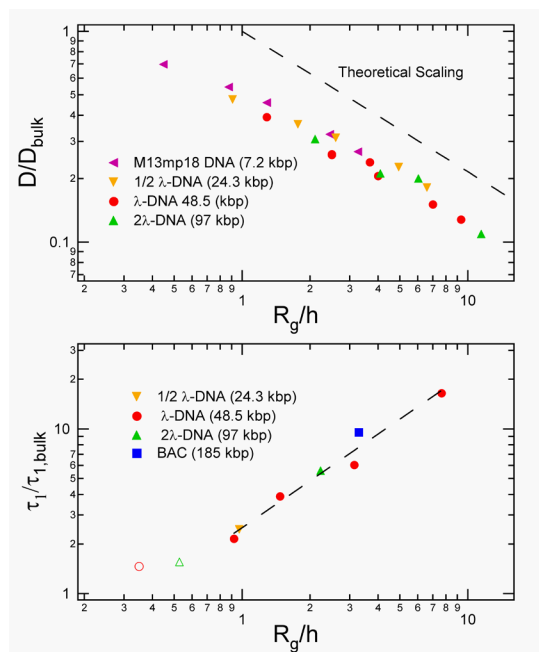
In dilute polymer solutions, the shape, motion, dynamic response, and solvent-interaction (HI) of single polymer molecules change when geometric constraints reach the length scales of the equilibrium polymer conformation. Our study seeks to understand these changes using double-stranded DNA as a model polymer and to utilize these confinement effects to tune the dynamic response of single molecules. This ability is useful in processes that rely on controlling the conformation of a biomolecule for analysis [1] or in the manipulation of molecules for separations and/or reactions

Our experiments [2-3] use thermally-bonded pyrex channels with heights ranging from 75 to 500 nm and widths of 150 μm . The Brownian motion of stained DNA molecules is observed using epi-fluorescence microscopy. By following the time evolution

of the center-of-mass and orientation of single molecules, we can obtain the diffusion coefficient (D) and longest relaxation time (τ_1) of the polymer independently. We find that scalings with molecular weight of both D and τ_1 agree with a free-draining polymer model, indicating that, in contrast to bulk solution, HI is not important in slit confinement at length scales comparable to the size of the molecule. We find that the relaxation time of the polymer increases with confinement, which promises easier manipulation of DNA conformations. Our results in well-defined nanofluidic devices may also provide insight into polymer behavior in the less-controlled confinement that occurs in concentrated polymer solutions. We are currently working to stretch DNA in confinement and to study the effects of confinement far from the equilibrium conformation of the polymer



▲ Figure 1: (a) An SEM micrograph of a 100-nm-tall channel. (b) Time-series images of a single 97-kbp DNA molecule undergoing Brownian motion in a 500-nm-tall channel.



▲ Figure 2: Variables D and τ_1 normalized by their bulk values versus a measure of confinement (equilibrium radius divided by gap height) for DNA molecules of varying molecular weight.

REFERENCES

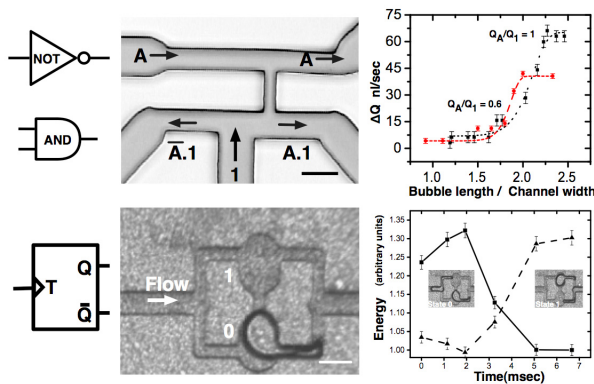
- [1] E.Y. Chan, N.M. Goncalves, R.A. Haeusler, A.J. Hatch, J.W. Larson, A.M. Maletta, G.R. Yantz, E.D. Carstea, M.Fuchs, G.G. Wong, S.R. Gullans, and R. Gilmanishin, "DNA Mapping using microfluidic stretching and single-molecule detection of fluorescent site-specific tags," *Genome Research*, vol. 14, no. 6, pp. 1137-1146, June 2004.
- [2] A. Balducci, P. Mao, J. Han, and P.S. Doyle, "Double-stranded DNA diffusion in slitlike nanochannels," *Macromolecules*, vol. 39, no. 18, pp. 623-628, Aug. 2006.
- [3] C.-C. Hsieh, A. Balducci, and P.S. Doyle, "An experimental study of DNA rotational relaxation time in nanoslits," *Macromolecules*, to be published.

Microfluidic Bubble Logic

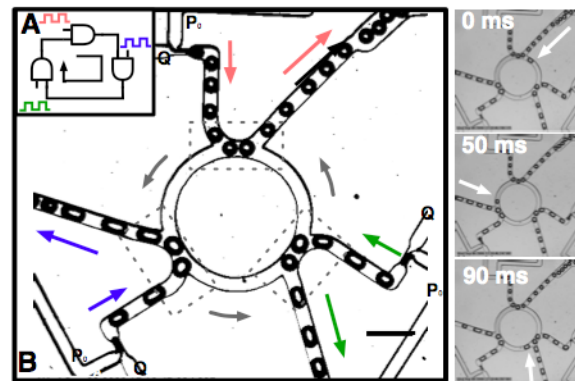
M. Prakash, N. Gershenfeld
 Sponsorship: Center for Bits and Atoms

Large-scale microfluidic integration promises to revolutionize the fields of biology and analytical chemistry. The “Lab-on-a-Chip” community has long sought the ability to precisely control very small volumes (nanoliters) of fluid packets. Current mechanisms for fluid routing depend on external control elements with no feedback, limiting scalability and integration. In [1] we describe Bubble logic, an all-fluidic universal logic family implemented in a two-phase microfluidic system. The presence or absence of a drop or a bubble represents a bit of information. Non-linear hydrodynamic interactions of these elements in microfluidic geometries are exploited to build logic gates (AND, NOT), bistable memory (toggle flip-flop), ring oscillators, ripple counters, and synchronizers. This provides an on-chip internal flow control mechanism with all the properties of a digital logic family including gain, bistability, cascadability, feedback and synchronization. Since no external control elements are required, bubble logic can also find applications in diagnostic instrumentation in resource-poor settings, controlled drug delivery or computation in harsh settings.

Previous attempts at an all-fluidic computation mechanism used inertial effects (significant only at high Reynolds numbers) or non-Newtonian fluids (like polymer blends). Bubble logic operates at both low Reynolds and capillary numbers, allowing us to reduce length scales further and thus operate in nanoliter or smaller regimes. Figure 1 depicts device geometries for universal AND-NOT logic gate and a toggle flip-flop. The devices are fabricated using soft-lithography in PDMS bonded to glass. Propagation time for the logic gate and toggle flip-flop is ~10ms. Figure 2 depicts a ring oscillator consisting of three AND gates and a delay line with photomicrographs of the device in operation (recorded by a high speed video camera). We are currently working on integrating bubble logic elements to build high-density, random-access chemical memories.



▲ Figure 1: Universal logic and memory. Top row depicts a universal logic gate (AND and NOT) with a plot depicting gain. Bottom row depicts one bit bistable memory, implemented as a toggle flip-flop with a plot of bistability (surface energy) as a bubble traverses the microfluidic geometry. Scale bar ~100 μm .



▲ Figure 2: Microfluidic ring oscillator depicting cascading and feedback. Top inset depicts the schematic with three microfluidic AND gates connected in a ring configuration. Right column depicts a time series of steady state operation of the oscillator at ~10Hz. Scale bar ~200 μm .

REFERENCES

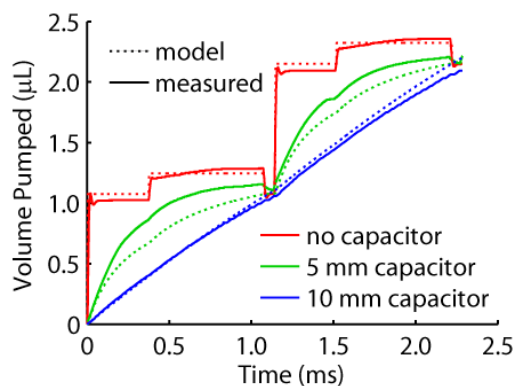
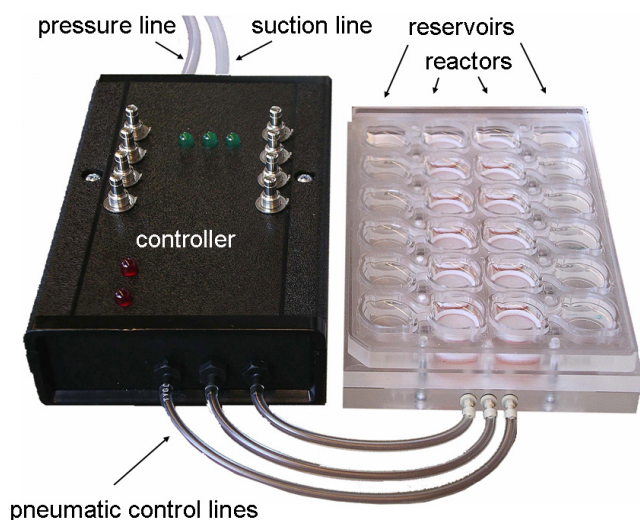
[1] M. Prakash and N. Gershenfeld., “Microfluidic bubble logic”, *Science*, vol. 315, no. 5813, pp. 832 – 835, Feb. 2007.

Perfused Multiwell Tissue Culture Plates for Development of Drug and Disease Models

K. Domansky, W. Inman, J. Serdy, B. Owens, S. Karackattu, J.R. Llamas Vidales, R. Littrel, M.H.M. Lim, L. Vineyard, L.G. Griffith
Sponsorship: DuPont-MIT Alliance, Pfizer, Biotechnology Process Engineering Center

A new platform for three-dimensional hepatic tissue engineering has been developed. It is based on the conventional multiwell tissue culture plate format but it allows the tissue to be continuously perfused with cell culture medium [1]. The new capability is achieved by a microfluidic perfusion system that re-circulates cell culture medium between reactors and reservoir (Figure 1). It features a network of microfluidic valves and pumps integrated into the plate [2]. Flow pulsatility is controlled by fluidic capacitors. In order to measure performance of fluidic capacitors, fluid was pumped through a capillary and a high-speed video camera was used to track the end position of the fluid. Figure 2 compares the performance of measured and modeled capacitors. As predicted by the model, the 10-mm capacitor effectively filters fluid pulses and generates a nearly constant flow. Flow with this characteristic is critical during the initial cell attachment time-period.

Phase contrast and fluorescent imaging, measurement of oxygen consumption, accumulation of taurocholic acid, gene expression profiling, and drug metabolism assays are used to characterize the performance of the 3D perfused cultures. Because the new system features a standard multiwell tissue culture plate footprint, it is readily amenable to numerous high-throughput assays compatible with automated technologies commonly used in pharmaceutical development. The system provides a means to conduct assays for toxicology and metabolism and can be used as a model for human diseases such as hepatic disorders, exposure-related pathologies, and cancer.



▲ Figure 1: Photograph of a 12-microbioreactor array with its electro-pneumatic controller. Cell culture medium is re-circulated between the reactor and reservoir wells. All reactor/reservoir pairs are fluidically isolated from each other.

▲ Figure 2: Comparison of measured capacitor performance to the capacitor model for 5- and 10-mm diameter capacitors and a flow rate of 0.05 mL/min.

REFERENCES

- [1] K. Domansky, W. Inman, J. Serdy, and L. G. Griffith, "Perfused multiwell tissue culture plates with integrated microfluidic system," in *Proc. of Tenth International Conference on Miniaturized Systems for Chemistry and Life Sciences (μ TAS)*, Boston, MA, Nov. 2006, pp. 951-953.
- [2] W. Inman, K. Domansky, J. Serdy, B. Owens, D. Trumper, and L. G. Griffith, "Design, modeling and fabrication of a constant flow pneumatic micro-pump," *Journal of Micromechanical Microengineering*, vol. 17, no. 5, pp. 891-899, May 2007.

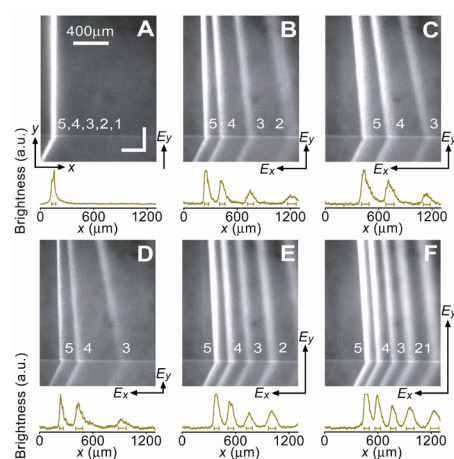
A Patterned Anisotropic Nanofilter Array for Continuous-flow Separation of DNA and Proteins

J. Fu, J. Han

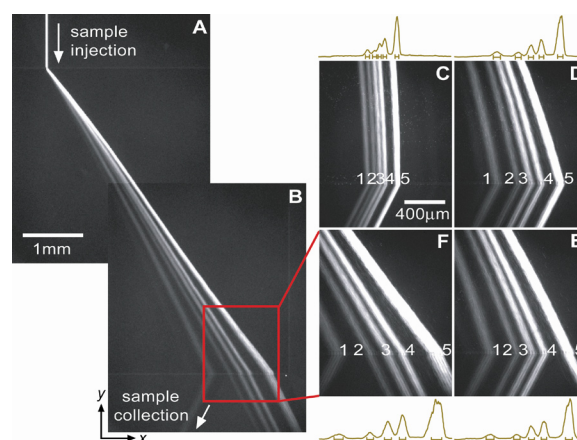
Sponsorship: NIH, NSF, Singapore-MIT Alliance (SMA-II, CE program)

Microfabricated regular sieving structures hold great promise as an alternative to gels to improve biomolecule separation speed and resolution. In contrast to the disordered gel porous network, these regular structures also provide well-defined environments ideal for study of molecular dynamics in confining spaces. However, previous regular sieving structures have been limited for separation of long DNA molecules, and separation of smaller, physiologically-relevant macromolecules, such as proteins, still remains as a challenge. Here we report a microfabricated anisotropic sieving

structure consisting of a two-dimensional periodic nanofluidic filter array (an Anisotropic Nanofilter Array, or ANA). The designed structural anisotropy in the ANA causes differently-sized molecules to follow different trajectories, leading to efficient separation. Continuous-flow Ogston sieving-based separation of short DNA and proteins as well as entropic trapping-based separation of long DNA were achieved, thus demonstrating the potential of the ANA as a generic sieving structure for an integrated biomolecule sample preparation and analysis system.



▲ Figure 1: Ogston sieving of the PCR marker through the ANA. For A, only E_y applied and $E_y=25$ V/cm; for B, $E_x=35$ V/cm, $E_y=25$ V/cm; for C, $E_x=60$ V/cm, $E_y=25$ V/cm; for D, $E_x=35$ V/cm, $E_y=12.5$ V/cm; for E, $E_x=35$ V/cm, $E_y=50$ V/cm; for F, $E_x=35$ V/cm, $E_y=75$ V/cm. Band assignment: (1) 50-bp; (2) 150-bp; (3) 300-bp; (4) 500-bp; (5) 766-bp.



▲ Figure 2: Entropic trapping of long DNA (the λ DNA-Hind III digest) through the ANA. Fluorescent photographs show separation of λ DNA-Hind III digest with different electric field conditions. In A, B, and F, $E_x=185$ V/cm and $E_y=100$ V/cm. In C, $E_x=50$ V/cm and $E_y=100$ V/cm. In D, $E_x=145$ V/cm and $E_y=100$ V/cm. In E, $E_x=170$ V/cm and $E_y=100$ V/cm. Band assignments are 2,322 bp (1), 4,361 bp (2), 6,557 bp (3), 9,416 bp (4), and 23,130 bp (5).

REFERENCES

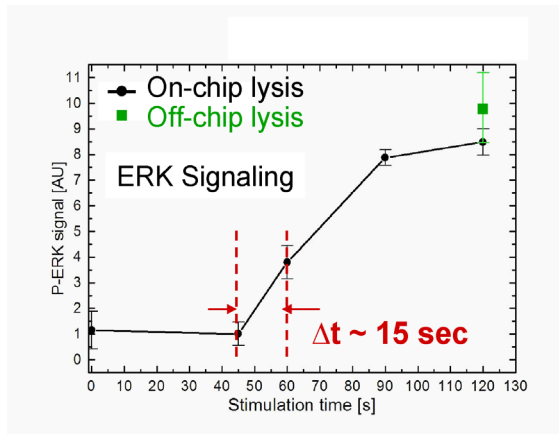
- [1] J. Fu and J. Han, "Nanofilter array chip for fast gel-free biomolecule separation," *Applied Physics Letters*, vol. 87, pp. 263902:1-3, Dec. 2005.
- [2] J. Fu, J. Yoo, and J. Han, "Molecular sieving in periodic free-energy landscapes created by patterned nanofilter arrays," *Physical Review Letters*, vol. 97, no. 1, pp. 018103:1-4, July 2006.
- [3] J. Fu, R.B. Schoch, A.L. Stevens, S.R. Tannenbaum, and J. Han, "A patterned anisotropic nanofluidic sieving structure for continuous-flow separation of DNA and proteins," *Nature Nanotechnology*, vol. 2, pp. 121-128, Feb. 2007.
- [4] J. Fu, "Nanofluidic devices for rapid analysis of DNA and proteins," Ph.D. thesis, Massachusetts Institute of Technology, Cambridge, MA, 2007.

Cell Stimulation, Lysis, and Separation in Microdevices

J. Albrecht, J. El-Ali, S. Gaudet, K.F. Jensen
Sponsorship: NIH

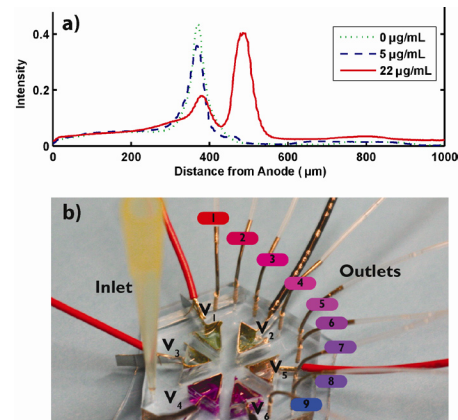
Quantitative data on the dynamics of cell signaling induced by different stimuli requires large sets of self-consistent and dynamic measures of protein activities, concentrations, and states of modification. A typical process flow in these experiments starts with the addition of stimuli to cells (cytokines or growth factors) under controlled conditions of concentration, time, and temperature, followed at various intervals by cell lysis and the preparation of extracts. Microfluidic systems offer the potential to do laborious assays in a reproducible and automated fashion [1].

Figure 1 shows quantification of the stimulation of a T-cell line with antibodies performed in a micro-fluidic device with integrated cell lysis. The device is capable of resolving the very fast kinetics of the cell pathways, with protein activation levels changing 4-fold in less than 15 seconds [2]. The quantification of the lysate is currently performed off-chip using electrophoretic separation. To effectively extract meaningful data from cellular preparations, many current biological assays require similar labor-intensive sample purification steps.



▲ Figure 1: The ERK signaling in Jurkat E6-1 cells stimulated with α -CD3 for different times. Stimulation and cell lysis were performed with the microfluidic device (chip stimulation) and with conventional methods (POS control). The error bars denote one standard deviation. This fast ERK response is resolved with relatively small variations between experiments performed with the same stimulation conditions, showing the reproducibility of the stimulation and effectiveness of the integrated lysis in the microfluidic device.

Micro-electrophoretic separators have several important advantages over their conventional counterparts, including shorter separation times, enhanced heat transfer, and the potential to be integrated into other devices on-chip. However, the high voltages required for these separations prohibit using metal electrodes inside the microfluidic channel. A PDMS isoelectric focusing device with polyacrylamide gel walls [3] has been developed to perform rapid separations by using electric fields orthogonal to fluid flow. This device and its variants have been shown to focus organelles, low-molecular-weight dyes, proteins, and protein complexes (Figure 2a) in seconds. Simulations have driven the development of improved device configurations, such as tandem IEF stages (Figure 2b).



▲ Figure 2: a) Focusing of Alexa 488 conjugated Protein G at various levels of unlabeled mouse IgG. Plotted are fluorescent intensities of Protein G alone (dotted line), 5 μ g/mL of IgG (dashed line), and 22 μ g/mL (solid line) that show the focusing of the IgG-Protein G complex. The proteins were focused in less than 20 seconds with an applied voltage of 30 V. b) Photograph of improved tandem-IEF device. Nine outlet fractions enable subsequent orthogonal separation and analysis.

REFERENCES

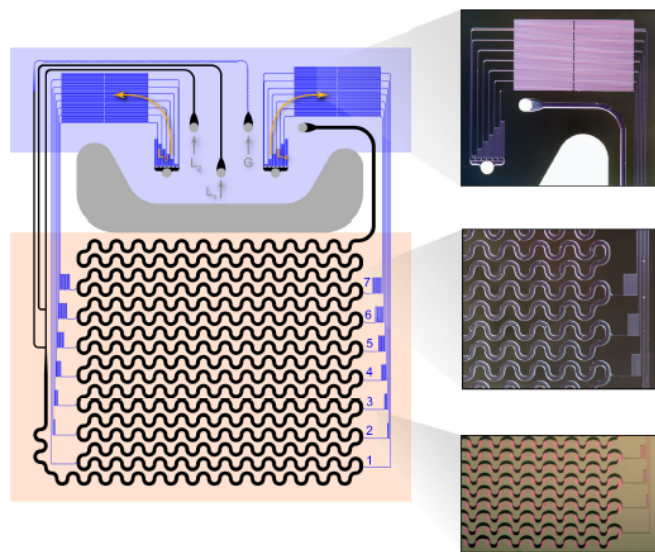
- [1] J. El-Ali, P.K. Sorger, and K.F. Jensen, "Condensed-matter physics: Coherent questions," *Nature*, vol. 443, no. 7110, pp. 403-411, Sept. 2006.
- [2] J. El-Ali, S. Gaudet, A. Guenther, P.K. Sorger, and K.F. Jensen, "Cell stimulation and lysis in a microfluidic device with segmented gas-liquid flow," *Analytical Chemistry*, vol. 77, no. 11, pp. 3629-3636, May 2005.
- [3] J. Albrecht and K.F. Jensen, "Micro free-flow IEF enhanced by active cooling and functionalized gels," *Electrophoresis*, vol. 27, no. 24, pp. 4960-4969, Dec. 2006.

Microreactors for Synthesis of Quantum Dots

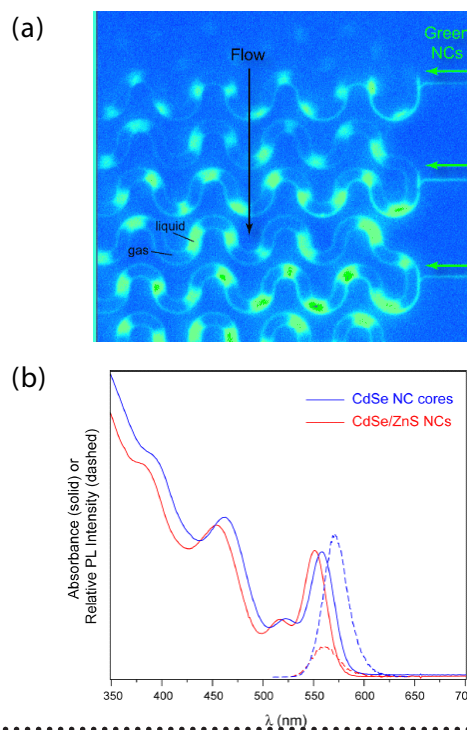
S. Marre, J. Guan, J. Park, M.G. Bawendi, K.F.Jensen
Sponsorship: NSF, ISN, Rhodia

We have fabricated gas-liquid, segmented-flow reactors with multiple temperature zones for the synthesis and the overcoating of quantum dots (QDs). In contrast to single-phase flow reactors, the segmented flow approach enables rapid mixing and narrow residence time distribution, factors which strongly influence the ultimate QD size distribution. The silicon-glass reactors accommodate a 1-m-long reaction channel (hydraulic diameter $\approx 400 \mu\text{m}$) and swallow side channels for multiple additional injections of precursors inside the main channel (Figure 1). Pressure-drop channels were added in order to avoid backflow into the side channels. Two temperature zones are maintained, a heated region ($> 260 \text{ }^\circ\text{C}$) and a cooled quenching region ($< 70 \text{ }^\circ\text{C}$). Measurements of the flow distribution (Figure 2a) show that this side manifold design results in very uniform distribution even at very low nominal flow rates. As a model system, monodispersed CdSe and CdSe/ZnS QDs were prepared using this reactor. For the preparation of

CdSe QDs, cadmium and selenium precursor solutions were delivered separately in the cooled region and were thereafter mixed in the heated region. An inert gas stream is introduced further downstream to form a segmented gas-liquid flow, thereby rapidly mixing the precursors and initiating the reaction, as was shown in a previous work [1]. In the case of the synthesis of CdSe/ZnS QDs, CdSe cores are introduced directly inside the main channel, while Zn and S precursors are added through the side swallow channels, allowing the overcoating. The reaction is stopped when the fluids enter the cooled outlet region of the device. When we vary the process parameters (temperature, precursors flow rates), the size of the cores material can be tuned without sacrificing the monodispersity. In addition, the overcoating of CdSe cores allows shifting the absorbance spectrum (5 nm), due to the presence of the ZnS layering (Figure 2b).



▲ Figure 1: Microreactor design with two feeder channels (blue) for adding precursor into the main stream. Each channel has a length of 14 cm and a hydraulic diameter of $50 \mu\text{m}$, whereas the main reaction channel (black) is 1 m long and has a hydraulic diameter of $400 \mu\text{m}$.



▲ Figure 2: (a) False-color fluorescence image used for measuring the flow distribution. Green-emitting nanocrystals are continuously injected from the side channels from the right into a gas-ethanol segmented flow in the main channel. (b) Absorbance and photoluminescence spectra of CdSe cores and CdSe/ZnS core/shell nanocrystals in hexane.

REFERENCES

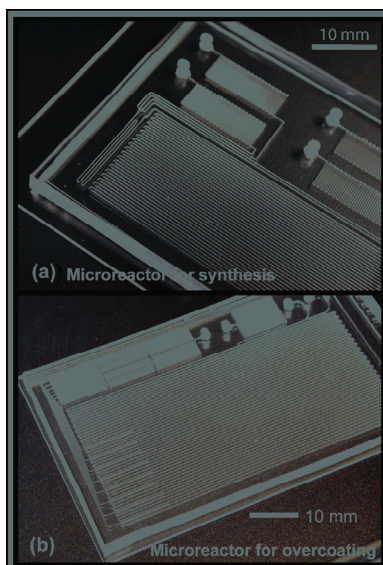
- [1] B.K.H. Yen, A. Günther, M.A. Schmidt, K.F.Jensen, and M.G.Bawendi, "A microfabricated gas-liquid flow reactor for high-temperature synthesis: The case of CdSe quantum dots," *Angewandte Chemie International Edition*, vol. 44, no. 34, pp. 5447-5451, Aug. 2005.

Microfluidic Synthesis and Surface Engineering of Colloidal Nanoparticles

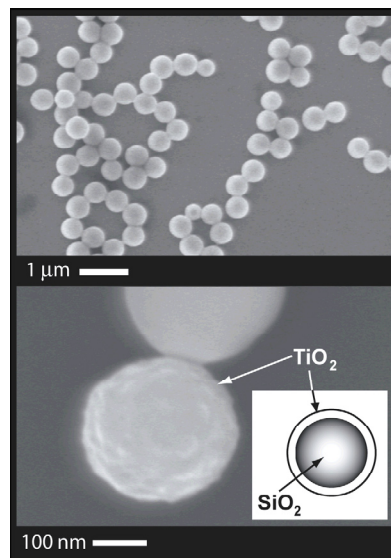
S.A. Khan, E.V. Loewer, K.F. Jensen

There has been considerable research interest over the last decade in fabricating core-shell materials with tailored optical and surface properties. For example, core-shell particles of silica and titania have drawn attention due their potential for trapping light at specific frequencies. This optical property depends on the formation of nanolayers on nano- or micro-cores. To obtain useful particles, these layers need to be uniform and even. These layered particles also need to be distinct and monodispersed. While nanolayer formation is successful in batch reactions, nonuniformity, agglomeration, and secondary nucleation often occur. We have developed microfluidic routes for synthesis and surface-coating of colloidal silica and titania particles.

The chief advantages of a microfluidic platform are precise control over reactant addition and mixing and continuous operation. Microfluidic chemical reactors for the synthesis and overcoating of colloidal particles are shown in Figures 1a and 1b, respectively [1-2]. Figure 2a is an SEM micrograph of silica particles synthesized in a microreactor (Figure 1a) operated in segmented gas-liquid flow mode. Figure 2b shows a silica nanoparticle coated with a thick shell of titania. We have also fabricated integrated devices combining synthesis and overcoating to enable continuous multi-step synthesis of core-shell particles.



▲ Figure 1: Microfluidic reactor for (a) synthesis of colloidal silica, fabricated in PDMS, and (b) overcoating thick titania shells on silica particles.



▲ Figure 2: (a) Silica synthesized in microreactor and (b) titania-coated silica.

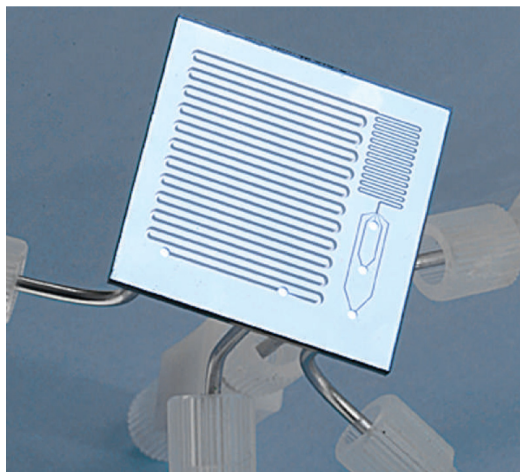
REFERENCES

- [1] S.A. Khan, A. Günther, M.A. Schmidt, and K.F. Jensen, "Microfluidic synthesis of colloidal silica" *Langmuir*, vol. 20, no. 20, pp. 8604-8611, June 2004.
- [2] S.A. Khan and K.F. Jensen, "Microfluidics surface-engineering of colloidal particles," in *Proc. μTAS 9*, Boston, MA, Oct. 2005, pp. 265-266.

Organic Synthesis in Microreactor Systems

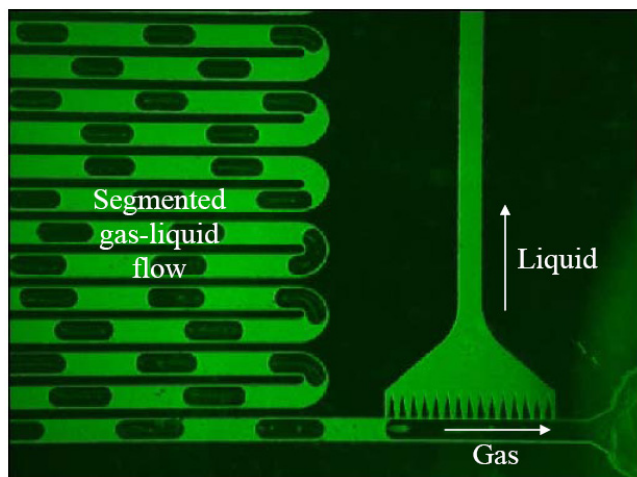
J.P. McMullen, N. Zaborenko, H.R. Sahoo, K.F. Jensen
Sponsorship: Pacific Scientific, Microchemical Systems Consortium

Enhanced heat and mass transfer, reduced reaction volume, and the ability to run several experiments in parallel render microreactors powerful instruments for scanning and optimizing chemical reaction conditions. Furthermore, the high mechanical strength and thermal conductivity of silicon microreactors permit the exploration of organic syntheses at higher temperatures and pressures than can be achieved with conventional bench-scale equipment. An example of these benefits is demonstrated in the aminocarbonylation reaction study [1]. Traditionally, these reactions are performed at atmospheric conditions and with temperatures at or below the boiling point of the solvent (toluene, 110°C). However, in silicon microreactors (Figure 1), it is possible to reach pressures exceeding 100 bar [2] and temperatures above 800°C [3]. Exploration of the aminocarbonylation reaction offers information that can be useful for the optimizing selectivity of the synthesis; higher CO pressures enhance α -ketoamide formation and increased temperatures favor amide formation.



▲ Figure 1: Silicon microreactor. Photograph, F. Frankel.

Once the chemical reaction is complete, it is desirable to separate the toxic gas from the liquid phase. Although negligible on the macro-scale, surface forces play a dominant role in microfluidics. Creating a capillary-based system (Figure 2) [4] makes it possible to take advantage of these forces. The liquid phase wets the capillaries and prevents the gas from penetrating the capillary matrix through the proper adjustments of pressure drops across the separator. Similarly, this concept can be applied to heterogeneous reactions that involve two immiscible liquids. Due to this micro-technology, microreactor systems can be assembled for multi-step synthesis and separation that could not easily be achieved in traditional laboratory environments. As a result, high throughput experiments can be performed and entire chemical processes can be optimized efficiently with microreactor systems.



▲ Figure 2: Capillary system for gas-liquid separation.

REFERENCES

- [1] E.R. Murphy, J.R. Martinelli, N. Zaborenko, S.L. Buchwald, and K.F. Jensen, "Accelerating reactions with microreactors at elevated temperatures and pressures: Profiling aminocarbonylation reactions" *Angewandte Chemie International Edition*, vol. 46, no. 10, pp. 1734-1737, Feb. 2007.
- [2] M.T. Timko, K.A. Smith, R.L. Danheiser, J.I. Steinfeld, and J.W. Tester, "Reaction rates in ultrasonic emulsions of dense carbon dioxide and water," *AIChE J.*, vol. 52, no. 3, pp. 1127-1141, Mar. 2006
- [3] L.R. Arana, S.B. Schaevitz, A.J. Franz, M.A. Schmidt, and K.F. Jensen, "A microfabricated suspended-tube chemical reactor for thermally efficient fuel processing," *J MEMS*, vol. 12, no. 5, pp. 600-612, Oct. 2003.
- [4] A. Gunther and K.F. Jensen, "Multiphase microfluidics: From flow characteristics to chemical and material synthesis," *Lab on a Chip*, vol. 6, no. 12, pp. 1487-1503, 2006.

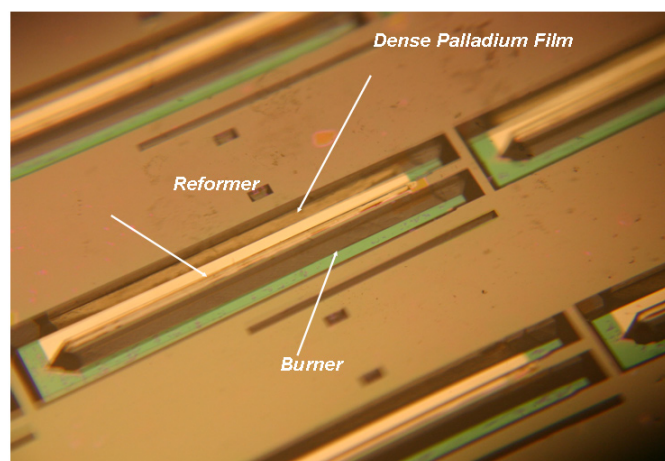
Autothermal Catalytic Micromembrane Devices for Portable High-purity Hydrogen Generation

K. Deshpande, M.A. Schmidt, K.F. Jensen
Sponsorship: ARO MURI

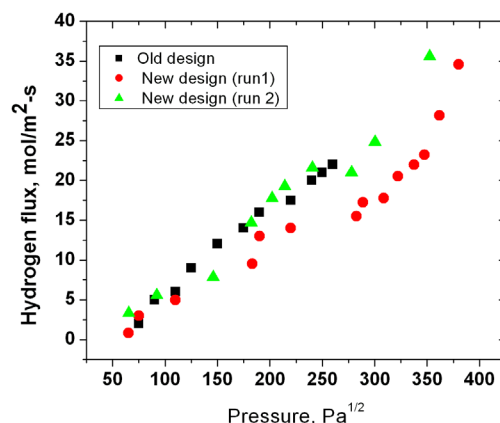
The high efficiency and energy density of miniaturized fuel cells provide an attractive alternative to batteries in the portable-power-generation market for consumer and military electronic devices [1-3]. The best fuel cell efficiency is typically achieved with hydrogen, but safety and reliability issues remain with current storage options. Consequently, there is continued interest in reforming of liquid fuels to hydrogen. The process typically involves high-temperature reforming of fuel to hydrogen combined with a low-temperature PEM fuel cell, which implies significant thermal loss. Owing to its high hydrogen content (66%) and ease of storage and handling, methanol is an attractive fuel. However, partial oxidation of methanol also generates CO, which can poison the fuel cell catalyst [1].

Previously [4] we have successfully demonstrated hydrogen purification using thin (~200 nm) Pd-Ag membranes using electrical heating. Further, integration of these devices with LaNiCoO_3 catalyst allowed methanol reforming at 475°C with 47% fuel conversion [5]. In the current work, we fabricate a novel autother-

mal reformer for hydrogen generation and purification using bulk micromachining techniques. This device combines the reforming unit with a catalyst loaded microreactor for combustion of hydrogen not recovered through the Pd-Ag membrane, generated CO, and unreacted methanol. The energy from the combustion heats the reformer to the operating temperature (~450°C). High thermal conductivity of silicon ensures efficient heat transfer from combustor to reformer. In the first phase, Pd-Ag membrane stability post-fabrication was tested; results indicated a pin-hole- and crack-free layer. Further, we successfully demonstrate high-pressure operation (up to 1.6 atm) of the device for enhanced hydrogen flux. The microburner has also been characterized with hydrogen oxidation over platinum catalyst. Work on reforming methanol for hydrogen generation and characterization of thermal responses is currently under progress.



▲ Figure 1: Fabricated reformer-burner unit with palladium membranes.



▲ Figure 2: Hydrogen flux comparison as a function of applied feed pressure.

REFERENCES

- [1] C.D. Baertsch, K.F. Jensen, J.L. Hertz, H.L. Tuller, S.T. Vengallatore, S.M. Spearing, and M.A. Schmidt, "Fabrication and structural characterization of self-supporting electrolyte membranes for a micro solid-oxide fuel cell," *Journal of Materials Research*, vol. 19, no. 9, pp. 2604-2615, Sept. 2004.
- [2] J.D. Morse, A.F. Jankowski, R.T. Graff, and J.P. Hayes, "Novel proton exchange membrane thin-film fuel cell for microscale energy conversion," *Journal of Vacuum Science and Technology A*, vol. 18, no. 4, pp. 2003-2005, July 2000.
- [3] J. Fleig, H.L. Tuller, and J. Maier, "Electrodes and electrolytes in micro-SOFCs: a discussion of geometrical constraints," *Solid State Ionics*, vol. 174, no. 1-4, pp. 261-270, Oct. 2004.
- [4] B.A. Wilhite, M.A. Schmidt, and K.F. Jensen, "Palladium-based micromembranes for hydrogen separation: Device performance and chemical stability," *Industrial and Engineering Chemistry Research*, vol. 43, no. 22, pp. 7083-7091, Oct. 2004.
- [5] B.A. Wilhite, S.J. Weiss, J. Ying, M.A. Schmidt, and K.F. Jensen "High-purity hydrogen generation in a microfabricated 23 wt % Ag-Pd membrane device integrated with 8:1 $\text{LaNi}_{0.95}\text{Co}_{0.05}\text{O}_3/\text{Al}_2\text{O}_3$ catalyst," *Advanced Materials*, vol. 18, no. 13, pp. 1701-1704, July 2006.

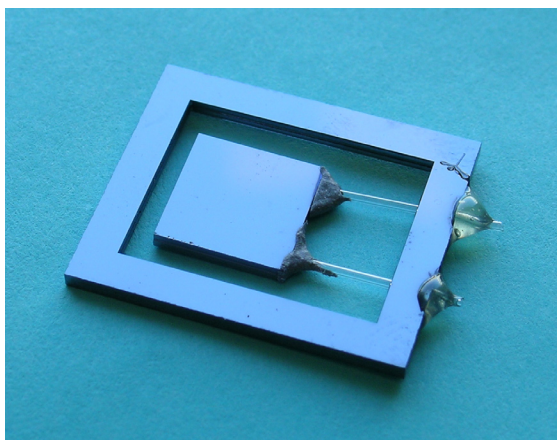
Thermal Management in Devices for Portable Hydrogen Generation

B. Blackwell, M.A. Schmidt, K.F. Jensen
Sponsorship: ARO MURI, Lincoln Laboratory

The development of portable-power systems employing hydrogen-driven solid oxide fuel cells continues to garner significant interest among applied science researchers. The technology can be applied in fields ranging from the automobile to personal electronics industries. This work focuses on developing microreaction technology that minimizes thermal losses during the conversion of fuels – such as light-end hydrocarbons, their alcohols, and ammonia – to hydrogen. Critical issues in realizing high-efficiency devices capable of operating at high temperatures have been addressed: specifically, thermal management, the integration of materials with different thermophysical properties, and the development of improved packaging and fabrication techniques.

A new fabrication scheme for a thermally insulated, high-temperature, suspended-tube microreactor has been developed. The new design improves upon a monolithic design proposed by Arana *et al.* [1]. In the new modular design (Figure 1), a high-temperature

reaction zone is connected to a low-temperature ($\sim 50^{\circ}\text{C}$) package via the brazing of pre-fabricated, thin-walled glass tubes. The design also replaces traditional deep reactive ion-etching (DRIE) with wet potassium hydroxide (KOH) etching, an economical and time-saving alternative. A brazing formulation that effectively accommodates the difference in thermal expansion between the silicon reactor and the glass tubes has been developed. Autothermal combustion of hydrogen, propane (Figure 2), and butane has been demonstrated in ambient atmosphere and in a vacuum.



▲ Figure 1: Suspended-tube microreactor showing 2 pre-fabricated SiO₂ tubes, a microfabricated Si reaction chip, and a microfabricated Si frame. The modular design is assembled via a glass braze.



▲ Figure 2: Autothermal combustion of propane under 25-mTorr vacuum.

REFERENCES

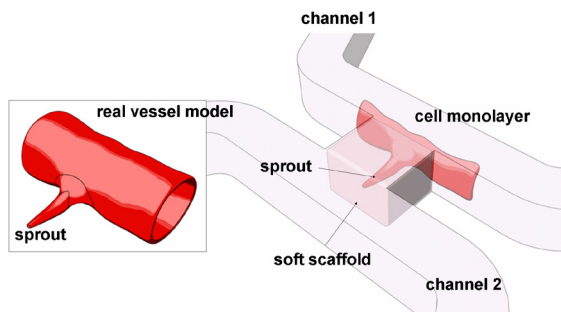
- [1] L.R. Arana, S.B. Schaevitz, A.J. Franz, M.A. Schmidt, and K.F. Jensen, "A microfabricated suspended-tube chemical reactor for thermally-efficient fuel processing," *Journal of MicroElectromechanical Systems*, vol. 12, no. 5, pp. 600-612, Oct. 2003.

Microfluidic Systems for the Study of Vascular Networks

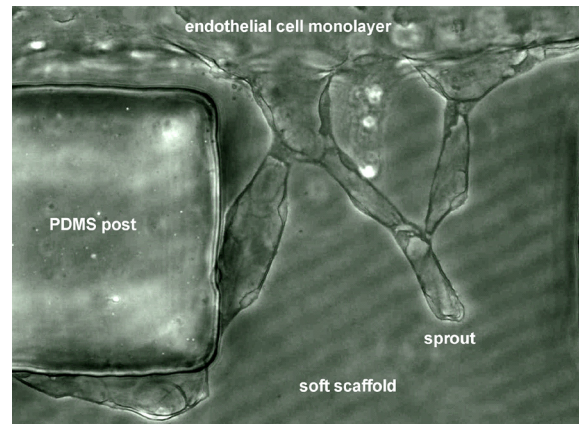
S. Chung, V. Vickerman Kelly, R. Sudo, R.D. Kamm
Sponsorship: Draper Labs, NIH NIBIB

Mechanical forces are important regulators of cell biology in health and disease. Cells in the vascular system are subjected to fluid shear stress, cyclic stretch, and differential pressure [1-3], and at the same time they receive multiple biochemical cues. All these factor into the integrated response of the tissue. A microfluidic bioreactor has been constructed to facilitate studies into the roles of both biophysical and biochemical factors on capillary morphogenesis. **The device is made of PDMS, cured on an SU-8 patterned wafer.** Then a scaffold material, collagen, is induced into a specific region of devices that was designed to keep its shape and properties. **Cells are seeded via one flow channel on the surface of the scaffold and then subjected to controlled mechanical factors like surface shear and trans-endothelial pressure, or biochemical angiogenic factors, inducing the**

formation of vascular sprouts that extend across the scaffold to a second flow channel. **With the bioreactor, cells on the scaffold form a confluent monolayer and generate sprouts. They show different responses and interactions with the scaffold, following the angiogenic factors, fluidic factors, surface characteristics and scaffold properties. Experiments are now under way to find the relations between cell responses and controlled factors. The developed system is the first system that can control biochemical and mechanical factors together, and it can be used for comparing the effects of angiogenic factors under controlled environment with enhanced view. It can also be applied to study the process of angiogenesis that entails the growth of vascular sprouts emanating from one endothelial surface and connecting with the other.**



▲ Figure 1: Concept drawing of the developed device. The seeded monolayer on the scaffold works as the wall of a real vascular system.



▲ Figure 2: The MVC sprout formed in collagen gel from the cell monolayer.

REFERENCES

- [1] L. You and C.R. Jacobs, "Cellular mechanotransduction," in *Nanoscale Technology in Biological Systems*, Boca Raton, Florida: CRC Press, 2005.
- [2] P. Carmeliet, "Angiogenesis in life, disease and medicine," *Nature*, vol. 438, pp. 932-936, Dec. 2005.
- [3] L. Coultas, K. Chawengsaksophak, and J. Rossant, "Endothelial cells and VEGF in vascular development," *Nature*, vol. 438, pp. 937-945, Dec. 2005.

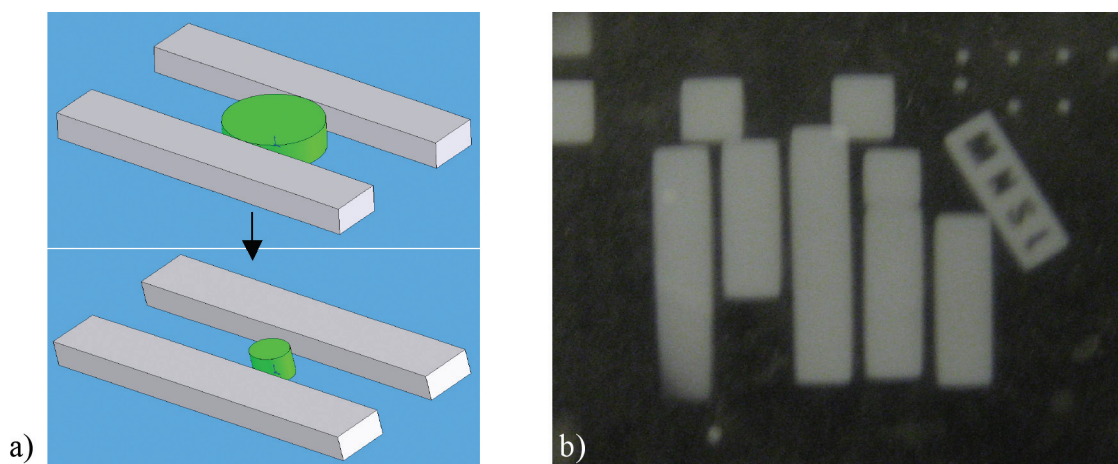
Patterning and Processing of Thermosensitive Hydrogels for Microfluidics Applications

N.E. Reticker-Flynn, H. Lee, S.G. Kim

Hydrogels have been an active area of research for a variety of applications due to their ability to retain large volumes of water within their polymer gel networks. Stimuli-responsive hydrogels provide the added advantage of the ability to control the water retention by means of external stimuli. For example, N-isopropylacrylamide (NIPAAm) is a thermosensitive hydrogel that exhibits a Lower Critical Saturation Temperature (LCST) around 32°C, above which the gel becomes hydrophobic and expels the water molecules, resulting in a drastic swelling/shrinking ratio. The goal of this project is to utilize this pseudo-binary transition in the fields of microfluidics and drug delivery.

By imbedding magnetic nanoparticles into the gel networks, the Hamad-Schifferli group [1] could control the temperature of the gels by inducing eddy currents by means of an oscillating magnet-

ic field. We are developing the concept further into micro-scale devices that can be monolithically integrated into many microfluidic systems. We have demonstrated the ability to photopattern the hydrogels and have shown control of the swelling behavior by controlling the amount of cross-linking in the network. This allowed for the creation of hydrogel valves for microfluidic devices. Unlike pressure controlled valves, these valves do not require any physical interconnects to macro-scale devices. This advantage could prove extremely useful in the commercialization of microfluidic analysis systems where users might not have equipment such as syringe pumps or air compressors available. In addition to valves, applications of the swelling behavior to micropumps are also being examined.



▲ Figure 1: (a) Controlable microfluidic valve activated by means of external magnetic field. (b) NIPAAm MIT logo with top of “T” removed from substrate.

REFERENCES

- [1] A. Wijaya, K.A. Brown, J.D. Alper, and K. Hamad-Schifferli, “Magnetic field heating study of Fe-doped Au nanoparticles,” *Journal of Magnetism and Magnetic Materials*, vol. 309, no. 1, pp. 15-19, Feb. 2007.

A Large-strain, Arrayable Piezoelectric Microcellular Actuator by Folding Assembly

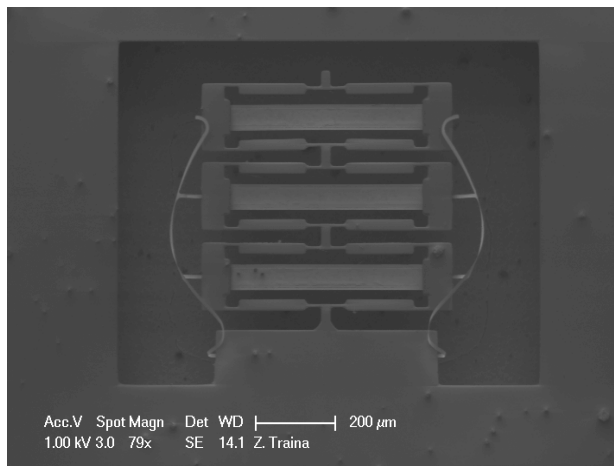
Z.J. Traina, S.G. Kim

Sponsorship: Korean Institute of Machinery and Materials

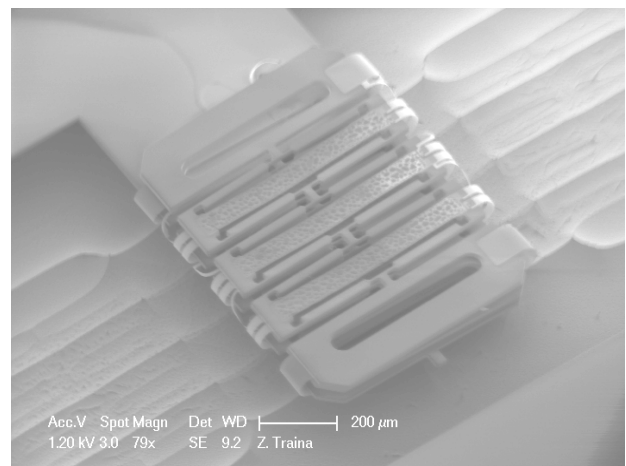
A low-power, piezoelectric, contracting cellular MEMS actuator has been developed that demonstrates a peak strain of 3% under a 10 V stimulus. Since the motion of the end effector is linear and in-plane, the actuator can be arrayed in series to amplify the total stroke or in parallel to amplify the total force, as needed. Location of the piezoelectric member through the structural center of stiffness reduces the potential for parasitic out of plane bending present in previous designs [1].

Cellular actuators arrays can be assembled into a larger array of actuators. We demonstrated that sets of cellular microactuators can be assembled out of plane by folding them over thin gold

hinges. To our knowledge, this study is the first effort in this field. The gold hinges serve dually as mechanical assembly guides and electrical interconnects. Long chains of devices may be assembled by rolling out of plane. Figure 2 shows a smaller collection, assembled by folding three actuator triplets onto one another. Actuation of the collection is contingent on the manufacturing of functional thin-film PZT.



▲ Figure 1: An array of three cellular actuators fabricated in series, which demonstrates a total static displacement of more than 15 μm under 10V stimulus. The strain of the assembly exceeds that of unmodified PZT by a factor of more than 29:1.



▲ Figure 2: A total of 9 actuators (three actuator triplets) assembled into one collection by folding out of plane over gold hinges. Actuation of a folded device collection is contingent on the manufacturing of functional thin film PZT.

REFERENCES

- [1] N.J. Conway, Z. Traina, and S.G. Kim, "Strain amplifying piezoelectric MEMS actuator," *Journal of Micromechanics and Microengineering*, vol. 17, no. 4, pp. 781-787, Apr. 2007.

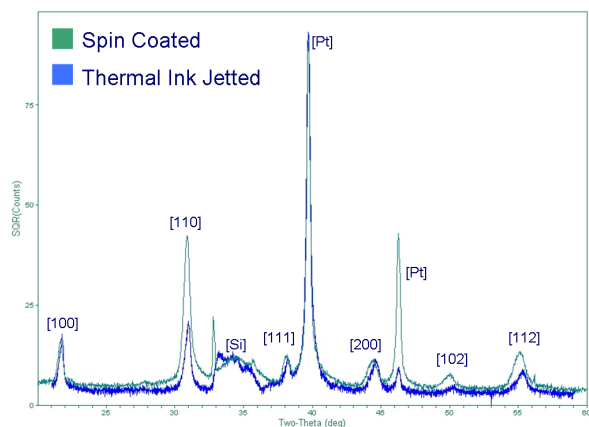
Thermal Ink Jet Printing of Lead Zirconate Titanate Thin Films

S. Bathurst, H.W. Lee, S.G. Kim
Sponsorship: DARPA, Hewlett-Packard

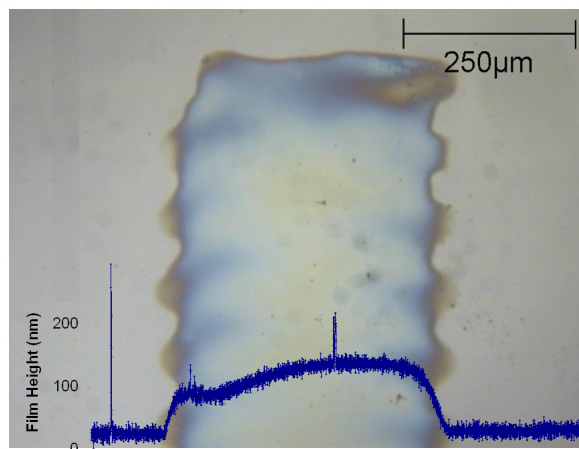
The ferromagnetic and piezoelectric properties of ceramic lead zirconate titanate (PZT) thin films have made PZT an appealing choice for micro-sensors and actuators. Significant work has been done integrating PZT with standard MEMS processes, including the development of PZT sol-gels for spin coating [1-2]. Cracking is often a problem with PZT spin coating due to the brittle nature of the films coupled with the thermal strain experienced during annealing. This propensity for cracking limits the overall thickness deposited and the size out of plane features over which PZT can be reliably coated. Furthermore, spin coating requires a large volume of the expensive PZT precursor solution. We propose thermal ink-jet printing of a modified PZT sol-gel as a new method of depositing PZT films for MEMS applications. Preliminary work has shown ink jetting to be a reliable method for depositing PZT films of the correct thickness for MEMS applications and that annealed films can crystallize into the piezoelectric perovskite phase using the same thermal process developed for spin-coated PZT (see Figure 1) [3]. The goal of this research is to develop a deposition process that will enable reliable manufacturing of high-quality PZT films with greater deposition flexibility and lower material costs than spin coating.

Thermal ink jetting technology supports a wide range of ink viscosities and solid particle contents. The ink composition can therefore be adjusted to control both the contact angle of solution with the substrate (1000Å Pt/ 200Å Ti) and the as-deposited film thickness. This flexibility allows for the deposition of films with thickness and uniformity that are acceptable for the fabrication of piezoelectric devices (see Figure 2). Multiple layers can be deposited to attain the thickness as needed. Currently, annealed films have been prepared as thick as 0.5 μm, corresponding to an as deposited thickness of approximately 1 μm. This is comparable to the current limit of standard spin-coated PZT sol-gel processed; printing of thicker films is under investigation.

We acknowledge Hewlett Packard for providing the POEMS thermal ink-jet printer.



▲ Figure 1: Comparison of X-ray diffraction of spin-coated PZT film with thermal ink-jetted film.



▲ Figure 2: Optical microscope image and profilometry of as deposited thermal ink-jetted lead zirconate titanate thin film.

REFERENCES

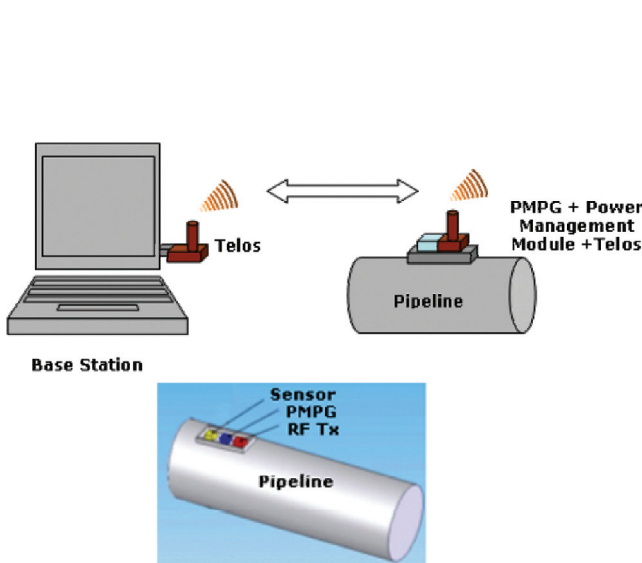
- [1] S.K. Dey, K.D. Budd, and D.A. Payne, "Thin-film ferroelectrics of PZT by sol-gel processing," *IEEE Trans. On Ultrasonics Ferroelectrics and Frequency Control*, vol. 35, no. 1, pp. 80-81, Jan. 1988.
- [2] C.D.E. Lakeman, J.F. Campion, C.T.A. Suchicital, and D.A. Payne, "An investigation into the factors affecting the sol-gel processing of PZT thin layers," *Applications of Ferroelectrics, 1990., IEEE 7th International Symposium on*, pp. 681 – 684, June 1990.
- [3] K.G. Brooks, I.M. Reaney, R. Klissurska, Y. Huang, L. Bursill, and N. Setter, "Orientation of rapid thermally annealed lead zirconate titanate thin films on (111) Pt substrates," *Journal of Materials Research*, vol. 9, no. 10, pp. 2540-2553, Oct. 1994.

Piezoelectric Micro-power-generator: MEMS Energy-harvesting Device for Self-powered Wireless Corrosion-monitoring System

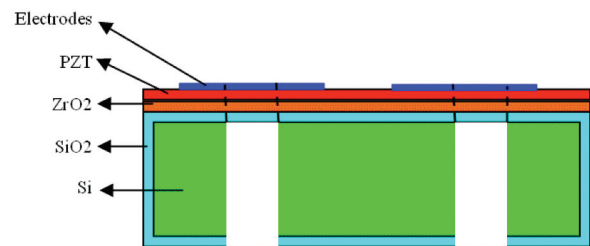
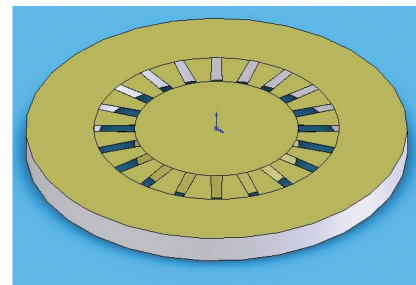
A. Hajati, S.G. Kim
 Sponsorship: NSF, Korean Institute of Machinery and Material

A novel thin-film, lead zirconate titanate $Pb(Zr,Ti)O_3$ (PZT), energy-harvesting MEMS device is being developed for autonomous wireless monitoring systems. It is designed to harvest energy from parasitic vibrational energy sources and convert it to electrical energy via the piezoelectric effect. We envision that harvesting parasitic energy from the vortex-induced vibration of the oil pipelines will deploy a massive number of microsensors along the hundreds of miles of pipeline in very cold and remote areas. The proposed system consists of a corrosion sensor, a radio transceiver, a microcontroller, a power management module, and a piezoelectric micro power generator (PMPG) to supply the needed power of the system without replacing batteries.

The new pie-shaped design for the harvester (about a size of a nickel) has a radical departure from previous design concepts. This energy harvester design can be regarded as revolutionary as the first self-rectifying piezoelectric power generator. The new design avoids the high Q resonance, which is also a big change from previous designs. This will enable more robust power generation even if the frequency spectrum of the source vibration varies unexpectedly. Furthermore, the beam shape is optimized to achieve uniform allowable strain throughout the PZT layer. Currently, the first prototype, which is shown schematically, is being fabricated at MTL.



▲ Figure 1: Wireless sensor system schematics. The self-powered sensor node transmits data to a receiver at the base station.



▲ Figure 2: The structure of a pie-shaped PMPG.

REFERENCES

- [1] Y.R. Jeon, Sood, J.H. Jeong, and S.G. Kim, "MEMS power generator with transverse mode thin-film PZT," *Sensors and Actuators A: Physical*, vol. 122, pp. 16-22, July 2005.
- [2] W.J. Choi, Y. Xia, J.A. Brewer, and S.G. Kim, "Energy-harvesting MEMS device based on thin-film piezoelectric cantilevers," in *Proc. of INSS05*, San Diego, CA, June 27-28, 2005.
- [3] R. Xia, C. Farm, W. Choi, and S.-G. Kim, "Self-powered wireless sensor system using MEMS piezoelectric micro-power-generator," in *Proc. IEEE Sensors 2006*, Daegu, Korea, 2006.

Lateral-line-inspired MEMS-array Pressure Sensing for Passive Underwater Navigation

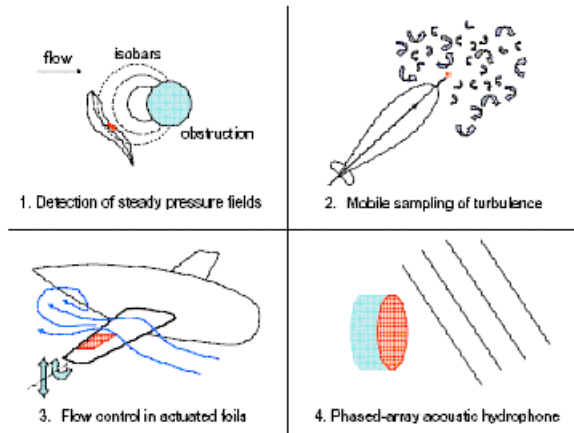
V. Fernandez, S. Hou, F. Hover, J. Lang, M. Triantafyllou
Sponsorship: NOAA: MIT Sea Grant College Program

A novel sensing technology for unmanned undersea vehicles (UUVs) is under development. The project is inspired by the lateral line sensory organ in fish, which enable some species to form three-dimensional maps of their surroundings [1-2]. The canal subsystem of the organ can be described as an array of pressure sensors [3]. Interpreting the spatial pressure gradients allows fish to perform a variety of actions, from tracking prey [4] to recognizing nearby objects [2]. It also aids schooling [5]. Similarly, by measuring pressure variations on a vehicle surface, an engineered dense pressure sensor array allows the identification and location of obstacles for navigation (Figure 1). We are demonstrating proof-of-concept by fabricating such MEMS pressure sensors by using KOH etching techniques on SOI wafers to construct strain-gauge diaphragms.

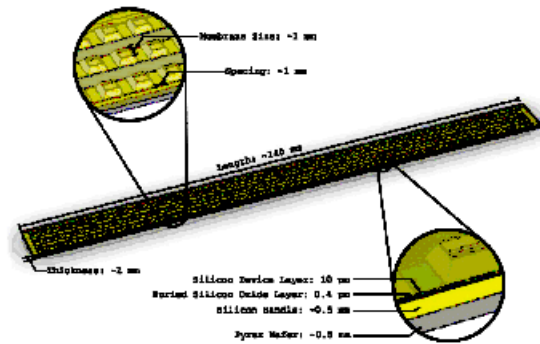
The system consists of arrays of hundreds of pressure sensors spaced about 2 mm apart on etched silicon and Pyrex wafers. The sensors are arranged over a surface in various configurations (Fig-

ure 2). The target pressure resolution for a sensor is 1 Pa, which corresponds to the noiseless disturbance created by the presence of a 0.1-m-radius cylinder in a flow of 0.5 m/s at a distance of 1.5 m. A key feature of a sensor is the flexible diaphragm, which is a thin (20 μm) layer of silicon attached at the edges to a silicon cavity. The strain on the diaphragm due to pressure differences across the diaphragm is measured. At this stage, the individual MEMS pressure sensors are being constructed and tested.

In parallel to the construction of a sensor array, techniques are being developed to interpret the signals from a dense pressure array by detecting and characterizing wake structures such as vortices and building a library of pressure distributions corresponding to basic flow obstructions. In order to develop these algorithms, experiments are being performed on coarse arrays of commercial pressure sensors



▲ Figure 1: Pressure-sensor array applications.



▲ Figure 2: Diagram of pressure-sensor array with basic structure depicted.

REFERENCES

- [1] J.C. Montgomery, S. Coombs, and C.F. Baker, "The mechanosensory lateral line system of the hypogean form of *Astyanax fasciatus*," *Env. Biol. Fishes*, vol. 62, nos. 1-3, pp. 87-96, Oct. 2001.
- [2] C. von Campenhausen, I. Riess, and R. Weissert, "Detection of stationary objects by the blind cave fish *Anoptichthys jordani* (Characidae)," *Journal of Comparative Physiology A*, vol. 143, no. 3, pp. 369-374, Sept. 1981.
- [3] S. Coombs, "Smart skins: Information processing by lateral line flow sensors," *Auton. Robots*, vol. 11, no. 3, pp. 255-261, Nov. 2001.
- [4] K. Pohlmann, J. Atema, and T. Breithaupt, "The importance of the lateral line in nocturnal predation of piscivorous catfish," *J. Exp. Biol.*, vol. 207, no. 17, pp. 2971-2978, Aug. 2004.
- [5] T.J. Pitcher, B.L. Partridge, and C.S. Wardle, "A blind fish can school," *Science*, vol. 194, no. 4268, pp. 963-965, Nov. 1976.

Fabrication of a Fully-integrated Multiwatt μ TurboGenerator

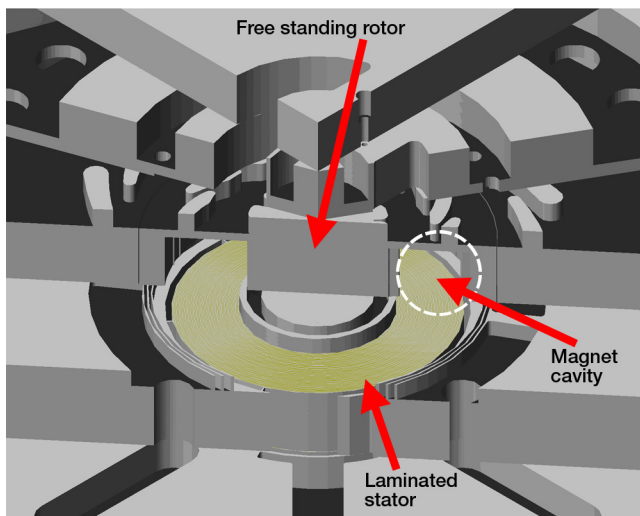
B.C. Yen, M. Allen, F.F. Ehrich, A.H. Epstein, F. Herrault, K.J. Hillman, L.C. Ho, S. Jacobson, J.H. Lang, H. Li, Z.S. Spakovszky, C.J. Teo, D. Veazie
Sponsorship: US Army Research Laboratory Collaborative Technology Alliance

There is a need for compact, high-performance power sources that can outperform the energy density of modern batteries for use in portable electronics, autonomous sensors, robotics, and other applications. Building upon the results presented in [1], the current research is aimed at fabricating a fully-integrated, multiwatt micro turbogenerator on silicon that can produce 10 W DC output power (Figure 1). One of the main challenges involves the seamless integration between silicon and the magnetic components required to generate power. The generator requires a NiFe soft magnetic back iron and laminated stator for flux redirection as well as NdFeB permanent magnet pieces to serve as flux sources (Figure 2). In addition, copper windings must be fabricated above the laminated stator to couple to the alternating flux in order to extract electrical power from the machine.

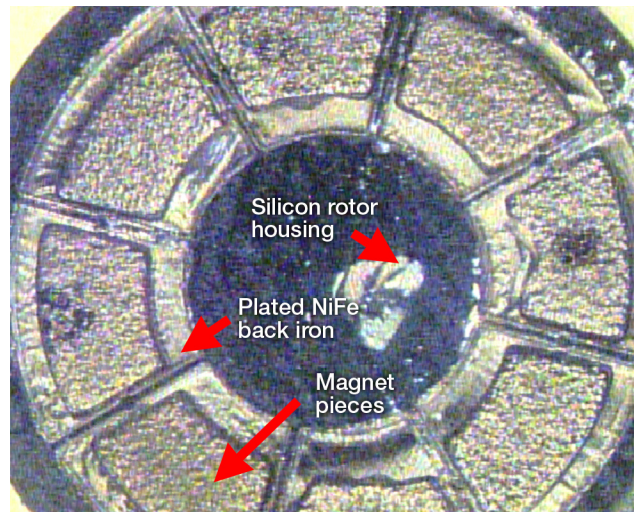
Great strides have been made in the past year to quantify the requirements on the magnet pieces that will go into the rotor housing. Manufacturing accuracy of the pieces is critical because variations in the magnet geometries create an overall rotor imbalance, which can cause the rotor to crash during

transcritical operation. A procedure in which the gaps around the magnet pieces are filled with solder and then polished back using chemical-mechanical planarization has been developed; this process can reduce the effective imbalance of the rotor by an order of magnitude.

The assembly and packaging procedure for the turbogenerator is also critical because the embedded permanent magnets cannot withstand temperatures much above 150 °C. This temperature restriction rules out the use of fusion bonding for the final die-level assembly after rotor insertion. Based on results presented by Choe, *et al.* [2], an eutectic In-Sn bonding scheme that requires only 140 °C has been researched. In this scheme, Cr/Au is deposited on one bonding surface and Cr/Sn/In/Au is deposited on the other surface; both depositions are done using an e-beam evaporator without breaking vacuum. By painting no-clean flux on both surfaces and compressing the dies together on a hot plate, we form the bond.



▲ Figure 1: Conceptual rendering of the fully-integrated generator. Back iron and magnet pieces will be inserted into the empty cavities of the rotor, which will be supported by gas thrust and journal bearings. Electrical connections are taken out from the backside of the die.



▲ Figure 2: Magnetic rotor test structure with back iron plated and sample magnet pieces inserted. The magnets shown in this photo were not manufactured to the correct size, but they demonstrate what a completed rotor might look like. (Courtesy of F. Herreault, GIT)

REFERENCES

- [1] B.C. Yen, *et al.*, "An Integrated Multiwatt Permanent Magnet Turbine Generator," in *Proc. MTL Annual Research Conference*, Waterville Valley, NH, Jan. 2006, p. 42.
- [2] S. Choe, W.W. So, and C.C. Lee, "Low temperature fluxless bonding technique using In-Sn composite," in *Proc. Electronic Components and Technology Conference*, pp. 114-118, May 2000.

A Portable Power Source Based on MEMS and Carbon Nanotubes

F A. Hill, T.F. Havel, C. Livermore

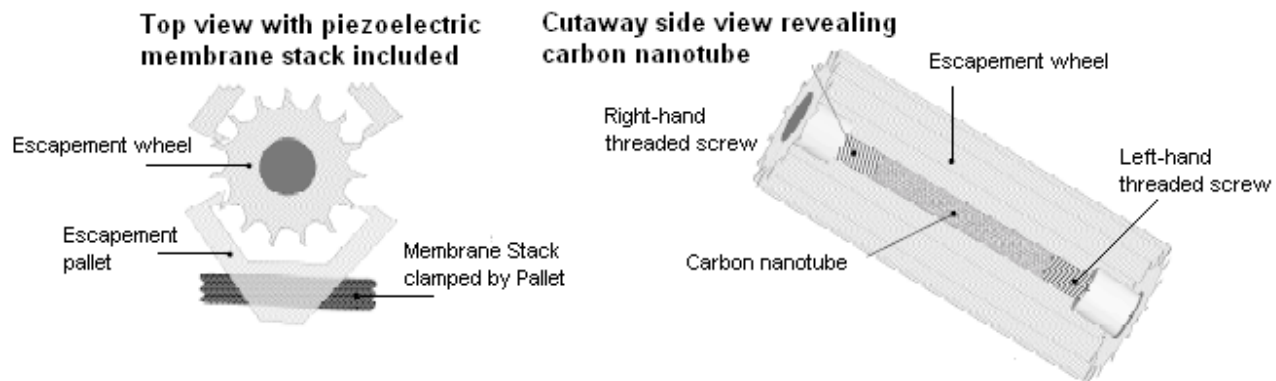
Sponsorship: Deshpande Center for Technological Innovation

There is a growing need for small, lightweight, reliable, highly efficient and fully rechargeable portable power sources. The focus of this project is the design and modeling of a system in which energy is stored in the elastic deformation of carbon nanotube (CNT)-based springs. The CNTs are coupled to a MEMS electric generator. When the CNT deformation is released, the stored energy actuates the generator, which then converts the energy into electricity. The MEMS generator may be operated in reverse, as a motor, in order to wind the CNT springs and recharge the system. Alternatively, the stored elastic energy may be used to supply a mechanical load directly. This project is motivated by recent research into the mechanical properties of CNTs. The CNTs have a high stiffness, low defect density, and a consequently high yield strain that enables them to store elastic energy with significantly greater energy density than typical spring materials such as high-carbon steel. Models suggest that CNTs can be reversibly stretched by up to 15% [1]; lower strains of up to 6% have been demonstrated experimentally to date [2-3].

This type of system offers several important potential advantages. First, due to CNTs' high strength, high flexibility, and low defect density, they can store energy at very high energy density. Considering just the CNT-based spring itself, the energy density of an array of CNTs stretched to a reversible 15% strain is about 1500 W-hr/kg, about ten times the energy density of Li-ion batteries.

The energy density of the final system will be lower because of the finite conversion efficiency of the generator and the weight of both the supporting structure and the generator hardware. In addition, because energy storage in the CNT system is based on stretching chemical bonds rather than breaking and reforming chemical bonds as in batteries, the CNT-MEMS generator system has the potential to operate at higher power densities, under harsher conditions, to deeper discharge levels, and through a greater number of charge-discharge cycles than a chemical battery.

The system architecture consists of a CNT-based energy storage element, an energy release rate mechanism, and a MEMS generator. This project is examining and modeling different variations on this system architecture that incorporate different modes of deformation of the CNT-based energy storage element, various types of generators, different types of coupling between the storage element and the generator, and different size scales for the various components. One conceptual example is illustrated below, in which the axial relaxation of an axially-stretched CNT-based storage element is converted to rotational motion of a wheel. The wheel is coupled to a piezoelectric generator through a mechanism that regulates the rate of energy release, much as in a mechanical watch.



▲ Figure 1: Schematic diagram showing the conceptual design of a MEMS-based energy storage device

REFERENCES

- [1] M.R. Falvo, G.J. Clary, R.M. Taylor, V. Chi, F.P. Brooks, S. Washburn and R. Superfine, "Bending and buckling of carbon nanotubes under large strain," *Nature*, vol. 389, no. 12, pp. 582-584, Oct. 1997.
- [2] D.A. Walters, L.M. Ericson, M.J. Casavant, J. Liu, D.T. Colbert, K.A. Smith, and R.E. Smalley, "Elastic strain of freely suspended single-wall carbon nanotube ropes," *Applied Physics Letters*, vol. 74, no. 25, pp. 3803-3805, June 1999.
- [3] M. Yu, B.S. Files, S. Arepalli, and R.S. Ruoff, "Tensile loading of ropes of single-wall carbon nanotubes and their mechanical properties," *Phys. Rev. Lett.*, vol. 84, no. 24, pp. 5552-5555, June 2000.

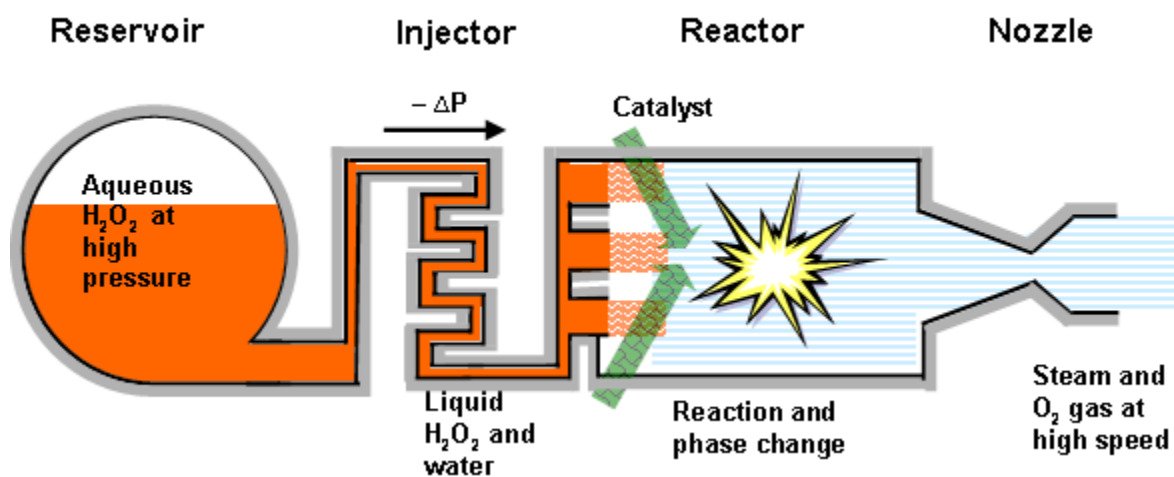
A MEMS Steam Generator

F. Eid, L.F. Velasquez-Garcia, A.H. Epstein, C. Livermore
Sponsorship: DARPA, MDA, AFRL

Previous work [1] has shown that MEMS technology has significant potential to create more compact, higher-performing hardware for chemical oxygen iodine lasers (COIL). In COILs, the laser medium is a flowing gas that must be pumped through the system at high mass flow rates to ensure proper system operation. As a result, compact pumps with high pumping rates are a key element of the COIL system. One promising component of a MEMS COIL system would be a compact MEMS pump system in which the pump action is provided in part by micro steam ejectors and the micro steam generators that supply their driving fluid. This work describes the design and modeling of a microscale hydrogen peroxide (H_2O_2)-based steam generator to supply such a MEMS pump system. Hydrogen peroxide is a readily available, inexpensive, nontoxic, and environmentally friendly fluid that may be catalytically decomposed to form steam. Steam generation by the catalytic decomposition of H_2O_2 also finds other important applications in the MEMS field beyond pumping, particularly in the area of thrust generation. Compared to their

macroscale counterparts, MEMS H_2O_2 -based steam generators offer better performance, notably improved mixing, and higher uniformity due to the absence of moving parts [2-3].

A complete MEMS steam generator consists of a peroxide reservoir, an injector, a reactor, and a converging-diverging nozzle to accelerate the exiting flow, as shown in Figure 1. Initial work focuses on the design of the reactor and nozzle. Liquid H_2O_2 in aqueous solution is injected into the reactor, where it decomposes into steam and oxygen gas upon contact with the catalyst. A continuous supply of homogeneous liquid catalyst is used, as it avoids the aging problem typically exhibited by heterogeneous catalysts [4]. The gaseous products of the reaction are then accelerated to supersonic velocities through the converging-diverging nozzle. The work to date indicates that a MEMS steam generator designed to minimize heat transfer to the environment can provide complete, compact, uniform decomposition of peroxide into steam suitable to drive a MEMS pumping system.



▲ Figure 1: Schematic diagram of a hydrogen peroxide-based MEMS steam generator, showing the peroxide reservoir, injector, reactor, and nozzle.

REFERENCES

- [1] B.A. Wilhite, C. Livermore, Y. Gong, A.H. Epstein, and K.F. Jensen, "Design of a MEMS-based microchemical oxygen-iodine laser (mCOIL) system," *IEEE J. of Quantum Electronics*, vol. 40, pp. 1041-1055, Aug. 2004.
- [2] W. Tanthapanichakoon, N. Aoki, K. Matsuyama, and K. Mae, "Design of mixing in microfluidic liquid slugs based on a new dimensionless number for precise reaction and mixing operations," *Chemical Engineering Science*, vol. 61, pp. 4220-4232, July 2006.
- [3] S. Bhaduri and D. Mukesh, *Homogeneous Catalysis: Mechanisms and Industrial Applications*, New York: John Wiley & Sons, Inc., 2000.
- [4] C. Xupeng, L. Yong, Z. Zhaoying, and F. Ruili, "A homogeneously catalyzed micro-chemical thruster," *Sensors and Actuators A: Physical*, vol. 108, pp. 149-154, June 2003.

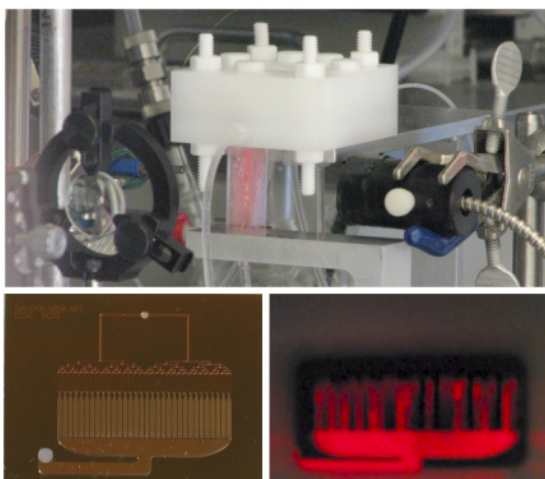
Microscale Singlet Oxygen Generator for MEMS-based COIL Lasers

T. Hill, L.F. Velásquez-García, A.H. Epstein, K.F. Jensen, C. Livermore
Sponsorship: DARPA, MDA, AFRL

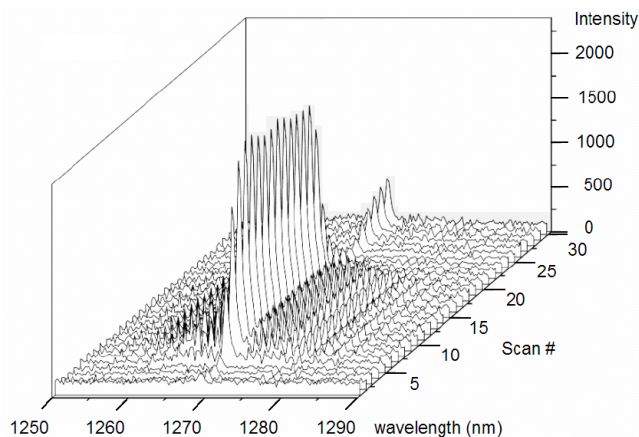
Conventional chemical oxygen iodine lasers (COIL) offer several important advantages for materials processing, including short wavelength (1.3 μm) and high power. However, COIL lasers typically employ large hardware and use reactants relatively inefficiently. This project is creating an alternative approach called microCOIL. In microCOIL, most conventional components are replaced by a set of silicon MEMS devices that offer smaller hardware and improved performance. A complete microCOIL system includes microchemical reactors, microscale supersonic nozzles, and micropumps. System models incorporating all of these elements predict significant performance advantages in the microCOIL approach [1].

Initial work is focused on the design, microfabrication, and demonstration of a chip-scale singlet oxygen generator (SOG), a microchemical reactor that generates singlet delta oxygen gas to power the laser. Given the extensive experience with microchemical reactors over the last decade [2], it is not surprising that a

microSOG would offer a significant performance gain over large-scale systems. The gain stems from basic physical scaling; surface-to-volume ratio increases as the size scale is reduced, which enables improved mixing and heat transfer. The SOG chip being demonstrated in this project employs an array of microstructured packed-bed reaction channels interspersed with microscale cooling channels for efficient heat removal [3]. To date the device has produced oxygen concentrations of 10^{17} cm^{-3} , yields approaching 80% and molar flowrates in excess of $600 \times 10^{-4} \text{ moles/L/sec}$ [4]. The yield and molar flowrates indicate a significant improvement over the macroscale SOG designs.



▲ Figure 1: A – View of chip surface showing glow resulting from singlet-oxygen production; B – View of packaging and optics surrounding microSOG; C – Photograph of microSOG.



▲ Figure 2: The IR spectra measured at the μSOG gas outlet versus time. The peak at 1268 nm indicates the spontaneous decay of singlet oxygen into its triplet state.

REFERENCES

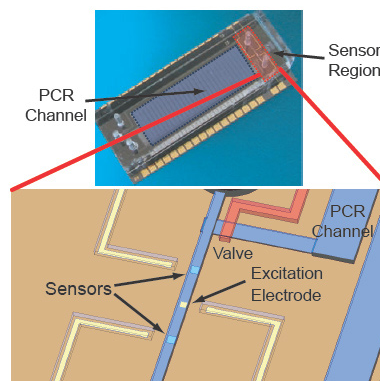
- [1] B.A. Wilhite, C. Livermore, Y. Gong, A.H. Epstein, and K.F. Jensen, "Design of a MEMS-based microchemical oxygen-iodine laser (mCOIL) system," *IEEE J. of Quantum Electronics*, vol. 40, pp. 1041-1055, August 2004.
- [2] M.W. Losey, M.A. Schmidt, and K.F. Jensen, "Microfabricated multiphase packed-bed reactors: Characterization of mass transfer and reactions," *Ind. Eng. Chem. Res.*, vol. 40, pp. 2555-2562, June 2001.
- [3] L.F. Velásquez-García, T.F. Hill, B.A. Wilhite, K.F. Jensen, A.H. Epstein, and C. Livermore, "A MEMS singlet oxygen generator – Part I: Device fabrication and proof of concept demonstration," *IEEE J. of Microelectromechanical Systems*, 2007, to be published.
- [4] T.F. Hill, L.F. Velásquez-García, B.A. Wilhite, W.T. Rawlins, S. Lee, S.J. Davis, K.F. Jensen, A.H. Epstein, and C. Livermore, "A MEMS singlet oxygen generator- Part II: Experimental exploration of the performance space," *IEEE J. of Microelectromechanical Systems*, 2007, to be published.

An Integrated Microelectronic Device for Label-free Nucleic Acid Amplification and Detection

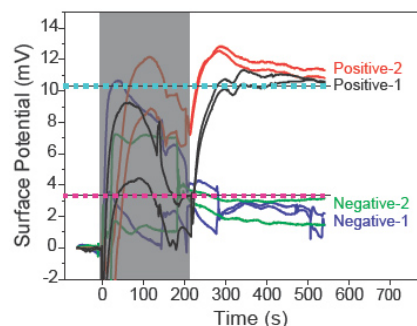
C.J. Hou, M. Godin, K. Payer, S.R. Manalis
Sponsorship: Hewlett-Packard, AFOSR

While there have been extensive advances in miniaturized polymerase chain reaction (PCR) systems, progress on integrated microfabricated readout mechanisms has been rather limited, and most systems rely on off-chip optical detection modules to measure the final product. Existing optical detection platforms typically include CCD cameras, photodiodes, and photomultiplier tubes. While such hardware has adequate sensitivity for detecting PCR products in sample volumes significantly lower than that of bench-top systems, most are difficult to miniaturize and integrate into a compact analytical system. For example, some portable systems incorporating external LEDs and photodetectors can weigh between 1 kg and 4 kg each. To address these limitations, several groups have successfully embedded photodetectors within integrated PCR platforms. However, these devices still rely on external excitation sources.

To address this limitation, we have developed an integrated microelectronic device for amplification and label-free detection of nucleic acids (Figure 1) [1]. Amplification by PCR is achieved with on-chip metal resistive heaters, temperature sensors, and microfluidic valves. We demonstrate a rapid thermocycling with rates of up to 50°C/s and a PCR product yield equivalent to that of a bench-top system. Amplicons within the PCR product are detected by their intrinsic charge with a silicon field-effect sensor. Similar to existing optical approaches with intercalators such as SYBR Green, our sensing approach can directly detect standard double-stranded PCR products while in contrast our sensor occupies a micron-scale footprint, dissipates only nano-watt power during operation, and does not require labeling reagents. By combining amplification and detection on the same device, we show that the presence or absence of a particular DNA sequence can be determined by converting the analog surface potential output of the field-effect sensor to a simple digital true/false readout.



▲ Figure 1: Device layout and concept. (top) Photograph of an integrated device with embedded sensors (right dotted area), PCR microfluidic channel with integrated valves (left dotted area), and metal-resistive heaters and temperature sensors (features above and below PCR channel). (bottom) A 3D rendering of the device centered on sensors (top and bottom squares) and an excitation metal electrode. Adjacent features include gold traces for electrical connections, inlet of the sensor channel, and an integrated valve controlling the interface to the PCR channel.



▲ Figure 2: The integrated PCR and field-effect sensing of product. The sensor was functionalized and pressure was applied to flow the content of PCR channel over electronic sensors, after which valves were closed and measurement buffer flow was restored. The PCR channel was replenished with starting PCR reagent as its contents flowed into the sensing channel. The greyed-out area indicates the period of PCR channel injection during which mechanical operations caused the sensor to lose its baseline value and drift temporarily. The higher and lower dotted segments are arbitrarily defined threshold levels for positive and negative signals, respectively.

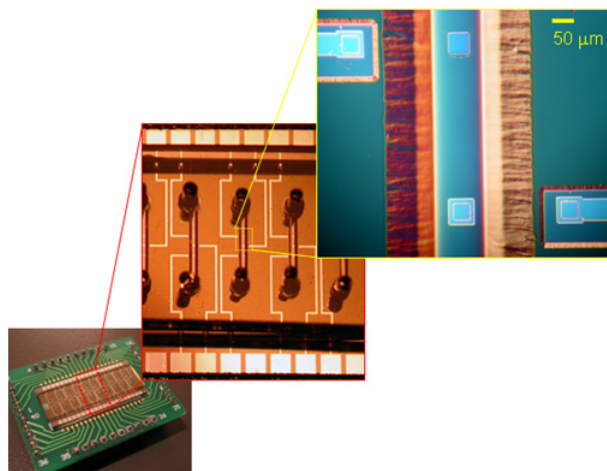
REFERENCES

- [1] C.J. Hou, M. Godin, K. Payer, R. Chakrabarti, and S.R. Manalis, "Integrated microelectronic device for label-free nucleic acid amplification and detection," *Lab on a Chip*, vol. 7, no. 3, pp. 347-354, Mar. 2007.

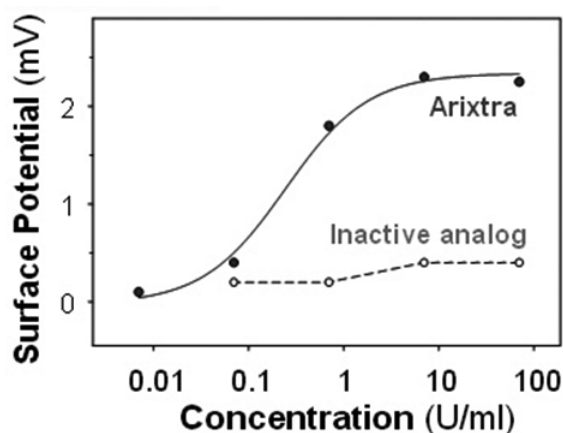
Monitoring of Heparin and its Low Molecular Weight Analogs by Silicon Field Effect

N. Milovic, J. Behr, M. von Muhlen, M. Godin, C.J. Hou, K.R. Payer, A. Chandrasekaran, P.R. Russo, R. Sasisekharan, S.R. Manalis
Sponsorship: Hewlett-Packard, AFOSR

Heparin is a highly sulfated glycosaminoglycan that is used as an important clinical anticoagulant. Monitoring and control of the heparin level in a patient's blood during and after surgery is essential, but current clinical methods are limited to indirect and off-line assays. We have developed a silicon field-effect sensor for direct detection of heparin by its intrinsic negative charge [1]. The sensor consists of a simple microfabricated electrolyte-insulator-silicon (EIS) structure encapsulated within microfluidic channels (Figure 1). As heparin-specific surface probes, we used the clinical heparin antagonist protamine or the physiological partner antithrombin III. The dose-response curves in 10% PBS revealed a detection limit of 0.001 U/ml, which is orders of magnitude lower than clinically relevant concentrations. We also detected heparin-based drugs, such as the low-molecular-weight heparin enoxaparin (Lovenox®) and the synthetic pentasaccharide heparin analog fondaparinux (Arixtra®) (Figure 2), which cannot be monitored by the existing near-patient clinical methods. We demonstrated the specificity of the antithrombin III functionalized sensor for the physiologically active pentasaccharide sequence. As a validation, we showed correlation of our measurements to those from a colorimetric assay for heparin-mediated anti-Xa activity. These results demonstrate that silicon field-effect sensors could be used in the clinic for routine monitoring and maintenance of therapeutic levels of heparin and heparin-based drugs and in the laboratory for quantitation of total amount and specific epitopes of heparin and other glycosaminoglycans.



▲ Figure 1: Optical micrograph of an array of silicon field-effect sensors for the detection of charged biomolecules such as heparin.



▲ Figure 2: Dose-response curve of the AT-III-sensor for the heparin-based pentasaccharide drug fondaparinux (●) and 6-O desulfated fondaparinux (○), which is known to exhibit low binding affinity for AT-III. Data points for fondaparinux fit with a Langmuir isotherm (solid line), and those for and 6-O desulfated fondaparinux are connected with a dashed line. Note that 0.2 U/mL ~ 1mg/ml ~ 50 nM.

REFERENCES

- [1] N. Milovic, J. Behr, M. Godin, C.J. Hou, K.R. Payer, A. Chandrasekaran, P.R. Russo, R. Sasisekharan, and S.R. Manalis, "Monitoring of heparin and its low-molecular-weight analogs by silicon-field effect," in *Proceedings of the National Academy of Sciences*, 2006, vol. 103. p. 13374.

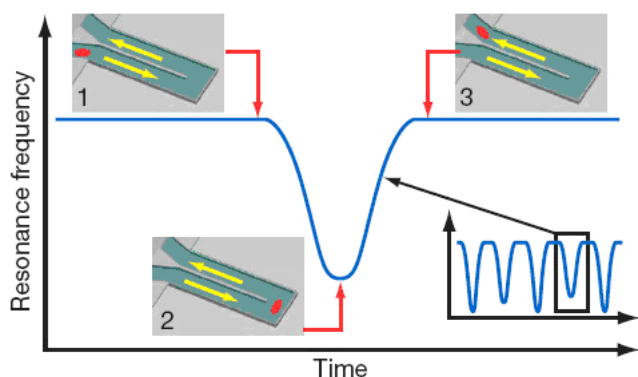
Weighing of Biomolecules, Single Cells and Single Nanoparticles in Fluid

T.P. Burg, M.Godin, W. Shen, G. Carlson, J.S. Foster, K. Babcock, S.R. Manalis

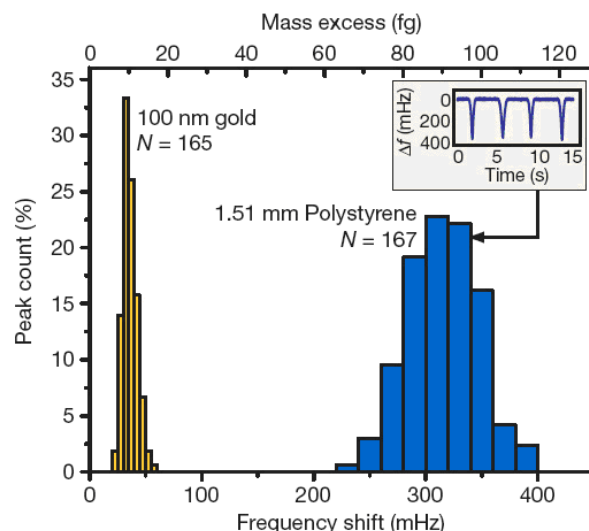
Sponsorship: NIH Cell Decision Process Center Grant, Institute for Collaborative Biotechnologies from the US Army Research Office, AFOSR

Nanomechanical resonators enable the measurement of mass with extraordinary sensitivity. Previously, samples as light as 7 zeptograms ($1 \text{ zg} = 10^{-21} \text{ g}$) have been weighed in vacuum, and proton-level resolution seems to be within reach. Resolving small mass changes requires the resonator to be light and to ring at a very pure tone—that is, with a high quality factor. In solution, viscosity severely degrades both of these characteristics, thus preventing many applications in nanotechnology and the life sciences where fluid is required. Although the resonant structure can be designed to minimize viscous loss, resolution is still substantially degraded when compared to measurements made in air or vacuum. An entirely different approach eliminates viscous damping by placing the solution inside a hollow resonator that is surrounded by vac-

uum (Figure 1). We have recently demonstrated that suspended microchannel resonators can weigh single nanoparticles (Figures 2), single bacterial cells, and sub-monolayers of adsorbed proteins in water with sub-femtogram resolution (1 Hz bandwidth). Central to these results is our observation that viscous loss due to the fluid is negligible compared to the intrinsic damping of our silicon crystal resonator. The combination of the low resonator mass (100 ng) and high quality factor (15,000) enables an improvement in mass resolution of six orders of magnitude over a high-end commercial quartz crystal microbalance [1]. This gives access to intriguing applications, such as mass-based flow cytometry, the direct detection of pathogens, or the non-optical sizing and mass density measurement of colloidal particles.



▲ Figure 1: A suspended microchannel translates mass changes into changes in resonance frequency. Fluid continuously flows through the channel and delivers biomolecules, cells, or synthetic particles. Sub-femtogram mass resolution is attained by shrinking the wall and fluid layer thickness to the micrometer scale and by packaging the cantilever under high vacuum. In one measurement mode, particles flow through the cantilever without binding to the surface, and the observed signal depends on the position of particles along the channel (inset 1 – 3). The exact mass excess of a particle can be quantified by the peak frequency shift induced at the apex.



▲ Figure 2: Synthetic particles of known size and density were measured to calibrate the mass sensitivity of the device. Gold nanoparticles ($100 \pm 8 \text{ nm}$) weighing 10 fg more than the water they displace produced a mean frequency shift of 36 mHz with a standard deviation of 6 mHz. On a different device, we measured a frequency shift of $310 \pm 30 \text{ mHz}$ for polystyrene microspheres ($1.51 \pm 0.01 \mu\text{m}$) with 90.1 fg mass excess.

REFERENCES

- [1] T.P. Burg, M. Godin, W. Shen, G. Carlson, J.S. Foster, K. Babcock, and S.R. Manalis, "Weighing of biomolecules, single cells, and single nanoparticles in fluid," *Nature*, to be published.

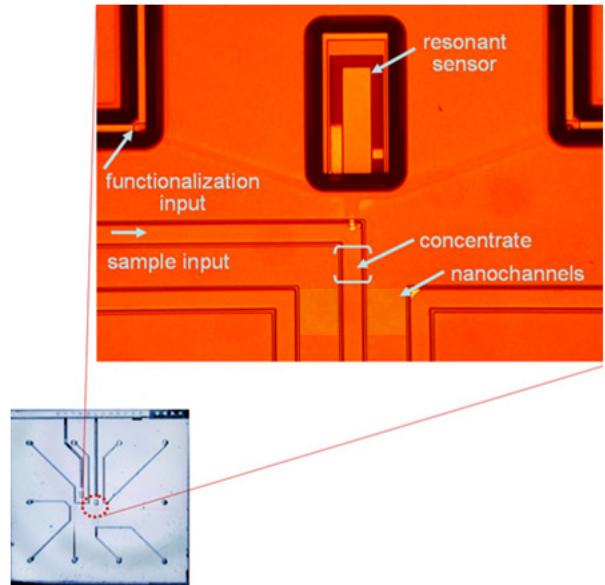
Integrated System for Cancer Biomarker Detection

P. Dextras, K. Payer, T. Burg, R. Chunara, Y.C. Wang, J. Han, S.R. Manalis
Sponsorship: NCI

There is evidence to suggest that the next generation of cancer-screening tests may employ not just one, but a small panel of less than ten biomarkers that together add statistical power to the detection of specific cancers. While immunoassays such as ELISA are well established for detection of antigen-based biomarkers, the fidelity of the assay is governed by the disassociation constant, K_d , of the antibody-antigen complex. If the antigen concentration is significantly below K_d , then the binding kinetics are slow and readout precision of the antigen-antibody complex can be degraded by noise.

We propose a general approach for improving the performance of ligand-receptor assays. The approach is based on a nano-fluidic device that controllably concentrates a dilute sample and an ultra-sensitive suspended microchannel resonant mass sensor that detects specific biomarkers within the concentrate. Since the amplification (or gain) of the concentrator is adjustable, the dynamic range and detection limit of the immunoassay can be governed by the properties of the concentrator and not K_d . Since the integrated concentration/detection system is batch-fabricated by conventional foundry-level processing techniques, the cost per device could potentially be less than ten dollars.

Over the past year, we have fabricated the first generation of integrated systems (Figure 1). The devices appear to be functional based on initial visual inspections. We are currently validating the performance of the system by using quantum dots for a calibration assay. We are also in the process of validating the performance of the concentrator and mass sensor (as individual components) with prostate-specific antigen so that we can make comparisons to existing methods in terms of sensitivity and selectivity.



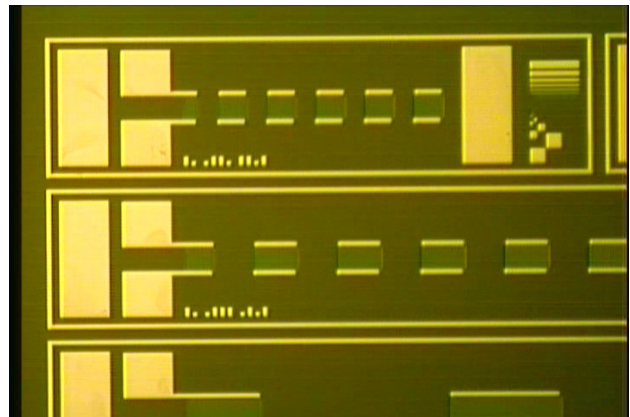
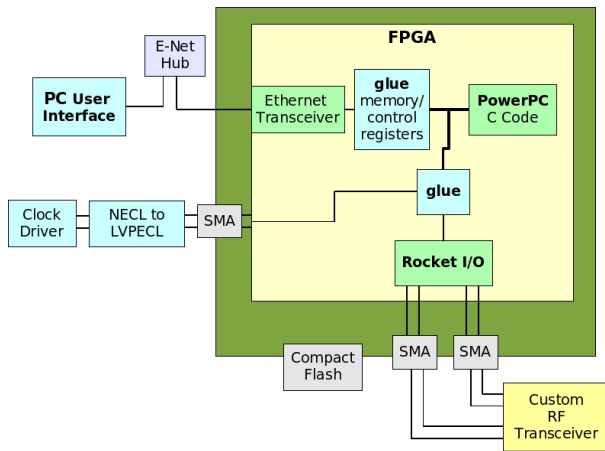
▲ Figure 1: Integrated system for concentration and detecting biomolecules.

Passive Microwave Transponders for Passive, Real-time, and High-sample-rate Localization

J. LaPenta, J. Paradiso
 Sponsorship: Media Laboratory, NanoStructures Laboratory

Passive surface acoustic wave (SAW) transponders have been used for RFID applications because of their zero-power and long-range (100m) capabilities. This work presents current research into utilizing SAW transponders for localizing objects. The SAW transponders have many advantages over existing localization solutions, including small size (mm x mm), zero-power, high-accuracy, longer range (100m), and kilohertz update rates. Unhindered localization of objects is desirable for many applications, from human computer interaction to product tracking to security. The SAW transponders offer improvements to existing solutions for asset tracking, location of lost articles, ubiquitous computing, tracking of people with special needs or prisoners, workers in hazardous situations, human machine interfaces, virtual training environments, security, location of short-range mobile sensors, and biomedical research. The goal of this project is to prototype this tracking system and evaluate the feasibility of a commercial system.

Multiple RADAR measurement stations use phase-encoded chirps to selectively track individual SAW transponders by triangulation of range and/or angle measurements. Update rates on the order of 10kHz with accuracies better than 10cm³ are conceivable. A 300-nm deep-uv contact-mask lithography nano-fabrication process to create these SAW devices is under development. Figure 1 shows the block diagram of the electronic test setup that is being used to characterize devices. Figure 2 shows a micrograph of a few of our fabricated devices. Recent results from this investigation will be presented, including the characterization of our first devices.



▲ Figure 1: Test electronics block diagram.

▲ Figure 2: The 3µm SAW devices.

REFERENCES

- [1] R. Brocato, "Passive microwave tags," Sandia National Laboratories, Livermore, CA, Sandia Report, 2004.
- [2] C. Campbell, *Surface Acoustic Wave Devices for Mobile and Wireless Communications*. San Diego: Academic Press, 1998.
- [3] K. Finkenzeller, *RFID Handbook, Second edition*. West Sussex, England: John Wiley & Sons, 2003.
- [4] H. Matthews, *Surface Wave Filters: Design, Construction, and Use*. New York: John Wiley & Sons, 1977.
- [5] P. Milstein and L. Das, "Surface acoustic wave devices." *IEEE Communications Magazine*, pp. 25-33, Sept. 1979.
- [6] L. Reindl, G. Scholl, T. Ostertag, H. Scherr, U. Wol, F. Schmidt, "Theory and application of passive saw radio transponders as sensors," *IEEE Transactions on Ultrasonics, Ferroelectrics and Frequency Control*, vol. 45, no. 5, pp. 1281-1292, Sep. 1998.
- [7] J. Bachrach and C. Taylor, "Localization in Sensor Networks." Cambridge, MA: Computer Science and Artificial Intelligence Laboratory at Massachusetts Institute of Technology, 2004.

Macroscopic Interfaces to Parallel Integrated Bioreactor Arrays

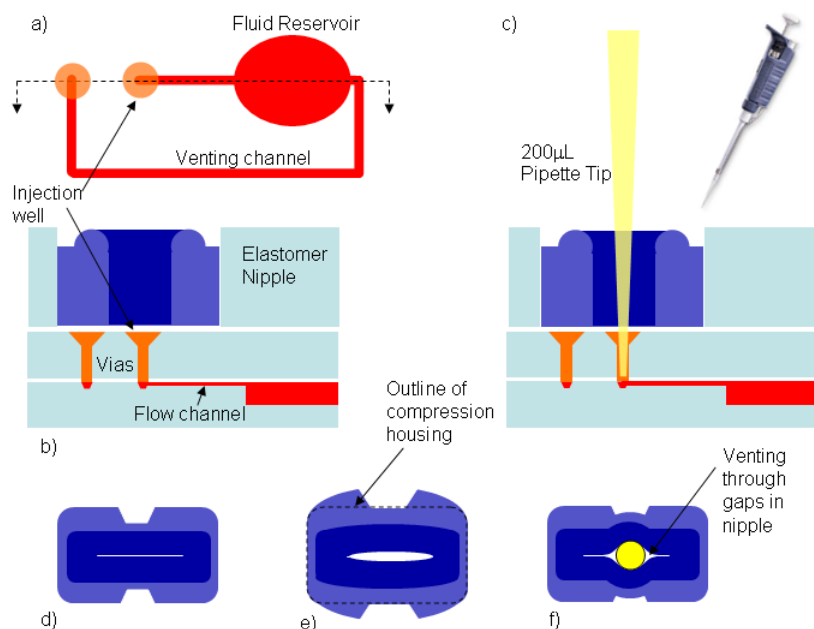
H. Lee, R.J. Ram, P. Boccazzi, A. Sinskey
Sponsorship: Lincoln Laboratory

Macroscopic fluidic interfaces are important for improving the usability of microfluidic devices. For example, in our previously developed parallel integrated bioreactor arrays [1], two needle punctures were required to fill each fluidic reservoir; one for fluid injection using a syringe and another needle to vent the air displaced by the injected fluid. While suitable for internal laboratory use, such an inconvenient fluid injection procedure impedes the adoption of this new bioreactor technology.

We have developed a fluid injection port that automatically vents the displaced air and is compatible with standard laboratory pipette tips. The principle of operation is shown in Figure 1. On opposite sides of each fluid reservoir (Figure 1a), there is a fluid injection channel and a vent channel. Both of these channels terminate in vias that connect the channels to the seat of the pipette interface nipple. The pipette-interface-nipple (Figure 1e) is an

elastomer structure, which, when compressed by its housing (Figure 1c), seals closed both vias such that fluid can neither escape nor enter the fluid reservoir. When a pipette tip is inserted into the interface-nipple, it is deformed and allows air to escape from the vent port (Figure 1f). Meanwhile, the inserted pipette tip seals to the via connected to the fluid injection channel and fluid can be injected into the reservoir. The particular bow-tie shape of the pipette-interface-nipple was chosen such that when it is inserted into a rectangular housing, sufficient compressive force would seal the central slit closed while also allowing space for the nipple to expand upon insertion of the pipette tip.

Fabricated devices exhibited good operating characteristics and provided a seal against a greater-than-10psi back pressure.



▲ Figure 1: Auto-venting and pipette compatible fluid injection port. a) Schematic view of an underlying microfluidic device with channels and a fluid reservoir. b) Cross-section showing device layers along with interface nipple and compression housing. c) Cross-section with inserted pipette tip. d) Interface-nipple inside compression housing; slit is sealed. e) Uncompressed, as-fabricated, interface nipple. Dotted line indicates compression housing dimensions. f) Compressed interface nipple showing inserted pipette tip and consequent deformation of the nipple.

REFERENCES

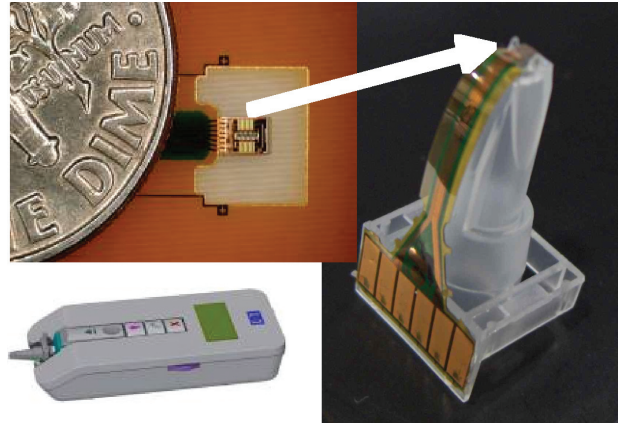
- [1] H.L.T. Lee, P. Boccazzi, A.J. Sinskey, and R.J. Ram, "Micro-bioreactor arrays with integrated mixers and fluid injectors for high-throughput experimentation with pH and dissolved oxygen control," *Lab on a Chip*, vol. 6, pp. 1229-1235, June 2006.

MIT-OSU-HP Focus Center on Non-lithographic Technologies for MEMS and NEMS

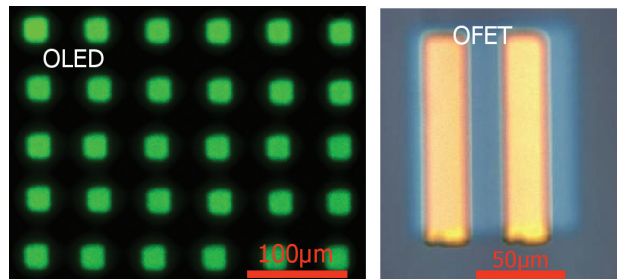
M.A. Schmidt (in coll. with S.G. Kim, C.G. Sodini, V. Bulović, MIT; D. Keszler, J. Wager, M. Subramanian, OSU; P. Benning, M. Chaparala, J. Stasiak, J. Thompson, Hewlett-Packard)
Sponsorship: AFOSR

This newly formed center is part of an overall set of centers on MEMS/NEMS fundamentals supported by DARPA. The MIT-OSU-HP Focus Center aims to develop new methods for fabrication of MEMS and NEMS that do not use conventional lithographic methods. The Center leverages the leading expertise of MIT and OSU in MEMS and printed devices, with the printing expertise of HP. The focus center is organized into four primary areas: tools, materials and devices, circuits, and demonstration systems.

In the area of tools, we are leveraging the existing thermal inkjet (TIJ) technology of HP and augmenting it with specific additional features, which expand the palette of available materials for printing. We are developing materials and devices over a broad spectrum from active materials, photonic and electronic materials, to mechanical materials. In the circuits area, we are studying the behavior of the devices that can be realized in this technology with the goal of developing novel circuit architectures. Lastly, we intend to build several “demonstration” systems that effectively communicate the power of the new technologies that will emerge from this center.



▲ Figure 1: An HP TIPS system for direct printing of a wide range of MEMS and electronic/photonic materials.



▲ Figure 2: Examples of printed optical and electronic devices.

A Micromachined Printhead for the Evaporative Printing of Organic Materials at Ambient Pressure

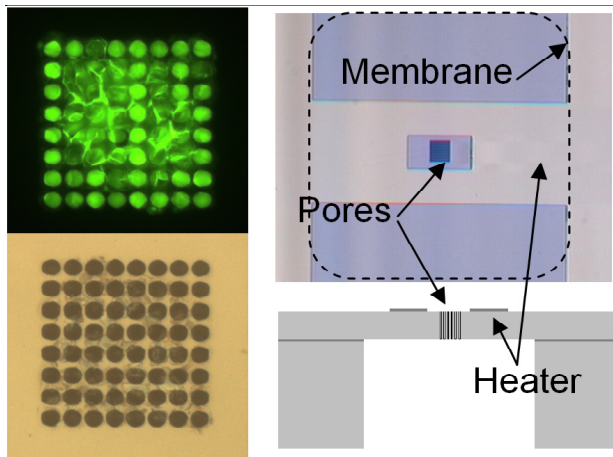
V. Leblanc, J. Chen, P. Mardilovich, V. Bulović, M.A. Schmidt
Sponsorship: Hewlett-Packard, DARPA

Organic optoelectronic devices are promising for many commercial applications if methods for fabricating them on large-area, low-cost substrates become available. Our project investigates the use of MEMS in the direct patterning of materials needed for such devices. By depositing the materials directly from the gas phase, without the liquid phase coming in contact with the substrate, we aim at avoiding the limitations due to inkjet printing of such materials.

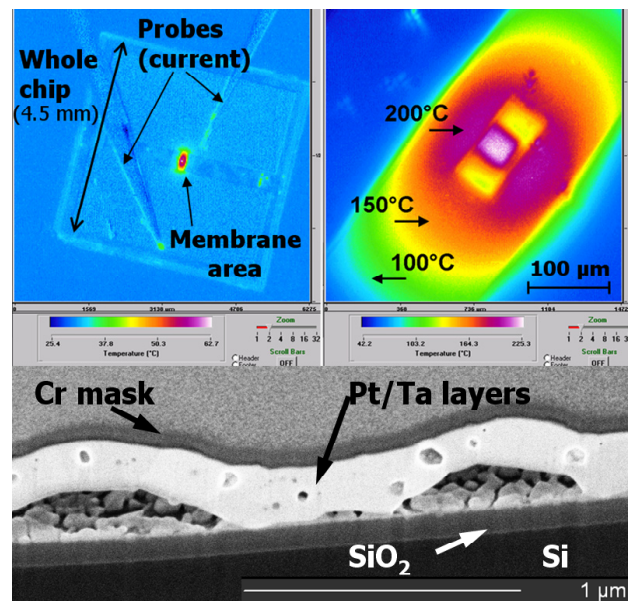
We developed a MEMS-enabled technique for evaporative printing of organic materials. This technique does not require a vacuum ambient, has a fast printing rate (1 kHz), and can be scaled up to an array of individually addressable nozzles. The MEMS printhead comports a microporous layer with integrated heaters for local evaporation of the materials. Figure 1 shows the micro-fabricated device: an array of 2 micron pores and an integrated

thin film platinum heater sit in the center of a silicon membrane. The material to be printed is delivered to the porous region in liquid or gas phase and deposits inside the pores (see Figure 1, top left). The integrated heater then heats up the porous area (see Figure 2, top) and the material is re-evaporated from the pores onto the substrate. The main limitation of this printhead is the failure of the thin-film platinum heater at temperatures above 800°C (see Figure 2 bottom).

This printhead was used, together with inkjet technology for the delivery of material to the pores, to print molecular organic semiconductors (see other abstract in this volume). Our technique enables printing of organic optoelectronics over large areas and can be used to print on a variety of substrates, does not require a vacuum ambient, and thus could enable low-cost printing of optoelectronics.



▲ Figure 1: Left: Pictures of the pores. Top: Fluorescent image after Alq3 material was loaded in the pores. Bottom: Optical image after re-evaporation of the material. Right: Top view and schematic of device.



▲ Figure 2: Top: Infrared microscope measurements of the temperature of a printhead chip. Bottom: An SEM image of a Focused Ion Beam cross-section of a failed heater.

REFERENCES

- [1] V. Leblanc, J. Chen, S.H. Kang, V. Bulović, and M.A. Schmidt, "Micromachined printheads for the evaporative patterning of organic materials and metals," *Journal of Microelectromechanical Systems*, to be published.
- [2] V. Leblanc, J. Chen, V. Bulović, and M.A. Schmidt, "A micromachined printhead for the direct evaporative patterning of organic materials," in *Proc. Digital Fabrication*, Denver, Sep. 2006, pp. 74-78.
- [3] V. Leblanc, J. Chen, P. Mardilovich, V. Bulović, and M.A. Schmidt, "Evaporative printing of organic materials at ambient pressure using a micromachined printhead," in *Proc. Fourteenth International Conference on Solid-State Sensors, Actuators and Microsystems*, Lyon, France, June 2007.

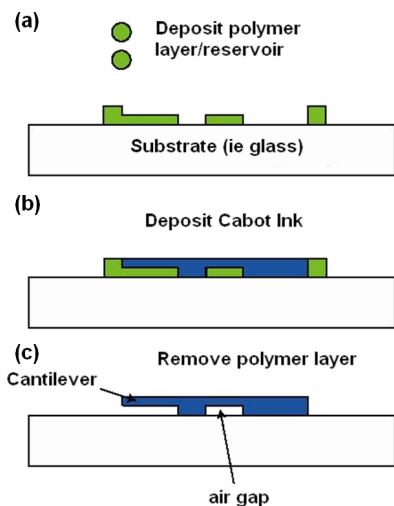
Surface Micromachining Processes using Non-lithographic Technologies

E.W. Lam, V. Leblanc, J. Chen, V. Bulović, M.A. Schmidt
 Sponsorship: DARPA, Hewlett-Packard

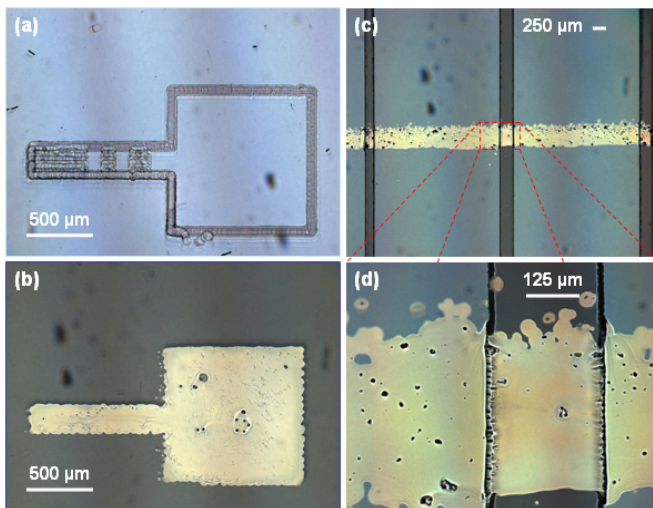
Conventional MEMS fabrication relies heavily on planar lithography and IC technology. While these techniques are well-suited for relatively flat devices such as the semiconductors, they are drastically limited in the design and fabrication of three-dimensional devices such as MEMS. From a commercial viewpoint, the semiconductor paradigm is also a poor fit for MEMS because the lower volume and demands make it more difficult to offset the high production costs. Ridding MEMS fabrication of its reliance on such techniques may introduce several advantages, namely a wider base of substrate materials and decreased costs.

Our project investigates severing MEMS fabrication from the semiconductor paradigm via non-lithographic technologies. We have previously shown how MEMS can be used for the direct patterning of small molecular organics [1]. Using similar concepts, we intend to show that surface micromachining can also be achieved.

The first stage of the project is to directly pattern a structural layer over a spacer and successfully release a cantilever. We have successfully patterned metal silver over various spacer materials, including polyethylene glycol (PEG), polyvinyl acetate (PVA), and UNITY™ sacrificial polymer, and we are currently working on the release process. This technique will ultimately be used to construct simple structures, such as cantilevers and bridges, to test the structural material's mechanical properties. The next stage of this project will consist of using this process to fabricate cantilevers and integrate them with other non-lithographic techniques to fabricate an accelerometer. Subsequent stages will consist of creating a library of non-lithographic processes so that entire MEMS devices can be fabricated without the use lithography.



▲ Figure 1: Basic approach of direct surface micromachining. (a) Spacer layer (green) is deposited. (b) Metal silver ink (blue) is deposited and sintered. (c) Spacer material is removed to release structure.



▲ Figure 2: Experimental results of directly processing spacer or structural materials. (a) Spacer material patterned as a reservoir with raised features. (b) Metal silver deposited in shape of reservoir (no spacer underneath). (c) Silver deposited over patterned photoresist (PR) lines. (d) Magnified view of silver over PR line.

REFERENCES

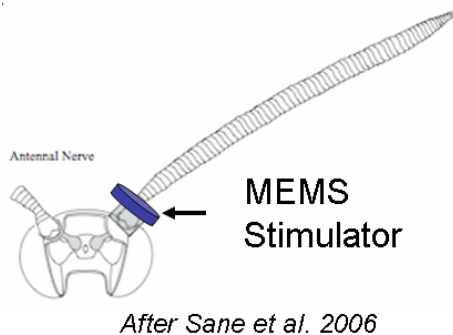
[1] J. Chen, V. Leblanc, S.-H. Kang, M.A. Baldo, P.J. Benning, V. Bulović, and M.A. Schmidt, "Direct patterning of organics and metals using a micro-machined printhead," in *Proc. MRS Spring 2005*, San Francisco, CA, Mar.-Apr. 2005, pp. H1.8:1-7

Micromechanical Actuators for Insect Flight Mechanics

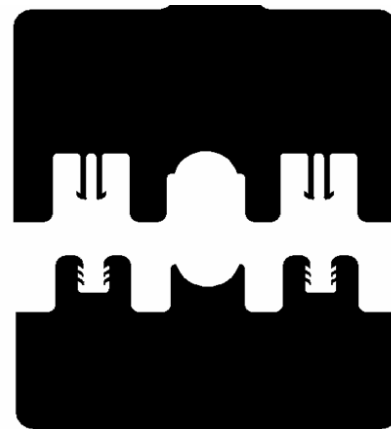
H. Zhou, M.A. Schmidt (in coll. with T.L. Daniel, University of Washington)
Sponsorship: AFOSR

This project aims to develop MEMS actuators to aid in the study of insect flight mechanics. Specifically, we are developing actuators that can stimulate the antennae of the crepuscular hawk moth *Manduca Sexta*. The possible mechanosensory function of antennae as airflow sensors has been suggested [1], and recent discoveries of our collaborators reveal that mechanosensory input from the antennae of flying moths serves a similar role to that of the hind wings of two-winged insects, detecting Coriolis forces and thereby mediating flight stability during maneuvers [2]. Early evidence suggests that mechanical stimulus of the antennae may enable flight control. In addition, the crepuscular hawk moth *Manduca Sexta* has a wide wingspan (~110 mm) and is capable of carrying at least one quarter of its own weight. Thus, studying the flight of *M. Sexta* by attachment of microsystems seems plausible. The goal of our project is to design and fabricate micromechanical actuators, which will be mounted onto the moth antennae (Figure 1). Our collaborators will study the flight control mechanism by mechanical stimulation.

Our first step is to fabricate “dummy” silicon rings for our biologist collaborators for implant experiments. The diameters along the antenna vary from tip to base, being thickest in the middle. As a result, in order to prevent the ring’s being thrown off, the mounting of the silicon ring onto the base cannot be as simple as pushing it from the tip with a large inner hole. On the other hand, the sizes of the antennae vary from moth to moth. Two-piece construction was designed and fabricated to be like a “zip strip” to meet the mounting requirements (Figure 2). Future work will focus on refining the design and fabrication of the mounting kit and integrating actuators into it. To generate adequate displacement, strain amplification will be needed, such as reported by Conway, et al. [3].



▲ Figure 1: Schematic view of mechanical actuators for hybrid insects MEMS.



▲ Figure 2: “Zip-strip-” like mounting kit for *M. Sexta* moth antennae.

REFERENCES

- [1] M. Gewecke, “Antennae: Another wind-sensitive receptor in locusts,” *Nature*, vol. 225, no. 5239, pp. 1263-1264, Mar. 1970.
- [2] S.P. Sane, A. Dieudonné, M.A. Willis, and T.L. Daniel, “Antennal mechanosensors mediate flight control in moths,” *Science*, vol. 315, pp. 863-866, Feb. 2007.
- [3] N.J. Conway and S.-G. Kim, “Large-strain, piezoelectric, in-plane micro-actuator,” in *Proc. 17th IEEE International Conference on Micro Electro Mechanical Systems*, Maastricht, the Netherlands, Jan. 2004, pp. 454 - 457.

MEMS Micro-vacuum Pump for Portable Gas Analyzers

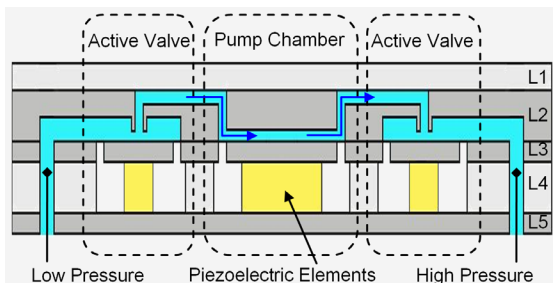
V. Sharma, M.A. Schmidt
Sponsorship: DARPA

There are many advantages to miniaturizing systems for chemical and biological analysis. Recent interest in this area has led to the creation of several research programs, including a Micro Gas Analyzer (MGA) project at MIT. The goal of this project is to develop an inexpensive, portable, real-time, and low-power approach for detecting chemical and biological agents. Elements entering the MGA are first ionized, then filtered by a quadrupole array, and sensed using an electrometer. A key component enabling the entire process is a MEMS vacuum pump, responsible for routing the gas through the MGA and increasing the mean free path of the ionized particles so that they can be accurately detected.

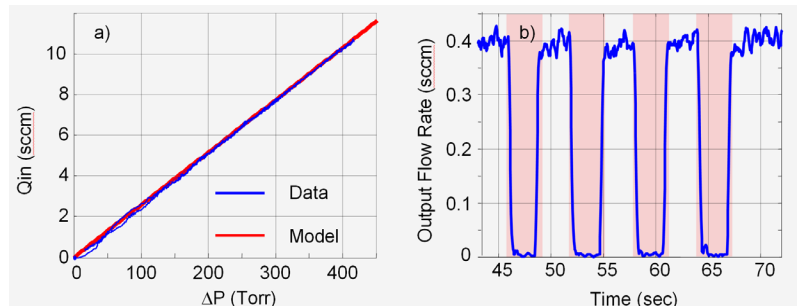
There has been a great deal of research done over the past 30 years in the area of micro pumping devices [1, 2]. We are currently developing a displacement micro-vacuum pump that uses a piezoelectrically driven pumping chamber and a pair of piezoelectrically driven active-valves; the design is conceptually similar to the MEMS pump reported by Li et al. [3]. We have constructed an accurate compressible mass flow model for the air flow [4] as well as a nonlinear plate deformation model for the stresses experienced by the pump parts [5]. Using these models,

we have defined a process flow and fabricated three generations of the MEMS vacuum pump over the past year and are currently working on the fourth.

A schematic of the pump is shown in Figure 1. For ease in testing we have initially fabricated only Layers 1-3 and have constructed a testing platform that, under full computer control, drives the pistons and monitors the mass flows and pressures at the ports of the device. The lessons learned from the first three generations of the pump have led to numerous improvements. Every step from the modeling to the etching and bonding to the testing has been modified and improved along the way. The most recent third generation pump test data is shown in Figure 2. Figure 2a shows the pressure versus flow rate characteristics of the pump; note that the data compares very well with models. Figure 2b shows the output flow rate versus actuation characteristics of the pump. Notice that the flow goes to zero each time the piston is actuated upwards (red bar). All three pistons demonstrated similar performance illustrating a pump with fully functioning pistons and tethers. Next, we hope to characterize the pumping characteristics of this and the upcoming fourth-generation pumps.



▲ Figure 1: Schematic of the MEMS Vacuum Pump. Layers 1 and 4 are glass, Layer 2 forming the chambers and channels is DSP silicon, Layer 3 forming the pistons and tethers is SOI silicon, and Layer 5 is SSP silicon.



▲ Figure 2: a) Pressure versus flow rate characteristics of the pump compares very well with models (ΔP = input pressure – output pressure). b) Output flow rate versus actuation characteristics of the pump. Notice that the flow goes to zero each time the piston is actuated upwards (actuation indicated by transparent red bar).

REFERENCES

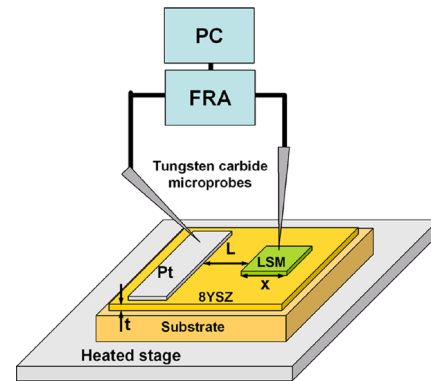
- [1] D.J. Laser and J.G. Santiago, "A review of micropumps," *J. of Micromechanics and Microengineering*, vol. 14, no. 6, pp. 35-64, June 2004.
- [2] P. Woias, "Micropumps—past, progress and future prospects," *Sensors and Actuators B: Chemical*, vol. 105, no. 1, pp. 28-38, Feb. 2005.
- [3] H.Q. Li, D.C. Roberts, J.L. Steyn, K.T. Turner, J.A. Carretero, O. Yaglioglu, Y.-H. Su, L. Saggere, N.W. Hagood, S.M. Spearing, M.A. Schmidt, R. Mlcak, and K. Breuer, "A high-frequency, high flow rate, piezoelectrically driven MEMS micro-pump," presented at the *IEEE Solid State Sensors and Actuators Workshop*, Hilton Head SC, June 2000.
- [4] A.K. Henning, "Improved gas flow model for micro-valves," in *Proc. Transducers 2003*, Boston, MA, USA, June 2003, pp. 1550-1553.
- [5] D.C. Roberts, O. Yaglioglu, J.Carretero, Y.-H Su, L. Saggere, and N.W. Hagood, "Modeling, design, and simulation of a piezoelectrically driven microvalve for high pressure, high frequency applications," in *Proc. SPIE - The International Society for Optical Engineering, Smart Structures and Materials 2001- Smart Structures and Integrated Systems*, Newport Beach, CA, Mar. 2001, pp. 366-380.

Microfabricated Electrodes for Solid Oxide Fuel Cells

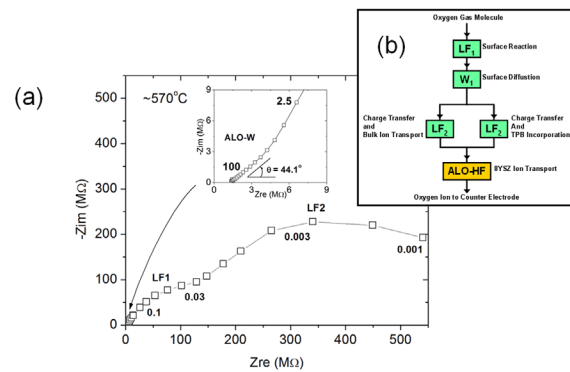
G.J. la O', Y. Shao-Horn
 Sponsorship: Ford-MIT Alliance, NSF, CMSE

The solid oxide fuel cell (SOFC) is an energy-conversion device that produces electricity directly through the electrochemical reaction of hydrogen (H_2) and oxygen (O_2). The SOFC also allows utilization of hydrocarbons, such as methane (CH_4), via internal reforming or direct electrochemical oxidation, giving these systems the flexibility of using a variety of commercially available fuels. The high energy-density of hydrocarbon fuels makes the SOFC attractive for large-scale stationary systems and as a replacement to batteries for powering portable electronic devices. Standard SOFCs operate in the temperature range of 800°C-1000°C and have an open circuit voltage of approximately 1-volt. The most common SOFC materials are yttria-stabilized zirconia (YSZ) for the electrolyte, strontium-doped lanthanum manganite (LSM) for the cathode and nickel (Ni)-YSZ for the anode. Although elevated temperature operation allows the use of non-noble metal catalysts and excellent high-grade heat exhaust to be used for additional power generating cycles, there are numerous advantages to lowering the SOFC operating temperature to around 600°C. Benefits such as lower thermal stress, reduced cell degradation, utilization of metallic components, and shorter startup times are a few. However, at these lower temperatures the poor electrochemical activity of the electrodes, in particular the LSM cathode, leads to unacceptable voltage losses that lower the efficiency and performance of the SOFC.

Oxygen reduction mechanisms on the perovskite material $La_xSr_{1-x}MnO_{3-d}$ (LSM) has been widely studied; however, no final conclusion on the molecular level mechanisms for oxygen reduction has been made. To probe the oxygen reduction reaction, we fabricate electrodes with precise geometries (50-200 μm) using thin-film deposition techniques (sputtering and laser ablation) and subsequent photolithography to investigate the fundamental electrode mechanisms and rate-determining reactions. The electrochemical impedance spectroscopy (EIS) response of a $La_{1-x}Sr_xMnO_{3-d}$ (LSM) microelectrode on 8YSZ is then analyzed as a function of geometry and temperature using a microprobe station equipped with a high temperature stage, as Figure 1 shows. Our preliminary EIS results¹ shown in Figure 2a show at least four distinct reaction processes for oxygen reduction on LSM/8YSZ: (i) ion transport in 8YSZ with average activation energy (E_a) of $1.16 \pm 0.02 eV$, (ii) surface diffusion on LSM with E_a ranging from $1.34 \pm 0.05 eV$ to $1.65 \pm 0.03 eV$, (iii) at least one surface chemical process on LSM with E_a ranging from $1.71 \pm 0.02 eV$ to $1.88 \pm 0.02 eV$ and an average capacitance $3.4 \times 10^{-4} F/cm^2$, and (iv) a mixed bulk/TPB charge transfer process with E_a ranging from $2.42 \pm 0.02 eV$ to $3.05 \pm 0.03 eV$ and an average capacitance of $3.2 \times 10^{-3} F/cm^2$. The overall oxygen reduction process is illustrated in Figure 2b, with the rate-limiting reaction for ORR found to be from mixed bulk/TPB charge transfer processes below 700°C and shifts to surface chemical reactions above 700°C.



▲ Figure 1: Electrochemical impedance spectroscopy configuration for microfabricated SOFC cathodes (LSM) tested using a microprobe station with high temperature stage.



▲ Figure 2: Nyquist plot of typical impedance response from LSM microelectrodes on 8YSZ at 570°C in air showing ALO-HF, ALO-W, LF1 and LF2 features that are correlated to 8YSZ ion transport, LSM surface diffusion, surface reaction, and tpb/bulk process, respectively.

REFERENCES

[1] G.J. la O', B. Yildiz, S. McEuen, and Y. Shao-Horn, "Probing oxygen reduction reaction kinetics of Sr-doped $LaMnO_3$ supported on yttria stabilized zirconia: An electrochemical impedance study of dense, thin-film microelectrodes," *Journal of the Electrochemical Society*, vol. 154, no. 4, pp. B427-B438, Apr. 2007.

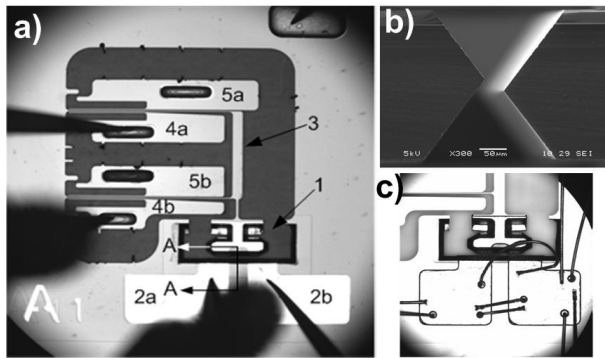
A MEMS-relay for Power Applications

A.C. Weber, J.H. Lang, A.H. Slocum
 Sponsorship: NSF Collaborative Research: Atomic Plane Electrical Contacts

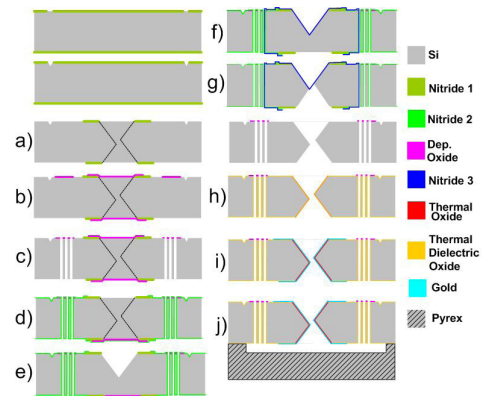
Contact travel and heat dissipation are important requirements of electrical power switching devices such as MEMS-relays and MEMS-switches. Whereas low-power MEMS-based RF switches have been vigorously studied, few studies have been reported on high-power MEMS-relays. This paper presents a MEMS-relay for power applications. The device is capable of make-break switching; has large contact travel, on the order of 10's of μm ; and has low contact resistance, on the order of 120 m Ω . Testing has demonstrated current carrying capacity on the order of several amperes and hot-switching of inductive loads, on the order of 10mH, without performance degradation.

The MEMS-relay, shown in Figure 1a, is bulk micromachined in (100) silicon and bonded to a glass substrate. Anisotropic etching

is used to fabricate the oblique and parallel (111) contact surfaces, having nanometer-scale surface roughness [1]. Figure 1b shows a cross section of the open fabricated contacts. An offset between the wafer-top and the wafer-bottom KOH masks produces the contact geometry shown. The silicon contact metal surfaces are created by evaporation and electroplating with a conductive film, shown in Figure 1c. A thermal oxide layer provides insulation between the actuators and the contacts. Deep reactive ion-etching (DRIE) is used to pattern a parallelogram-flexure compliant mechanism and a pair of rolling-point “zipper” electrostatic actuators [2]. Nested masks are used to pattern both wafer-through etches. Figure 2 illustrates the process used to fabricate the device.



▲ Figure 1: Device after fabrication. Die top view (a), contact cross section A-A of oblique contacts as shown in Figure 1a (b), contact electroplating (c).



▲ Figure 2: Fabrication Process. Nitride mask for KOH-etch (a), sacrificial oxide (b), DRIE (c), nitride passivation; patterning with shadow wafer (d), top KOH-etch (e), nitride passivation (f), bottom KOH-etch (g), dielectric oxide growth (h), metallization (i), bonding (j).

REFERENCES

- [1] A.C. Weber, J.H. Lang and A.H. Slocum, “{111} Silicon etched planar electrical contacts for power MEMS-relays,” in *Proc. 53rd IEEE Holm Conference on Electrical Contacts*, Pittsburgh, PA, Sep. 2007
- [2] J. Li, M.P. Brenner, T. Christen, M.S. Kotilainen, J.H. Lang, and A.H. Slocum, “Deep-reactive ion-etched compliant starting zone electrostatic zipping actuators”, *Journal of MEMS*, vol. 14, no. 6, pp. 1283-1297, Dec. 2006.

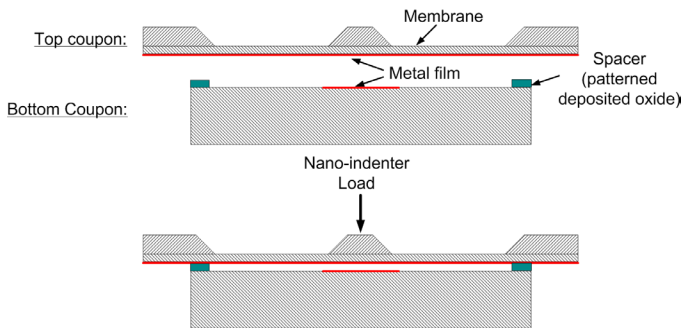
A Silicon-etched, Electrical-contact Tester

A.C. Weber, A.H. Slocum, J.H. Lang
Sponsorship: NSF Collaborative Research, Atomic Plane Electrical Contacts

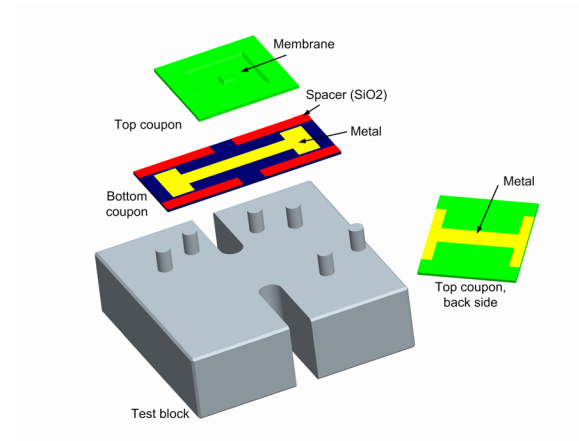
We are developing a bulk micromachined contact tester to investigate the electro-tribological performance of micro- and nano-structured planar electrical contacts [1]. The test device features parallel, planar, nanometer-scale surface roughness contacts etched in silicon coated with thin conductive films. Contacts used in microsystems, probes and interconnects are subject to heat dissipation and to electro-mechanical tribological effects. With an understanding of how nanoscale surface and subsurface material structure affect electrical contact resistance and mechanical contact wear, a deterministic manufacturing process could be developed to design electrical contacts from crystalline plane surfaces as potential high performance contacts for MEMS devices and related applications.

The microfabricated contact tester, shown in Figure 1 and in Figure 2, consists of a pair of parallel planar contact surfaces with nanometer roughness patterned onto two (100) Si substrates. Anisotropic etching is used on one of the substrates to create a membrane that serves as a compliant mechanism for the contact tester. A thin conductive film, i.e., Au, is patterned onto the

contacts in a Kelvin configuration. The two-piece tester architecture allows for inspection of the contacts before, during, or after testing without destruction of the test device. In one embodiment of the tester, a quasi-kinematic coupling enables the alignment between the substrates while providing the initial gap between the contacts. Similar quasi-kinematic designs fabricated in silicon substrates have reported repeatability on the order of 1 micrometer [2]. In a second embodiment of the MEMS-tester a patterned oxide film is used to provide the initial space between the contacts. The tester will be loaded using a commercial nanoindenter to bring the surfaces into contact as contact resistance is measured as a function of the force.



▲ Figure 1: Schematic view of the contact tester.



▲ Figure 2: Exploded view of the contact tester. The back side of the top coupon indicates the patterned metal used for the Kelvin contact configuration.

REFERENCES

- [1] A.C. Weber, G. Bassiri, B.M. Dvorak, A.H. Slocum, D.A. Lucca, and J.H. Lang, "Atomic Plane Electrical Contacts", in *Proceedings of the 7th European Society of Precision Engineering (EUSPEN) International Conference*, Bremen, Germany, May 2007
- [2] A.H. Slocum and A.C. Weber, "Precision passive mechanical alignment of wafers," *Journal of MEMS*, vol. 12, no. 6, pp. 826-834, Dec. 2003

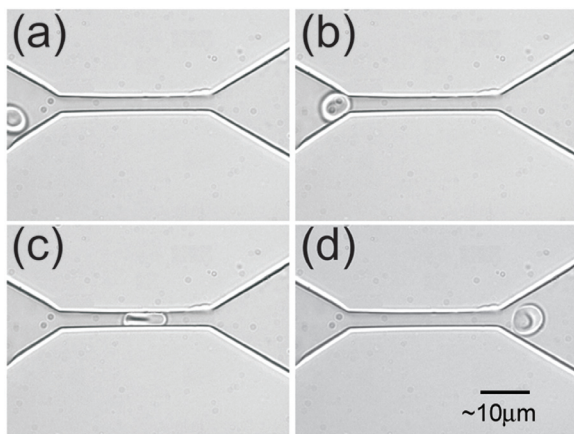
Microfluidic Studies of Biological Cell Deformability and Rheology

D. Quinn, S. Navlakha, N. Walter, A. Micoulet, S. Suresh
Sponsorship: Singapore-MIT Alliance, NSF

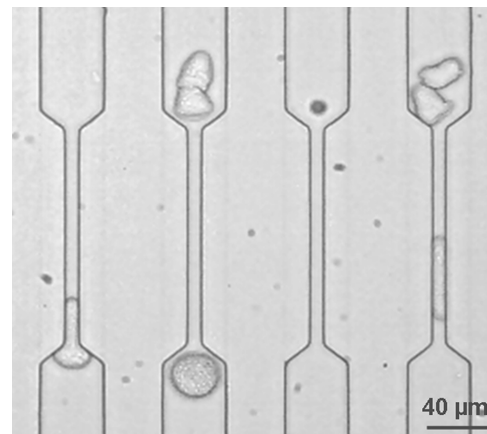
It is well known that many hereditary or infectious diseases, as well as certain types of cancer, produce alterations in mechanical properties of human cells. In certain diseases, such as malaria, infected cells exhibit reduced deformability and increased cytoadherence. Such changes alter the circulatory response of red blood cells (RBCs) and limit physiological responses to such diseases, such as splenic clearance of parasitized RBCs, and restrict circulation of RBCs in the microvasculature. In other diseases, such as pancreatic cancer under certain conditions, cancerous cells may exhibit enhanced deformability, which may contribute to an increased probability of metastasis.

Several projects in the Suresh research group aim to utilize microfabricated structures to experimentally evaluate the circulatory response of diseased human cells. In these studies, microfabricated channels of polydimethylsiloxane (PDMS) are used in conjunction with a fluidic system and a high-speed camera to quantify the biorheological behavior of cells under different conditions. In the case of diseases involving RBCs, cells are made to pass through a

narrow (~3 micrometer square) channel under a known pressure differential. During this process, shown in Figure 1, the average velocity and characteristic entrance and exit and shape recovery times are indicative of the overall biorheological response of the cell during microcirculation. Current results indicate large differences in rheological behavior of cells of different ages and incubation times. In addition, initial results from *Plasmodium falciparum* parasitized RBCs indicate a possible effect of exported proteins from the malaria-inducing parasite to the surface of the RBC membrane on the rheological behavior of RBCs. Similar experiments are also being conducted on pancreatic cancer cells (Panc-1), as seen in Figure 2. In these cells, the biorheology of cells is assessed in environments similar to those experienced during metastasis. Future work with these systems will aim to further identify particular proteins or biochemical interactions that affect the biorheological and circulatory behavior of diseased cells with the aim of developing enhanced understanding of the mechanisms of disease progression and possible avenues for treatment.



▲ Figure 1: An experimental *in vitro* demonstration of the “fluidization” of a healthy human RBC through a microfluidic channel at room temperature. The series of images show the shape of an RBC as it is squeezed through a 4 μm x 4 μm channel, made of polydimethylsiloxane (PDMS), under a pressure differential of 1-2 mm of water at approximately 0.4 seconds/frame. Note the recovery of shape upon egress from the channel.



▲ Figure 2: Pancreatic cancer cells (Panc-1) passing through narrow constrictions. The cells pass through 8 μm x 18 μm PDMS channels under an applied flow rate of ~0.5 $\mu\text{l}/\text{min}$ and an approximate pressure differential of 4kPa.

REFERENCES

- [1] S. Suresh, “Mechanical response of human red blood cells in health and disease: Some structure-property-function relationships,” *Journal of Materials Research*, vol. 21, pp. 1871-1877, Aug. 2006.
- [2] S. Suresh, J. Spatz, J.P. Mills, A. Micoulet, M. Dao, C.T. Lim, M. Beil, and T. Sefferlein, “Connections between single-cell biomechanics and human disease states: Gastrointestinal cancer and malaria,” *Acta Biomaterialia*, vol. 1, pp. 15-30, Jan. 2005.

Phase Change Materials for Actuation in MEMS

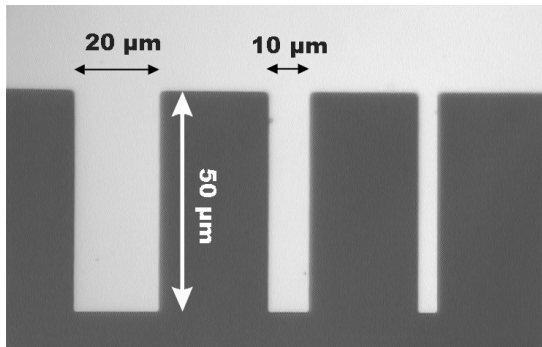
J.A. Kalb, Q. Guo (Singapore-MIT Alliance), X.Q. Zhang (National University of Singapore), C.H. Sow (National University of Singapore), Y. Li (National University of Singapore), C.V. Thompson
Sponsorship: Alexander von Humboldt Foundation, Singapore-MIT Alliance

Phase change materials (Sb and Te alloys) are used for optical data storage in commercial phase change memories, such as rewritable compact discs (CD±RW) and rewritable digital video disks (DVD±RW, DVD-RAM) [1]. Recently, they have also shown high potential for the development of phase change random access memories (PC-RAMs or PRAMs), which might replace flash memories in the future [2]. In this project, thin films of phase change materials are systematically analyzed with regard to their transformation behavior under laser-induced amorphization and crystallization. The goal of this project is to gain a better understanding of the relationship among the laser parameters, the material-specific transformation kinetics, and the involved volume changes (and associated mechanical stresses) over a wide range of alloy compositions.

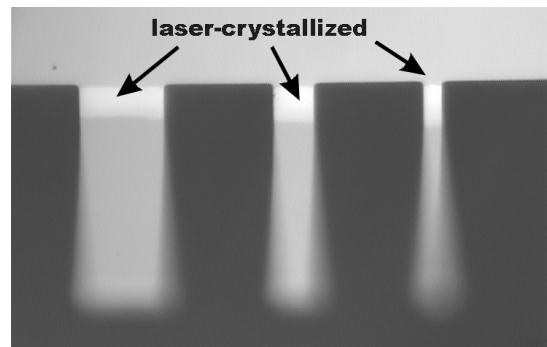
The approach to pursuing this goal is to use microfabricated SiN cantilevers as substrates for thin film deposition: The SiN cantilevers are manufactured by chemical vapor deposition of low-stress SiN on Si wafers, patterning the SiN film using optical lithography and revealing the cantilevers using dry etching and wet etch-

ing. Thin films of phase change materials are subsequently sputter-deposited on these SiN cantilevers and are locally switched by laser heating from the amorphous to the crystalline phase (and vice versa). The associated stresses induce a cantilever bending, which is measured by optical microscopy and non-contact interferometry as a function of laser annealing parameters, laser quench rate and alloy composition (Figures 1 and 2). Additionally, amorphous films are hot-stage crystallized, which allows the study of the kinetics associated with the crystallization process as well as the force associated with the cantilever bending.

The results of this project will help to increase the number of write-erase cycles and the data transfer rate in phase change memories and may lead to other applications of phase change materials in MEMS actuation.



▲ Figure 1: Optical micrograph of SiN cantilevers fabricated by optical lithography and dry/wet etching. An amorphous $\text{Ge}_2\text{Sb}_2\text{Te}_5$ film has been deposited on top.



▲ Figure 2: The $\text{Ge}_2\text{Sb}_2\text{Te}_5$ film has been crystallized with a scanning HeNe laser near the support of the cantilevers. As a consequence, the reflectivity increases and the cantilever end moves up by about $7.5 \mu\text{m}$, which reveals the laser-induced strain and stress in the film.

REFERENCES

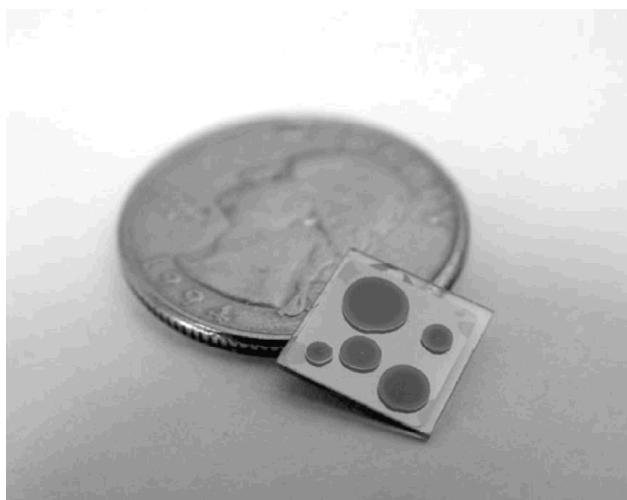
- [1] N. Yamada, "Erasable phase-change optical materials," *MRS Bulletin*, vol. 21, no. 9, pp. 48-50, Sep. 1996.
- [2] S. Hudgens and B. Johnson, "Overview of phase change chalcogenide nonvolatile memory technology," *MRS Bulletin*, vol. 29, no. 11, pp. 829-832, Nov. 2004.

Microfabricated Thin-film Electrolytes and Electrodes for Solid Oxide Fuel Cells

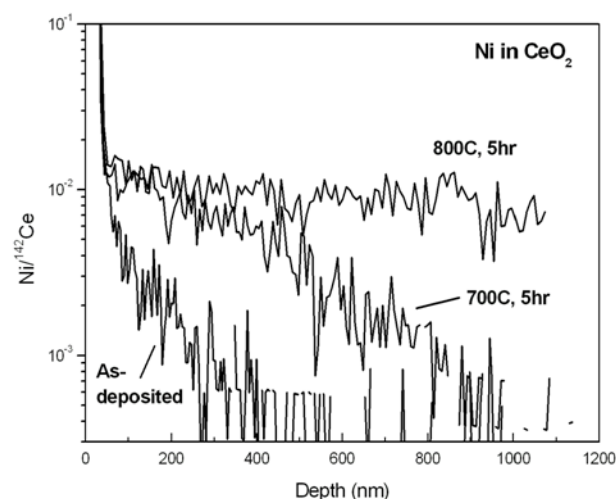
J.L. Hertz, S.J. Litzelman, W.C. Jung, W.S. Kim, A. Rothschild, H.L. Tuller (in coll. with K.F. Jensen, B.L. Wardle, M.A. Schmidt, E. Ivers-Tiffée, D. Gerthsen, U. Karlsruhe; M. Martin, R. DeSousa, U. Aachen)
Sponsorship: DOD MURI, NSF, DOE

There is growing interest in the microfabrication of electrodes for solid oxide fuel cells (SOFCs) in microionic devices [1]. Recently, we reported the fabrication of Pt/(Zr,Y)O₂ (YSZ) nanocomposite electrodes by reactive magnetron co-sputtering [2]. Use of X-ray diffraction and X-ray photoelectron spectroscopy (XPS) characterization show these composites to be a two-phase system with no change of oxidation state from the constituent compounds. Electrical characterization via impedance spectroscopy demonstrated promising electrochemical properties at low temperatures; an area-specific resistance of 500 Ω cm² was achieved at 400°C. To test whether microfabricated thin-film electrolytes may suffer from degradation due to grain boundaries acting as short-circuit-

ing diffusion pathways, sputtered NiO diffusion source films were in-diffused along grain boundaries into nanocrystalline CeO₂ thin films grown by pulsed laser deposition (PLD), at temperatures from 700-800°C. The diffusion profiles were measured by Time-of-Flight Secondary Ion Mass Spectrometry (ToF-SIMS) at the Institute for Physical Chemistry at RWTH Aachen University, Germany. These SIMS spectra, shown in Figure 2, point to a single diffusion mechanism, believed to be grain boundary diffusion, at these relatively low temperatures. Further work to systematically determine the unique opportunities and challenges associated with microstructured SOFCs is currently underway.



▲ Figure 1: Photograph of a Pt/YSZ composite microelectrode device fabricated by reactive magnetron sputtering. Five microelectrodes lie on the surface and the counter electrode is visible through the transparent YSZ substrate².



▲ Figure 2: The ToF-SIMS spectra of Ni diffusion in CeO₂. The as-deposited profile is shown, as are profiles resulting from anneals at 700 and 800°C for 5 hours. In the 800°C sample, Ni has diffused through the entire film.

REFERENCES

- [1] J. Fleig, H.L. Tuller, and J. Maier, "Electrodes and electrolytes in micro-SOFCs: A discussion of geometrical constraints," *Solid State Ionics*, vol. 174, no. 1-4, pp. 261-270, Oct. 2004.
- [2] J.L. Hertz and H.L. Tuller, "Nanocomposite platinum-yttria stabilized zirconia electrode and implications for micro-SOFC operation," *Journal of the Electrochemical Society*, vol. 154, no. 4, pp. B413-B418, Feb. 2007.

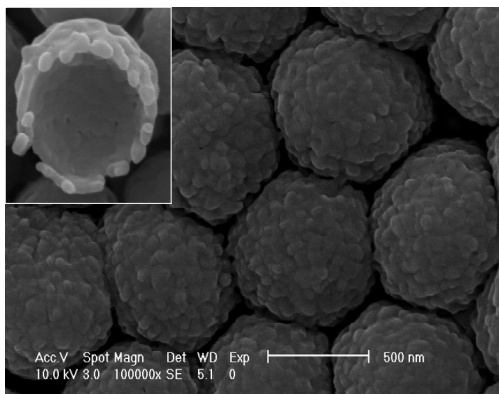
Nanowire- and Microsphere-templated Gas Sensors

A. Rothschild, K. Sahner, G. Whitfield, H.L. Tuller (in coll. with I.D. Kim)
Sponsorship: NSF

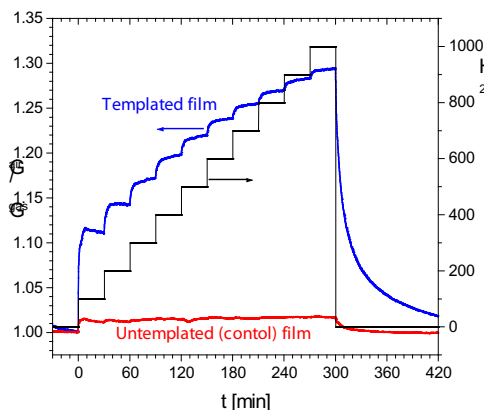
Novel materials synthesis techniques were used to fabricate nanostructured and macroporous semiconducting metal oxide (SMO) films exhibiting exceptionally high sensitivity to reducing and oxidizing gases, as compared to conventionally prepared specimens. Increased sensitivity resulted from an elevated surface area and reduced specimen cross section. Several processing routes were pursued including electrospinning of semiconducting metal oxide (SMO) nanowires into a highly porous mat structure and microsphere templating followed by pulsed laser deposition (PLD) of macroporous SMO material onto the microsphere templates.

The TiO_2 /poly(vinyl acetate) composite nanofiber mats were electrospun onto interdigitated Pt electrode arrays, producing a mesh of 200-500 nm sheaths filled with ~ 10 nm thick single-crystal anatase fibrils. Testing in the presence of NO_2 gas at 300°C demonstrated a minimum detection limit (MDL) of below 1

ppb¹. Chemical and physical synthesis routes were combined to prepare macroporous $\text{CaCu}_3\text{Ti}_4\text{O}_{12}$ and TiO_2 thin films by PLD onto PMMA microsphere-templated substrates. Stable quasi-ordered hollow hemispheres with diameter and wall thicknesses of 800 nm and 100 nm, respectively, were obtained (Figure 1). Current-voltage and impedance spectroscopy measurements point to the crucial role played by grain boundary barriers in controlling the electrical properties of these films. The macroporous $\text{CaCu}_3\text{Ti}_4\text{O}_{12}$ films exhibited a much superior H_2 gas sensitivity (55ppm MDL) to non-templated films² (Figure 2), while macroporous TiO_2 films exhibit excellent NO_x sensitivity. Studies are continuing to more carefully correlate sensor response with SMO microstructure, morphology, and chemistry.



▲ Figure 1: Two SEM micrographs of the macroporous CCTO films. The inset emphasizes the grain structure of the hemispheres.



▲ Figure 2: The resistance response of CCTO films deposited on templated (blue curve) and plain substrates (red curve) during exposure to increasing concentrations (between 100 and 1000 ppm) of H_2 in air.

REFERENCES

- [1] I.-D. Kim, A. Rothschild, B.H. Lee, D.Y. Kim, S.M. Jo, and H.L. Tuller, "Ultrasensitive Chemiresistors Based on Electrospun TiO_2 Nanofibers," *Nano Lett.*, vol. 6, pp. 2009-2013, Sep. 2006.
- [2] I.-D. Kim, A. Rothschild, T. Hyodo, and H. L. Tuller, "Microsphere Templating as Means of Enhancing Surface Activity and Gas Sensitivity of $\text{CaCu}_3\text{Ti}_4\text{O}_{12}$ Thin Films," *Nano Letters*, vol. 6, pp. 193-198, Feb. 2006.

BioMEMS for Control of the Stem Cell Microenvironment

L. Kim, A. Rosenthal, S. Sampattavanich, A. Skelley, J. Voldman
Sponsorship: NIH

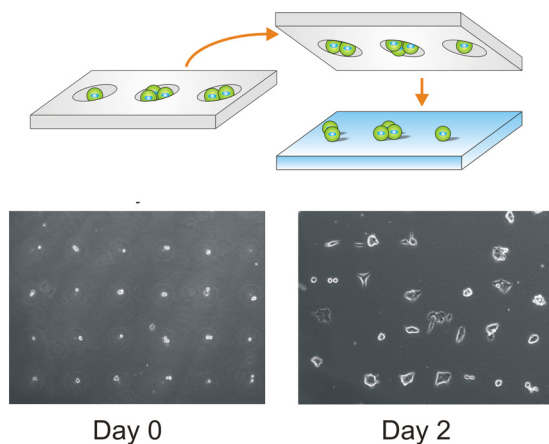
The stem cell microenvironment is influenced by several factors including cell-media, cell-cell, and cell-matrix interactions. Although conventional cell-culture techniques have been successful, they offer poor control of the cellular microenvironment. To enhance traditional techniques, we have designed a microscale system to perform parallel cell culture on a chip while controlling the microenvironment in novel ways.

To control cell-matrix and cell-cell interactions, we use cell patterning. We have developed a simple cell-patterning technique (Figure 1 upper) that can pattern single cells onto arbitrary substrates [1]. Using this technique, we patterned clusters of mouse embryonic stem cells (mESCs) with different numbers of cells in each cluster (Figure 1 lower). We have also developed methods for single-cell patterning using dielectrophoresis (DEP), which uses non-uniform AC electric fields to position cells on or between electrodes [2].

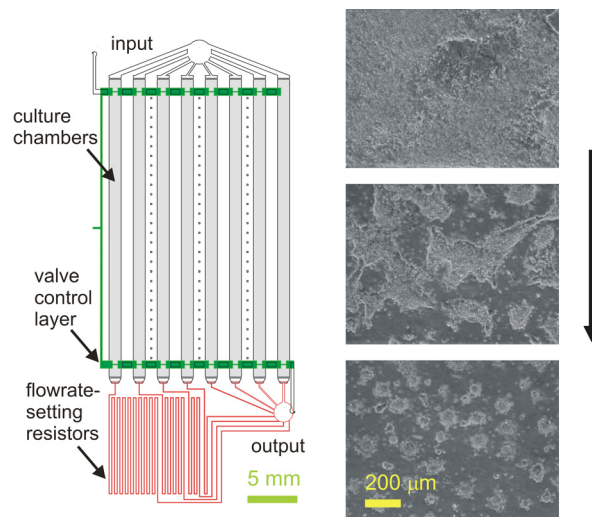
To control cell-media interactions, we have developed a microfluidic device for culturing adherent cells over a logarithmic range

of flow rates [3]. The device (Figure 2, left) controls flow rates via a network of geometrically-set fluidic resistances connected to a syringe-pump drive. We use microfluidic perfusion to explore the effects of continuous flow on the soluble microenvironment. We cultured mESCs in standard serum-containing media across a 2000× range of flow rates. On day 1, colony areas were roughly constant along the axis of perfusion, implying negligible nutrient depletion. However, by day 3, we observed a significant decrease in colony size along the axis of perfusion at mid-range flow rates (Figure 2, right). At higher flow rates, colonies were uniformly large along the axis of perfusion, implying that nutrient depletion was not significant above certain flow rates.

This microfabricated system will serve as an enabling technology that can be used to control the cellular microenvironment in precise and unique ways, allowing us to perform novel cell biology experiments at the microscale.



▲ Figure 1: The mESCs patterned onto tissue culture polystyrene and tracked over multiple days. The cells attach, proliferate, and move.



▲ Figure 2: Microfluidic 1×8 array of cell culture chambers for creating a logarithmic range of flow rates (left). The three photographs at the right show day 3 mESC colonies at upstream, middle, and downstream locations in a single culture channel. Colony size decreased along the axis of perfusion. Arrow indicates direction of flow (right).

REFERENCES

- [1] A. Rosenthal, A. Macdonald and J. Voldman, "Cell patterning chip for controlling the stem cell microenvironment," *Biomaterials*, 2007, to be published.
- [2] A. Rosenthal and J. Voldman, "Dielectrophoretic traps for single-particle patterning," *Biophysical Journal*, vol. 88, pp. 2193-2205, Mar. 2005.
- [3] L.Y. Kim, M.D. Vahey, H.-Y. Lee, and J. Voldman, "Microfluidic arrays for logarithmically perfused embryonic stem cell culture," *Lab on a Chip*, vol. 6, no. 3, pp. 394-406, Mar. 2006.

Microfabricated Devices for Sorting Cells Using Complex Phenotypes

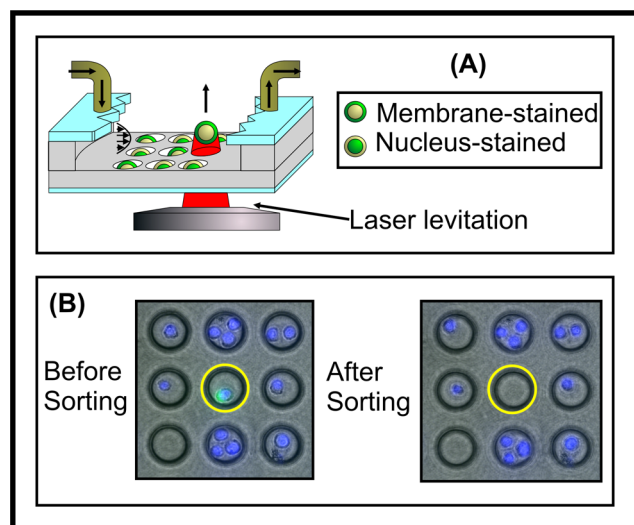
S. Desai, J. Kovac, N. Mittal, B. Taff, J. Voldman
Sponsorship: NIH, DOD, Singapore-MIT Alliance

This research involves the development of numerous microfabricated sorting cytometer architectures for genetic screening of complex phenotypes in biological cells. Our various approaches combine the ability to observe and isolate individual mutant cells within surveyed populations. In this work we merge benefits of both microscopy and flow-assisted cell sorting (FACS) to offer unique capabilities in a single platform. Biologists will leverage these new affordances to isolate cells on the basis of observed dynamic and/or intracellular responses, enabling novel avenues for population screening.

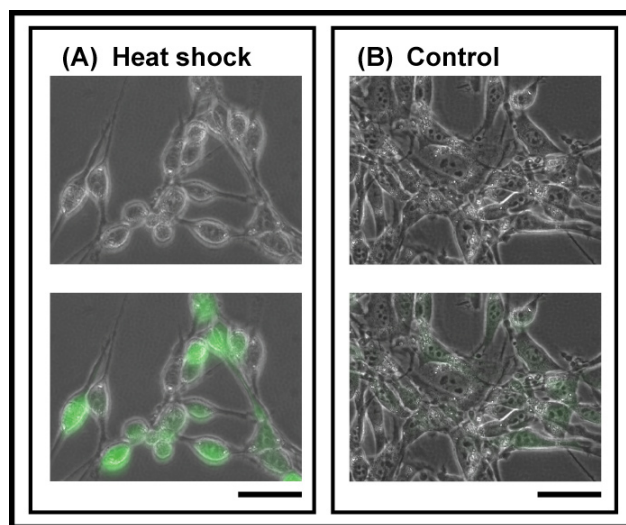
Our most recent approach to image-based sorting, which complements our earlier work, utilizes a microfabricated array of PDMS microwell structures positioned in the floor of a microfluidic flow chamber (Figure 1) [1-2]. These microwells capture and hold cells in place for microscopy-based imaging, and can be optimized to trap single cells. After inspecting the array using microscopy to determine cells of interest, we apply radiation pressure from an

infrared (IR) laser diode to levitate target cells out of the wells and into a flow stream. Released cells can be collected downstream for further analysis. The interconnect-free architecture scales easily; we have presently implemented trap arrays containing more than 10,000 sites.

Manipulating live cells, irrespective of the technique, will certainly have some effect on cellular behavior and physiology. It is imperative that we understand the effects of our sorting techniques (both optical and electrical) on cellular physiology over a range of operating conditions for two main reasons: (1) to determine whether there are any gross effects (such as viability and changes in proliferation), and (2) to determine whether there are more subtle effects that alter complex phenotypes of interest. To this end we are designing a microfabricated device to perform electrical and optical “dose responses” to determine optimal regions of operation and using fluorescence-based stress reporter cell lines as sensors of physiological state (Figure 2).



▲ Figure 1: Microwell-based optical sorting. (A) Schematic sort based on fluorescence localization (nucleus vs. cytoplasm). Laser levitates target cells into the flow stream for downstream collection. (B) Section of well array. We remove a membrane-stained cell from a population of purely nuclear-stained cells. We used an argon laser here; we now use IR-beams to mitigate cell-damage concerns.



▲ Figure 2: Sensing physiological state. (A) Green fluorescent protein (GFP) based stress reporter cell line which shows significant increase in fluorescence intensity, compared to control (B) after a 30-minute heat shock at 44°C and a 14-hour recovery at 37°C. Such a live cell sensor will allow us to perform fluorescence-based cell health assays on thousands of cells. Scale bars 20 μm .

REFERENCES

- [1] J. Kovac and J. Voldman, “Facile image-based cell sorting using OPTO-FluCS (Opto-fluidic cell sorting),” in *Proc. of μTAS 2006 Conference*, Tokyo, Japan, Nov. 2006, pp. 1483-1485.
- [2] J. Kovac and J. Voldman, “Intuitive, visual, complex phenotype cell sorting using OPTO-FluCS (Opto-fluidic cell sorting),” presented at the *Biomedical Engineering Society Fall Meeting 2006*, Chicago, IL, Oct. 2006.

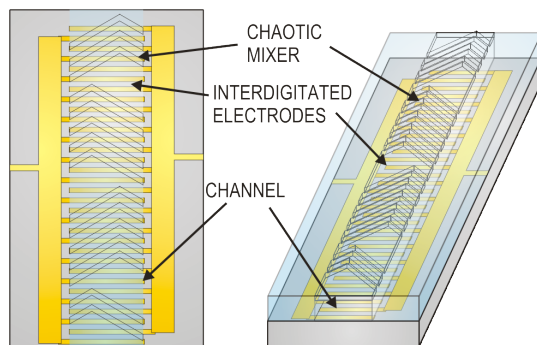
Combined Microfluidic/Dielectrophoretic Microorganism Concentrators

H.-Y. Lee, K. Puchala, J. Voldman
Sponsorship: NASA, Draper Labs

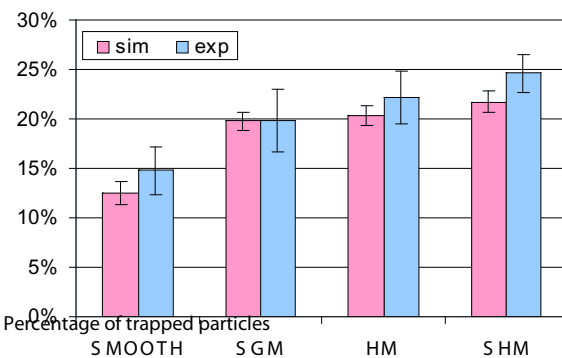
This project focuses on the development of microfabricated microfluidic/dielectrophoretic devices capable of concentrating micron-size particles from complex liquids. The concentrated particles of interest, such as pathogenic bacteria and spores, can then be delivered in small aliquots to the appropriate sensor for identification. Our micro-concentrator exploits the phenomenon of dielectrophoresis (DEP)—the force on polarizable particles in spatially non-uniform electric field [1]—to trap particles from the flow stream in order to subsequently concentrate them by release into a smaller volume of liquid. We create the non-uniform electric field using interdigitated electrodes (IDE) at the bottom of the flow channel (Figure 1).

To maximize the exposure of particles to the DEP field, we employ a passive microfluidic mixer to circulate the liquid (Figure 1). One question that arises is how to determine the optimal mixer geometry for circulating the liquid, which may differ from the ideal geometry for mixing two liquids. To answer this question we

developed modeling tools and an experimental methodology to quantitatively predict the trapping behavior of particles in these systems. As Figure 2 shows, our modeling is able to predict the efficiency of different mixer configurations, without any fitting parameters. Among the four mixers tested (herringbone mixer (HM) slanted groove mixer (SGM), staggered herringbone mixer (SHM), and smooth channel (SMOOTH)), the HM and SHM perform similarly. This result is unexpected, as the HM is known to be a poor mixer of two liquids, while here we show that it is fine for circulating one liquid [2].



▲ Figure 1: Device overview. Illustration of the assembled devices, showing the PDMS channel and gold interdigitated electrodes (IDEs) on the Pyrex substrate.



▲ Figure 2: Comparison of simulated and experimental trapping efficiency. The fabricated devices have 16- μm wide electrodes with 24- μm spacing and a groove-to-channel aspect ratio of 0.22 (SGM), 0.23 (HM), and 0.25 (SHM).

REFERENCES

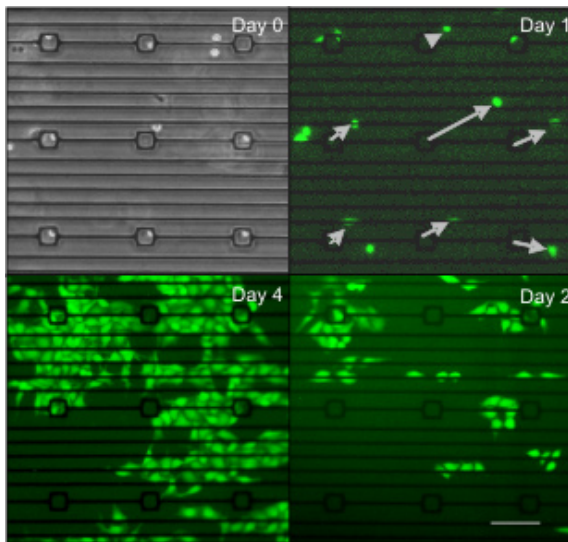
- [1] J. Voldman, "Electrical forces for microscale cell manipulation," *Annu. Rev. Biomed. Engr.*, vol. 8, pp. 425-454, 2006.
- [2] H.-Y. Lee and J. Voldman, "Optimizing micromixer design for enhancing dielectrophoretic microconcentrator performance," *Analytical Chemistry*, vol. 79, no. 5, pp. 1833-1839, Mar. 2007.

DEP Cell-patterning for Controlling Cellular Organization

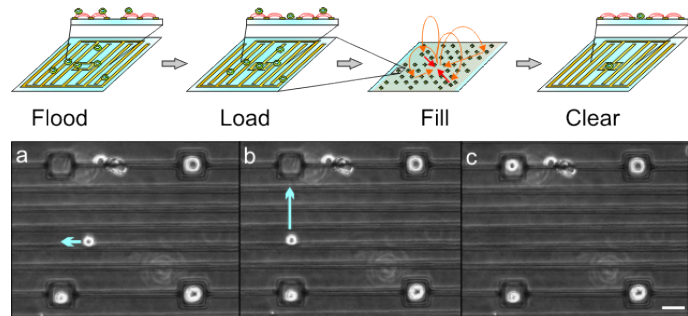
N. Mittal, J. Voldman
Sponsorship: Singapore-MIT Alliance

The ability to place cells at specific locations on a substrate is a useful tool to study and engineer interactions between cells [1], perform image-based cell selection [2], and create cell-based biosensors [3]. The ability to pattern with single-cell resolution is necessary in order to perform studies of single-cell physiology in which these cells are interacting with other cells. We have previously created nDEP-based traps that were used to hold single micron-size *beads* at chosen locations on a substrate [4]. We have recently extended this work by modifying the design to allow us to manipulate and pattern single *cells*. We accomplished this modification by adding interdigitated electrodes to minimize non-specific cell adhesion and determining operating parameters

that minimized heating and electric field exposure. The resulting structures are termed nDEP microwells to reflect that fact that they present an electrical microwell to incoming cells, allowing only cell-substrate attachment inside the DEP trap. With these nDEP microwells we have been able to place non-adherent cells and pattern adherent cells (Figure 1). Additionally, we have demonstrated that our cell-patterning technique does not affect gross cell phenotype as measured by morphology and proliferation. Finally, we have developed a method that combines pressure-driven and convective flows to manipulate cells in two dimensions (Figure 2).



▲ Figure 1: Phase and fluorescent images of GFP-expressing HeLa cells trapped in an nDEP microwell array, showing that they exhibit normal morphology and proliferation over 4 days after being trapped at 1 V_{pp} and 10 MHz. Arrows in the Day 1 figure (top, right) show the displacement of cells that moved out of the trap. The scale bar represents 100 μm .



▲ Figure 2: Top: Schematic of operating procedure. In the "Fill" step, orange lines show the motion of the fluid while red lines show the motion of (two) untrapped cells. The flow must be kept slow enough ($< 5 \mu\text{m/s}$) so that cells do not get lifted with the flow. Bottom: Use of convective flow to pattern cells. (a) \rightarrow (b): Convective flow pushes untrapped cells towards the center of the electrode array (not shown at this scale) when electrodes are driven at 2.5 V_{pp} . Blue arrows show the movement of cells between frames. This flow is used to align cells with the trap. (b) \rightarrow (c): Transition is made to pressure-driven flow using a syringe pump. All untrapped cells move in the same direction, along the array. The pressure-driven flow is used to push aligned cells into the traps. The scale bar represents 25 μm .

REFERENCES

- [1] S.N. Bhatia, M.L. Yarmush, and M. Toner, "Controlling cell interactions by micropatterning in co-cultures: Hepatocytes and 3T3 fibroblasts," *Journal of Biomedical Materials Research*, vol. 34, no. 2, pp. 189-199, Feb. 1997.
- [2] B.M. Taff and J. Voldman, "A scalable, addressable positive-dielectrophoretic cell-sorting array," *Analytical Chemistry*, vol. 77, no. 24, pp. 7976-7983, Dec. 2005.
- [3] D.A. Stenger et al., "Detection of physiologically active compounds using cell-based biosensor," *Trends in Biotechnology*, vol. 19, no. 8, pp. 304-309, Aug. 2001.
- [4] A. Rosenthal and J. Voldman, "Dielectrophoretic traps for single-particle patterning," *Biophysical Journal*, vol. 88, no. 3, pp. 2193-2205, Mar. 2005.

Iso-dielectric Cell Separation

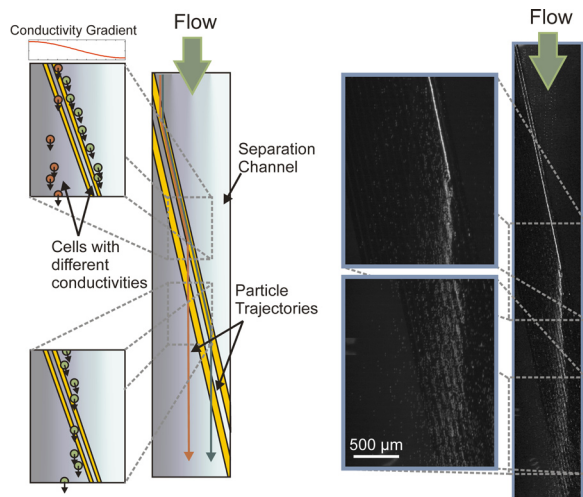
M.D. Vahey, J. Voldman

Sponsorship: NIH NIBIB, MIT Buschbaum Fund, Singapore-MIT Alliance, CSBi/Merck Graduate Fellowship

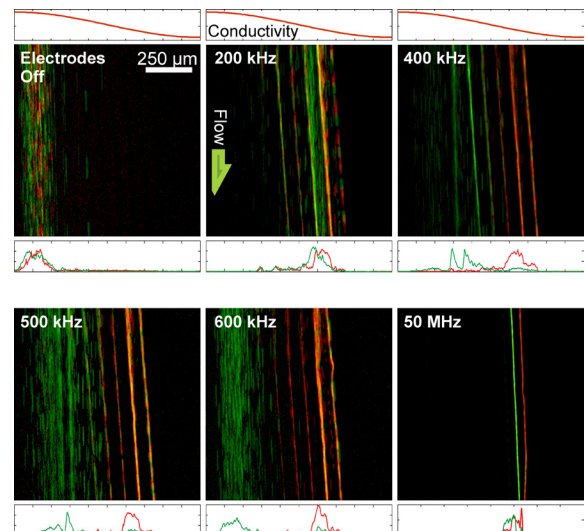
Increased throughput in the techniques used to engineer new metabolic pathways in unicellular organisms demands similarly high throughput tools for measuring the effects of these pathways on phenotype. For example, the metabolic engineer is often faced with the challenge of selecting the one genomic perturbation that produces a desired result out of tens of thousands of possibilities [1]. We propose a separation method – iso-dielectric separation, or IDS – which separates microorganisms continuously based on their intrinsic dielectric properties [2-3]. Because IDS is an equilibrium method, sorting cells according to their unique equilibrium positions in an energy landscape, it offers enhanced specificity over other label-free separation methods [4]. This technology would enable high throughput screening of cells based upon electrically distinguishable phenotypes.

Iso-dielectric separation uses dielectrophoresis (DEP) and media with spatially varying conductivity to create the energy landscape in which cells are separated according to their effective conduc-

tivity (Figure 1). It is similar to iso-electric focusing, except that it uses DEP instead of electrophoresis, and is thus applicable to uncharged particles, such as cells [5]. The IDS leverages many of the advantages of microfluidics and equilibrium gradient separation methods to create a device that is continuous-flow, capable of parallel separations of multiple (>2) subpopulations from a heterogeneous background, and label-free. We demonstrate the simultaneous separation of three types of polystyrene beads based upon surface conductance as well as sorting non-viable from viable cells of the budding yeast *Saccharomyces cerevisiae* (Figure 2). Current efforts are focused on the separation of *Escherichia coli* based upon the amount of the intracellular polymer poly(hydroxybutyrate) each cell contains.



▲ Figure 1: (Left) Illustration of iso-dielectric separation, depicting cells with different electric properties following different trajectories in a conductivity gradient. (Right) Fluorescence micrograph showing the trajectory of a single type of polystyrene beads flowing through the device.



▲ Figure 2: Separation of viable and non-viable yeast cells using IDS, showing in particular the frequency-dependent behavior of live and dead cells in the device ($f_h = 0.047$ S/m, $f_l = 0.0093$ S/m, $Q = 3\mu\text{l}/\text{min}$, $V = 20$ V_{pp}). Optimal separation is observed at ~600 kHz.

REFERENCES

- [1] G. Stephanopoulos, "Metabolic fluxes and metabolic engineering," *Metabolic Engineering*, vol. 1, no. 1, pp. 1-11, 1999.
- [2] M.D. Vahey and Voldman, J. "Iso-dielectric separation: A new method for the continuous-flow screening of cells," *Micro Total Analysis Systems '06*, vol. 2, pp. 1058-1060, 2006.
- [3] M.D. Vahey and Voldman, J. "Iso-dielectric separation: A new technology for continuous-flow cell screening," presented at the *BMES Fall Meeting*, Sep.-Oct. 2006.
- [4] P.H. O'Farrell, "Separation techniques based on the opposition of 2 counteracting forces to produce a dynamic equilibrium," *Science*, vol. 227, pp. 1586-1589, Mar. 1985.
- [5] H.A. Pohl and J.S. Crane, "Dielectrophoresis of cells," *Biophysical Journal*, vol. 11, pp. 711-727, 1971.

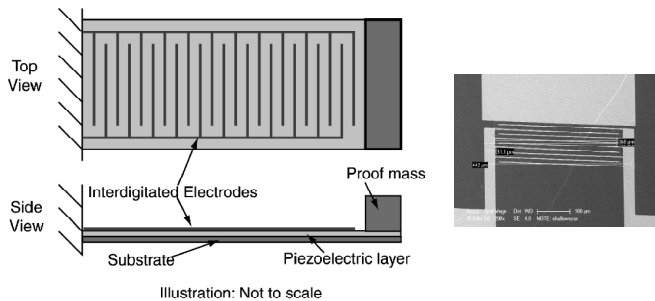
MEMS Vibration Harvesting for Wireless Sensors

W.S. Kim, A. Mracek, Y. Manioux, B.L. Wardle (in coll. with S.G. Kim)
 Sponsorship: AFOSR, NSF Fellowship

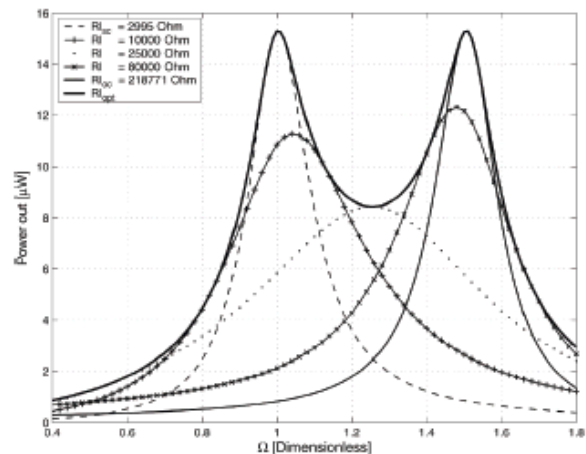
The recent development of “low power” (10’s-100’s of μW) sensing and data transmission devices, as well as protocols with which to connect them efficiently into large, dispersed networks of individual wireless nodes, has created a need for a new kind of power source. Embeddable, non-life-limiting power sources are being developed to harvest ambient environmental energy available as mechanical vibrations, fluid motion, radiation, or temperature gradients [1]. While potential applications range from building climate control to homeland security, the application pursued most recently has been that of structural health monitoring, particularly for aircraft.

This SHM application and the power levels required favor the piezoelectric harvesting of ambient vibration energy. Current work focuses on harvesting this energy with MEMS resonant

structures of various geometries. Coupled electromechanical models for uniform beam structures have been developed to predict the electrical and mechanical performance obtainable from ambient vibration sources. The optimized models have been validated by comparison to prior published results [2] and verified by comparison to tests on a macro-scale device [3]. A non-optimized, uni-morph beam prototype (Figure 1) has been designed and modeled [4-5]. Dual optimal frequencies with equal peak powers and unequal voltages and currents are characteristic of the response of such coupled devices when operated at optimal load resistances (Figure 2). Design tools to allow device optimization for a given vibration environment have been developed for both geometries. Future work will focus on fabrication and testing of optimized uni-morph and proof-of-concept bi-morph prototype beams. System integration and development, including modeling the power electronics, will be included.



▲ Figure 1: Illustration of MPVEH uni-morph configuration (left) and SEM of a prototype device.



▲ Figure 2: Power vs. normalized frequency with varying electrical load resistance [4].

REFERENCES

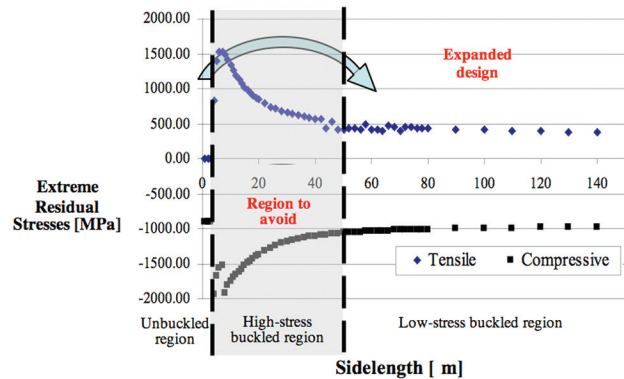
- [1] S. Roundy, P.K. Wright, and J.M. Rabaey, *Energy Scavenging for Wireless Sensor Networks with Special Focus on Vibrations*, Norwell, MA: Kluwer Academic Publishers, 2004.
- [2] H.A. Sodano, G. Park, and D.J. Inman, "Estimation of electric charge output for piezoelectric energy harvesting," *Strain*, vol. 40, no. 2, pp. 49-58, May 2004.
- [3] N.E. duToit and B.L. Wardle, "Experimental verification of models for microfabricated piezoelectric vibration energy harvesters," presented at the 47th AIAA Structures, Dynamics, and Materials Conference, Newport, RI, May 2006.
- [4] N.E. duToit, B.L. Wardle, and S.G. Kim, "Design considerations for MEMS-Scale piezoelectric mechanical vibration energy harvesters," *Integrated Ferroelectrics*, vol. 71, pp. 121-160, 2005.
- [5] N.E. duToit and B.L. Wardle, "Performance of microfabricated piezoelectric vibration energy-harvesters," *Integrated Ferroelectrics*, vol. 83, pp.13-23, 2007.

Design, Fabrication, and Testing of Multilayered Microfabricated Solid Oxide Fuel Cells (SOFCs)

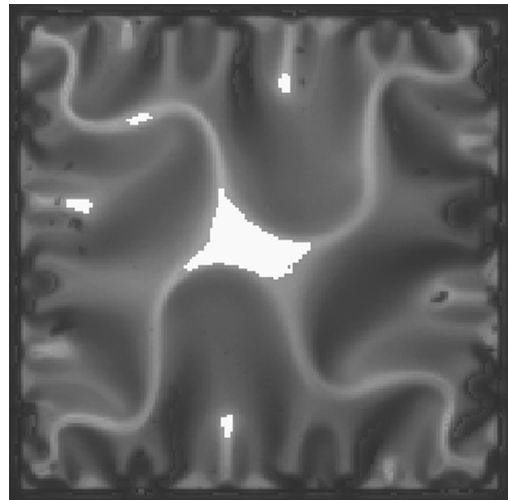
N. Yamamoto, D. Quinn, P. Capozzoli, N. Wicks, B.L. Wardle, S.M. Spearing (in coll. with B.A. Wilhite, J. Hertz, J. Cui, K.F. Jensen, H.L. Tuller, M.A. Schmidt)
Sponsorship: ARO

Microfabricated solid oxide fuel cells were investigated for portable power applications requiring high energy densities [1]. The thickness of the electrolyte, the travel length of oxygen ions, was reduced down to $\sim 150\text{nm}$. The tri-layers (yttria-stabilized zirconia (YSZ) as an electrolyte and platinum-YSZ cermet as cathode/anode) were sputter-deposited on a silicon wafer, and then they were released as square plates by KOH etching the silicon through patterned silicon nitride masks on the back side. High intrinsic and extrinsic (thermal) stresses due to fabrication and operation ($25\text{-}600^\circ\text{C}$) [2], respectively, require careful thermomechanically stable design of μSOFCs .

First, material properties of the ultra-thin YSZ were characterized experimentally and found to be significantly different than those of bulk YSZ [3]. Second, based on the obtained properties, maximum stresses in the plates at 625°C were analyzed using non-linear von Karman plate theory [4]. The stresses showed three regions with sidelength variation: an un-buckled regime, a buckled regime with high stresses, and post-buckling regime with lower stresses (see Figure 1). The μSOFCs were fabricated in the post-buckling regimes with $\sim 80\text{-}180\mu\text{m}$ sidelength and total $\sim 450\text{nm}$ thickness. With the plates buckled as shown in Figure 2, the μSOFCs produced power output of 0.008mW/cm , lower than the expected power from their electrochemical test. Given the high-performance predicted for the underlying nano-structured ultra-thin electrolyte, anode, and cathode layers, additional studies are needed to improve specimens and test setup and to assess μSOFCs ' long-term operational stability.



▲ Figure 1: Maximum stress evolution with sidelength of YSZ square membranes with $\sim 450\text{nm}$ thickness cycled to 600°C .



▲ Figure 2: Top-view of highly buckled, but unfailed, square membrane.

REFERENCES:

- [1] C.D. Baertsch, et al., "Fabrication and structural characterization of self-supporting electrolyte membranes for a μSOFC ," *Journal of Matls Research*, vol. 19, pp. 2604-2615, Sep. 2004.
- [2] D.J. Quinn, M.S. Spearing, B.L. Wardle, "Residual stress and microstructural evolution in thin film materials for a micro solid oxide fuel cell (SOFC)," *Mater. Res. Soc. Symp. Proc.*, vol. 854E.
- [3] N. Yamamoto, "Thermomechanical Properties and Performance of Microfabricated Solid Oxide Fuel Cell (μSOFC) Structures," Master's thesis, Massachusetts Institute of Technology, Cambridge, MA, 2006.
- [4] N. Yamamoto, N. Wicks, B.L. Wardle, "Twice-buckled cermet composite laminate under equibiaxial compression," *Proceedings of 48th AIAA/ASME/ASCE/AHS/ASC Structures, Structural Dynamics, and Materials Conference*, Honolulu, HI, Apr. 2007.